SOME ASPECTS OF NONLINEAR DYNAMICS

K. M. VALSAMMA

THESIS SUBMITTED IN
PARTIAL FULFILMENT OF THE REQUIREMENTS
FOR THE DEGREE OF
DOCTOR OF PHILOSOPHY

DEPARTMENT OF PHYSICS
Cochin University of Science and Technology
KOCHI

1992

C E R T I F I C A T E

Certified that the work reported in the present thesis is based on the bonafide work done by Ms. Valsamma K.M. under my guidance in the Department of Physics, Cochin University of Science and Technology, and has not been included in any other thesis submitted previously for award of any degree.

Cochin-682022

17-2-1992

Prof. K. Babu Joseph
(Supervising Teacher)
Professor and Head of the
         Department of Physics
Cochin University of Science
         and Technology
Cochin-682 022.

C O N T E N T S

P R E F A C E

The thesis entitled 'Some Aspects of Nonlinear Dynamics'
deals with investigations carried out on the universal para-
meters associated with the transition to chaos in nonlinear
dissipative systems. The analysis is based on an analytic
perturbative procedure, developed to solve the renormalisation
group equations, and the method is applied to specific one
hump and circle maps. The universal function obtained in the
latter case has been used to compute the singularity spectrum
of the circle map. Finally certain aspects of the continuous
symmetries of dissipative systems are discussed and applied
to specific models like Lorenz and Rössler, followed by
detailed numerical analysis.

The thesis consists of five chapters. Chapter 1 gives
a general introduction to deterministic chaos in dissipative
as well as conservative systems along with a discussion of
the different routes to chaos. Commonly used concepts in
nonlinear analysis such as generalised dimension, fractal
dimension, information and correlation dimension are discussed.
Multifractals and singularity spectrum are also introduced.
The universality theory developed by Feigenbaum in the context
of 1-d maps is briefly discussed towards the end of this
Chapter.

In Chapter 2, the perturbative scheme of solving the RG equations is presented and the procedure is applied to specific cases such as $z=2,4$ and 6. The asymptotic series in the expressions for the universal constants α and δ are replaced by Padé approximants to obtain results exhibiting faster convergence.

Chapter 3 gives a brief introduction to circle maps and extending the perturbative method, the constants α and δ corresponding to the sine circle map are calculated and reported. Choosing a polynomial circle map, the dependence of the universal constants on z is studied. The corresponding universal function $g(x)$ is used to find the singularity spectrum of the associated attractor.

Chapters 4 and 5 form a separate section of the thesis. Chapter 4 introduces the symmetry concept in the context of dissipative systems. Here we formulate a general theory of rotational, translational and scale symmetry for dissipative systems. It gives a clue about how translational, rotational and scale symmetry behave in the phase-space as the control parameter is tuned.

Chapter 5 treats within the symmetry framework specific models of dissipative systems in detail alongwith numerical results and conclusions. The investigations carried out provide material for the following papers:

1 'Use of Padé approximants in the Evaluation of α and δ for 1-d maps. Pramana (J. Phys.) <u>30</u> (1988) 501

2 'Perturbative Analysis of Quasiperiodic Route to Chaos in the Circle Map. Phy. Scr. <u>42</u> (1990) 19

3 'Aspects of Symmetries of Dissipative Systems' Research Reports in Physics: Symmetries and Singularity Structures. ed: M. Lakshmanan, M. Daniel Springer-Verlag, Berlin (1990) 78

4 'Multifractals in Polynomial Circle Maps' – Communicated to Physics Letters A

CHAPTER I

INTRODUCTION

1.1 Chaos in non-linear systems

It has been established recently that deterministic evolution laws may sometimes lead to chaotic behaviour even in the absence of external noise. This phenomenon, called deterministic chaos, is essentially due to a sensitive dependence on initial conditions and has great relevance in the description of many physical systems whose dynamics is modelled by ordinary nonlinear differential equations or by discrete maps. That is, in the case of certain nonlinear systems we cannot predict, to any significant accuracy, its future evolution even when the governing laws are deterministic or the motion is periodic. The observation that complex behaviour can be generated even in systems of a very low number of degrees of freedom, governed by completely deterministic rules, has stimulated a lot of research interest. With the development of ideas in this direction, several phenomena such as hydrodynamics, turbulence, and chemical kinetics are being explained in a better and more satisfactory way than before. Deterministic chaos arises due to an intrinsic property of a dynamical system and non-linearity is the essential condition for a system to slip into chaos.

Let the time evolution of a dynamical system be described by a set of n first order differential equations,

$$\frac{d}{dt} \vec{x}(t) = \vec{f}(\vec{x}, t) \tag{1.1}$$

Here $\vec{x}(t)$ represents a vector in $\mathbb{R}^n$ and $\vec{f}$ a vector field over this space [1]. If $\vec{f}$ does not depend on time explicitly, it is called an autonomous flow. On the other hand, when $\vec{f}$ does depend explicitly on time it is a nonautonomous flow. Study of solutions to (1.1) is facilitated by a method due to Poincaré, popularly known as Poincaré surface of section, wherein we find the successive intersections of the trajectory of points in a specified direction of evolution with an appropriate plane S rather than directly in $\mathbb{R}^n$. The transformation leading from one point to the next is a continuous mapping T of S into itself, called the Poincaré map [2]:

$$x_{k+1} = T(x_k) = T(T(x_{k-1})) = T^2(x_{k-1}) = \cdots \tag{1.2}$$

As is evident from the above relation, x_o determines x_1, which in turn determines x_2, and so on. T is an invertible mapping of S into itself. The scheme based on the Poincaré section replaces a continuous time evolution with a discrete mapping.

The Poincaré surface of section converts an n dimensional flow into an (n-1) dimensional difference map, and usually has the following appearance: a point or a number of points located along a single curve or on a surface; for example, for a periodic system the Poincaré section is a single point in a plane called the fixed point of the map T, represented by

$$x_o = T(x_o) = T^2(x_o) = \ldots \qquad (1.3)$$

For a quasi-periodic system, the Poincaré section has a number of points which look like a simple curve, and in the commensurate case, the curve has only a limited number of points, while for incommensurate frequencies it will be densely filled. Hence under strong dissipation, (1.1) can be abstracted by a difference map

$$x_{n+1} = f_\lambda (x_n) \qquad (1.4)$$

Dynamical systems in general are usually classified into conservative and dissipative types. Conservative systems are those which preserve the phase-space volume during time evolution and are more fundamental than dissipative systems. The dissipative systems on the other hand, are characterised by internal friction, which entails a continuous decrease of the energy. As a result the asymptotic motion (t→∞) takes place on a subspace of the

original phase space, on which the initial condition has no influence. The specific subspace which is asymptotically reached in time is called an attractor. The set of initial conditions that evolve to an attractor is called the basin of attraction. For 1-d flow the only possible attractor is the fixed point, whereas in the case of a 2d-flow the possible attractors are fixed point and limit cycle. A third type of attractor is the torus T^r which corresponds to a quasiperiodic regime with r independent frequencies.

A chaotic attractor [3] corresponds to unpredictable motions, which exhibit the property of sensitive dependence on initial conditions. By this is meant that nearby points diverge on an average, exponentially. This results from the fact that trajectories on a chaotic attractor are successively stretched and folded, as a consequence of which, errors in estimating the initial state of the system undergo continuing amplifications. Put differently, the microscopic perturbations are amplified to get the macroscopic perturbations.

Discrete maps of the form (1.4) are often used to model the dynamics of a wide variety of physical, chemical and biological systems effectively [4,5], $f_\lambda (x_n)$ depends on a control parameter λ , the variation of which can drive

the map through asymptotically different states. The
study of 1-d maps helps one to understand many of the
scaling and universal properties of chaotic transitions
observed in higher dimensional systems. The function
$f_\lambda(x)$ often has the following properties:

(1) $f_\lambda(x)$ maps an interval (a_1, a_2) into itself.

(2) $f_\lambda(x)$ increases monotonically as x increases through
the range $o \leq x \leq A$, with A being the maximum of the map
and $f_\lambda(x)$ decreases monotonically as x increases
beyond A. That is, it is unimodal, with $f(a_1)=f(a_2)=o$.

(3) $f_\lambda(x)$ has a unique maximum at x = A in this interval,
such that $f'(x) > o$ for $x < A$ and $f'(x) < o$ for $x > A$.

Such maps are called one hump maps.

One class of such unimodal maps satisfying the above
requirements is described by the relation

$$x_{n+1} = 1 - \lambda |x_n|^z \qquad\qquad (1.5)$$

on the interval $(-1, 1)$ with $o < \lambda < 2$, where z is usually a
positive integer that labels the different universality
classes.

1.2 Routes to chaos

As remarked in the opening section, the temporal
evolution of a system can be characterised by the trajectory

of a point in phase space. A trajectory on a chaotic attractor exhibits most of the properties associated with random motions, although no randomness is explicitly introduced. The equations of motion are purely deterministic, but the random behaviour spontaneously emerges from the system. Over short periods, small differences in position are greatly amplified, making long term prediction impossible even for the simplest systems whose parameters are determined exactly.

Usually, the behaviour of a dissipative system depends on a control parameter which determines the asymptotic behaviour. The phenomenon by which the system switches from one stable state to another under a variation of the control parameter, is called bifurcation. There are three main types of bifurcation [6,7]. As the control parameter λ of the system is tuned, the stable attractor becomes unstable and at some parameter value $\lambda = \lambda_0$ there undergoes a bifurcation to a pair of fixed points, one of which is stable and the other is unstable. The creation of these two new fixed points at $\lambda = \lambda_0$ is called tangent bifurcation. In pitchfork bifurcation a stable fixed point is destroyed and two new stable fixed points are created. Here in pitchfork bifurcation the periodicity of the existing attractors has

doubled. In a third type of bifurcation a fixed point loses stability and a limit cycle is produced. This is termed a Hopf bifurcation and can occur only in 2d-flows. In higher dimensional systems, a Hopf bifurcation may give rise to a torus, instead of a limit cycle.

Depending on the type of bifurcation involved, there are three commonly observed routes or scenarios by which a transition from regular to chaotic motion can occur in dissipative systems. The three routes of significant relevance are:

(1) period-doubling (Feigenbaum scenario)

(2) quasiperiodicity (Ruelle-Takens-Newhouse scenario)

(3) intermittency (Pomeau-Manneville scenario)

Feigenbaum Scenario

The most widely known and best understood route to chaos is period-doubling, discovered by Feigenbaum[8-9,11], in which a stable fixed point bifurcates to a periodic orbit which then proceeds via an infinite number of period-doubling bifurcations to chaotic behaviour, as the control parameter is varied. This route has been observed in a number of experimental situations like Rayleigh-Bénard convection [2,10], Belousov-Zhabotinsky reaction [12,13] etc. Two universal constants can be associated with this type of transition:

1) Scale factor α : At each period-doubling the separation between any two adjacent elements of a periodic attractor is scaled by a constant factor α, defined by

$$\alpha = \lim_{n \to \infty} \frac{\Delta x_n}{\Delta x_{n+1}} \qquad (1.6)$$

where Δx_n is half the separation between fixed points in the 2^n cycle.

2) Bifurcation rate δ: For each period-doubling the control parameter is approximately scaled by a factor δ:

$$\delta = \lim_{n \to \infty} \frac{\lambda_{n+1} - \lambda_n}{\lambda_{n+2} - \lambda_{n+1}} \qquad (1.7)$$

where λ_n represents the value at which nth bifurcation occurs.

Ruelle-Takens-Newhouse Scenario [2,14,16]

In Ruelle-Takens-Newhouse route a steady state gives way to an oscillatory state (limit cycle) by means of Hopf bifurcation, as the knob is turned. Then another bifurcation occurs and the motion becomes doubly periodic corresponding to a toroidal surface in phase-space.

Finally a third bifurcation occurs in which the doubly periodic toroidal motion gives way to a chaotic attractor.

Pomeau-Manneville Scenario [15]

The intermittency route to chaos was proposed by Pomeau and Manneville. It is associated with the collision of a stable fixed point with an unstable fixed point. Unlike period-doubling or Ruelle-Takens-Newhouse scenario, there is no indication as to when the transition occurs. It merely describes a situation where the motion alternates between periodic behaviour and bursts of chaos. At the onset of chaos, these bursts are far apart in time, but as the control parameter is varied beyond onset, the bursts become more and more frequent.

1.3 Characterisation of chaos

After having described the various types of bifurcation and the routes which these follow, we will discuss some aspects of chaotic attractors whose onset these various scenarios are meant to describe. We know that within some basin of attraction in phase space a dissipative system will settle down to an attracting set or attractor which may or may not be chaotic. Chaotic attractors have a complicated form with interweaving trajectories on it

[3,17-19]. This multilayered nature makes the attractor behave strangely. Strangeness refers to the dynamics unrelated to its geometry. The typical geometry of a strange attractor is a set of self-similar structures that repeat on finer and finer scales and has a fractional dimension. Experimental evidence for the existence of strange attractor was first given by E.N. Lorenz [96,20]. The characterisation of a strange attractor employs such notions as Lyapunov exponents, various dimensions and entropies.

The topological dimension of an attractor is the minimum number of co-ordinates needed to specify in it the location of a point. It is also a lower bound on the number of essential variables needed to model the dynamics. Using any reasonable definition of dimension, we note that a fixed point has dimension zero, a limit cycle has dimension one etc. Unlike these structures, chaotic attractors, however have a structure that is not simple, and frequently have a highly fractured structure.

To fully understand the properties of a chaotic attractor, one must take into account the distribution or density, of points on the attractor. The natural or probabilistic measure provides a notion of the relative frequency with which an orbit visits different regions of the attractor. Accordingly

there are two types of dimensions, the metric and proba-
bilistic dimensions. The metric dimension characterises
the sets as geometrical objects which are determined by
their metric properties. The probabilistic dimension
takes into account with what probability a typical traje-
ctory of a dynamical system visits different regions of
the attractor.

Capacity or Fractal Dimension

A typical example of a set with noninteger dimension
is the middle thirds Cantor set [21,22] obtained by divid-
ing the interval (0,1) into thirds, discarding the middle
thirds and repeating the operation for the remaining
intervals and so on, ad infinitum. Thus a Cantor set is
a compact metric space that is totally disconnected,
uncountable and may have measure zero and exhibits rescal-
ing invariance. This structure has close correspondence
with that of the strange attractor and gives considerable
insight into some of the general properties of the
attractor.

The capacity or fractal dimension is defined by [5]

$$D_o = \lim_{\epsilon \to 0} \frac{\ln N(\epsilon)}{\ln (1|\epsilon)} \tag{1.8}$$

where $N(\epsilon)$ is the minimum number of p-dimensional cubes
of side ϵ needed to cover the set. For the Cantor set

obtained by the limiting process of deleting middle thirds, if we choose $\epsilon = (\frac{1}{3})^m$, then $N(\epsilon) = 2^m$ and the above equation yields,

$$D_c = \lim_{m \to \infty} \frac{\ln 2}{\ln 3} = 0.630 \tag{1.9}$$

The fractal or capacity dimension is a metric dimension. Actually many attractors have a Cantor set like structure.

Being a purely geometric measure, the fractal dimension D_o does not reflect the inhomogenity of the strange set, since points rarely visited are counted on an equal footing with points frequently visited in the course of the flow. The information dimension defined next, gives the visitation probability in different points of the attractor.

Information Dimension D_1

An important measure which is sensitive to the frequency of visiting is the information entropy defined by [22]

$$I(\epsilon) = - \sum_{i=1}^{N(\epsilon)} P_i(\epsilon) \ln P_i(\epsilon) \tag{1.10}$$

Then D_1 is defined:

$$D_1 = \lim_{\epsilon \to 0} \frac{I(\epsilon)}{\ln(1/\epsilon)} \tag{1.11}$$

where P_i is the probability for a point of the attractor to be contained in the ith box, $N(\epsilon)$ the number of boxes visited. If every box is visited with the same probability

$$P_i(\epsilon) = \frac{1}{N(\epsilon)}, \quad \forall_i$$

giving

$$I(\epsilon) = -\ln N(\epsilon)$$

and $D_1 = D_0$ (1.12)

That is, D_1 reduces to the fractal dimension D_0. For all other cases, $D_1 < D_0$. The difference $D_1 - D_0$ provides some measure of the non-uniformity with which different parts of the attractor are covered by the flow.

Correlation Dimension D_2

The correlation integral is obtained from the correlation between random points on the attractor. Consider the set of points on the attractor obtained from a time series $x_1 \ldots x_N$ with fixed increment τ between successive measurements. Due to the exponential divergence of trajectories, most pairs (x_i, x_j) with $i \neq j$ will be dynamically uncorrelated. The points are spatially correlated on the attractor if the distance is less than a preset number ϵ. The spatial correlation is defined according to the

correlation integral

$$C(\epsilon) = \frac{1}{N^2} \sum_{i,j=1}^{N} \Theta(\epsilon - (|x_i - x_j|)) \qquad (1.13)$$

where $\Theta(x) = 1 \qquad$ if $x > 0$

$\qquad\qquad\quad = 0 \qquad$ if $x \leq 0$

For proper choice of ϵ, $C(\epsilon)$ grows like

$$C(\epsilon) \sim \epsilon^{\nu} \qquad (1.14)$$

When this scaling relation holds for a clear range of ϵ values it makes sense to calculate correlation dimension.

Hence the correlation dimension is defined:

$$D_2 = \lim_{\epsilon \to 0} \frac{\ln C(\epsilon)}{\ln \epsilon} \qquad (1.15)$$

The correlation exponent ν gives a useful measure of the local structure of the strange attractor. The correlation dimension is made use of in experimental situations involving higher dimensional systems.

Higher Order Information Dimension D_q

A complete physical characterisation of a strange attractor is possible only in terms of the generalised dimensions D_q. For a strange attractor the set D_q contains information on the appearance and statistical properties of the attractor. The fractal dimension D_0, the information dimension D_1 and the correlation dimension D_2, are particular

cases of the qth order generalised dimension defined
by [7]

$$D_q = \frac{1}{q-1} \lim_{\epsilon \to 0} \frac{\ell n(\sum_{i=1}^{N(\epsilon)} P_i^q)}{\ell n(\epsilon)}$$ (1.16)

for q = 0,1,2

Lyapunov Characteristic Exponent [3,22]

Probably the most important quantitative measure of characterisation of chaos in both conservative and dissipative systems is the Lyapunov characteristic exponent. A crucial step in our study of dynamics is to concentrate on the analysis of separation in time of infinitely close points. In order to describe stretching and contraction in more detail, we need the notion of the Lyapunov characteristic exponent.

For a definition of Lyapunov characteristic exponent for a system of differential equations given by (1.1), we consider two nearby trajectories with initial conditions x_o and $x_o + \Delta x_o$ respectively. These evolve in time yielding the tangent vector $\Delta x(x_o, t)$ with its Euclidean norm

$$d(x_o, t) = || \Delta x(x_o, t) ||$$ (1.17)

The time evolution of Δx is given by linearising (1.17)

$$\frac{d}{dx}(\Delta x) = M(x(t)) \Delta x$$ (1.18)

where $M(x(t)) = \dfrac{\partial f(x)}{\partial x}\Big|_{x\,=\,x(t)}$ is the Jacobian matrix.

The mean exponential rate of divergence of nearby trajectories is

$$\sigma(x_0) = \lim_{\substack{t \to \infty \\ d(o) \to o}} \frac{1}{t} \, \ell n \, \frac{d(x_0,\,t)}{d(x_0,\,o)} \qquad (1.19)$$

Choosing an M-dimensional basis $(\hat{e}_i)$, σ takes on M values

$$\sigma_i(x_0) = \sigma(x_0, \hat{e}_i) \qquad (1.20)$$

which are the Lyapunov exponents. For an M dimensional system, there exist M, σ's which can be ordered:

$$\sigma_1 \geq \sigma_2 \geq \cdots \geq \sigma_M \qquad (1.21)$$

These M Lyapunov exponents quantify the sensitivity of the system dynamics to its initial conditions and also indicate the degree to which nearby phase space trajectories diverge.

For a conservative flow, all Lyapunov exponents sum upto zero, $\sum_i \sigma_i = o$. The sum is negative for a dissipative system, implying phase space contraction. A positive Lyapunov characteristic exponent signals the transition to chaotic behaviour. The signature of the Lyapunov characteristic exponents provides a classification scheme for

attractors [22]. For example,

(-,-,-,-) fixed point

(o,-,-,-) periodic motion

(o,o,o,-) quasiperiodic motion on a torus

(+,0,-,-) chaos

(+,+,o,-) superchaos

Lyapunov exponents can be defined for maps as well:

$$\sigma_i^{map} = \lim_{n \to \infty} \ell n(M_i(n)) \qquad (1.22)$$

with $M = \frac{\partial f}{\partial x}$, the Jacobian of the map. Here $M_i(n)$ is defined by the eigenvalues of the product of the Jacobian matrices at the nth iterate. The sum of Lyapunov exponents also represents the average information lost by the system in unit time. The computation of the largest Lyapunov exponent has been used as a tool for the dynamic characterisation of chaos in dissipative systems.

f-α Spectrum

Fractal objects are seen to appear in a variety of applications [23-32] and in particular, occur in the context of chaotic dynamical systems [33-37]. The concept of a fractal object was explicitly formulated and made popular in various scientific disciplines in recent years by Mandelbrot [30]. Fractals are complicated objects

exhibiting self-similar scaling properties. The most basic
property of an attractor is considered to be its dimension.

The singular measures associated with most fractals
are described by a hierarchy of different dimensions, D_q,
referred to earlier as higher order dimensions, giving a
measure of the inhomogenity in the distribution of points
on the attractor. These more complex objects are called
multifractals. By multifractality we mean that points
corresponding to a given type of singularity typically form
a fractal set, whose dimension depends on the type of
singularity. Put differently, multifractals are sets, with
an interwoven family of different fractal sets $s(\alpha)$, on which
the measure has a singularity of type α. To characterise
the global scaling characteristics of these sets, a conti-
nuous spectrum of scaling indices [22,37,38] has been
proposed. The spectra display a range of scaling indices
and their singularities in the set.

The fractal dimension defined through equation (1.8)
takes into account only the geometrical self-similarity of
the attractor. To distinguish this from the more general
statistical self-similarity, we define $d\mu(x)$ as the
normalised invariant measure on the attractor. Then the
probability associated with the ith box of volume ℓ^d, con-
sidering d-dimensional hypercubes of size ℓ put on a

fractal, is

$$P_i = \int_{ith\ box} d\mu(\vec{x}) \qquad\qquad (1.23)$$

with $\sum\limits_{i} P_i = 1$

For a uniform fractal of dimension D, with a uniform dis-
tribution on it $P_i(\epsilon) \sim \epsilon^D$, where ϵ is the fraction $\frac{\ell}{L}$ with
L being the total linear size. When a non-uniform fractal
with distribution having infinitely many singularities is
considered, the probability $P(\epsilon)$ of finding a point in a
box of fractional size ϵ scales as

$$P(\epsilon) \sim \epsilon^{\alpha} \qquad\qquad (1.24)$$

where $\epsilon \ll 1$, and α corresponds to the strength of the local
singularity of the measure and can take a range of values
depending on the given region of the measure. The number
of boxes with the same singularity scales with

$$N_\alpha(\epsilon) \sim \epsilon^{-f(\alpha)} \qquad\qquad (1.25)$$

$f(\alpha)$ is the fractal dimension of the subset of boxes
characterised by the exponent α. The exponent α falls in
the interval $[\alpha_{min}, \alpha_{max}]$, and $f(\alpha)$ is usually a single
humped function with a maximum:

$$\max_{\alpha} f(\alpha) = D_o \qquad\qquad (1.26)$$

To characterise the distribution of singularities, we divide the portion of the space occupied by the attractor into boxes of size ϵ and compute for each box i, the probabaility $P_i(\epsilon)$ that a point sampled according to the invariant measure $d\mu(x)$ belongs to the ith box. Then the moments of the distribution $P_i(\epsilon)$ are

$$M_q(\epsilon) = \sum_i P_i(\epsilon)^q \qquad (1.27)$$

for $-\infty < q < \infty$. For $q = o$

$$M_o(\epsilon) = N(\epsilon) \sim \epsilon^{-D_o} \qquad (1.28)$$

On account of the complexity of multifractal distributions, the scaling of $M_q(\epsilon)$ for $\epsilon \to o$ is of the following pattern:

$$M_q(\epsilon) \sim \epsilon^{(q-1) D_q} \qquad (1.29)$$

where D_q is the qth order generalised dimension. The factor $(q-1)$ is chosen in the exponent so that $M_1(\epsilon) = 1$. Correspondingly, $D_q > o$ for all q and D_q monotonically decreases with increasing q. For uniform fractals all the D_qs are equal to D.

For nonuniform distributions, we collect points of singularity lying between α and $\alpha + d\alpha$ into a subset Λ_α; the fractal dimension of this subset is f_q. That is, the number of boxes scales like

$$N_q(\epsilon) \sim \epsilon^{-f_q} \qquad (1.30)$$

and the probability

$$P_q \sim \epsilon^{\alpha_q} \qquad (1.31)$$

for $\epsilon \to 0$, the f_q and α_q defined by (1.30) and (1.31) provide an alternative description of fractal measures with regard to (1.25) and (1.24) and $f_0 > f_q$ for $q \neq 0$. f_q as a function of growing q increases upto D and then decreases monotonically, while α_q for growing q is a monotonically decreasing one with q, since the dominant contribution comes from boxes with greater probability.

Taking $M_q(\epsilon)$ as

$$M_q(\epsilon) \simeq N_q(\epsilon) \, P_q^{\,q} \qquad (1.32)$$

and grouping together boxes with the same singularity we have,

$$M_q(\epsilon) \sim \int_{\alpha_\infty}^{\alpha_{-\infty}} \epsilon^{(q\alpha' - f(\alpha'))} d\alpha' \qquad (1.33)$$

For $\epsilon \ll 1$, the principal contribution to the integral would be from the value of α that minimises the exponent. Hence we introduce the minimising conditions to yield

$$\left. \frac{df(\alpha)}{d\alpha} \right|_{\alpha_q} = q \qquad (1.34)$$

with α_q the value that corresponds to the minimum of $q\alpha - f(\alpha)$. As is evident from (1.31), (1.30) and (1.32) we have

$$(q-1) \ D_q = q \ \alpha_q - f_q \tag{1.35}$$

Since $\alpha_q = \alpha(q)$

and $f_q = f(\alpha(q))$ we have

$$D_q = \frac{1}{(q-1)} (q \ \alpha(q) - f(\alpha(q))) \tag{1.36}$$

or

$$\tau_q = (q-1)D_q = q \ \alpha(q) - f(\alpha(q)) \tag{1.37}$$
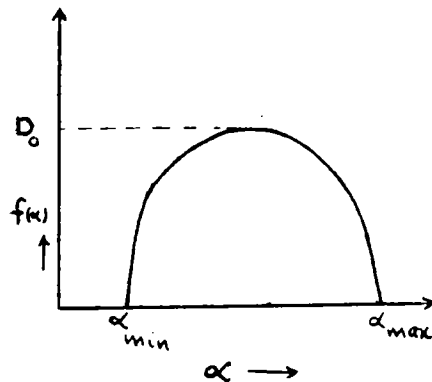
Alternatively we are led to

$$\alpha_q = \alpha \ (q) = \frac{d}{dq} \ (q-1) \ D_q \tag{1.38}$$

At $q=1$ we have the information dimension D_1:

$$D_1 = \alpha_1 = f_1 \quad \text{or} \quad D_1 = \alpha(1) = f(1) \tag{1.39}$$

A distribution with $D_1 < D$, is necessarily a fractal measure. A typical f-α curve is shown below.

The properties of the f-α curve are:

(1) f is a convex function, as $f'' < 0$.

(2) $f(\alpha)$ is monotone increasing for $q > 0$ and decreasing for $q < 0$, since $\dfrac{df}{d\alpha} = q$.

(3) $D_o = f(\alpha(q))\big|_{q=0}$ occurs at the maximum point of the f-α curve.

(4) $f(\alpha)$ curve intersects the bisector $f = \alpha$ at $q = 1$ where the relation $D_1 = \alpha(1) = f(\alpha(1))$ holds.

(5) If the $f(\alpha)$ curve intersects the α-axis, then it intersects vertically at α_∞ and $\alpha_{-\infty}$ since $\dfrac{df}{d\alpha} = \pm\infty$ at $q = \pm\infty$.

Graphically we can determine D_q as follows: Draw a straight line of slope q, $y = q\alpha + b$, and make it to have contact with the $f(\alpha)$ curve at point C which determines $\alpha(q)$ and the corresponding $f(\alpha(q))$ with $b = f(\alpha(q)) - q\alpha(q)$. Hence

$$y = f(\alpha(q)) + q(\alpha - \alpha(q))$$

This line intersects the bisector at the point G with the same $\bar{\alpha}$ for both y and α. This gives

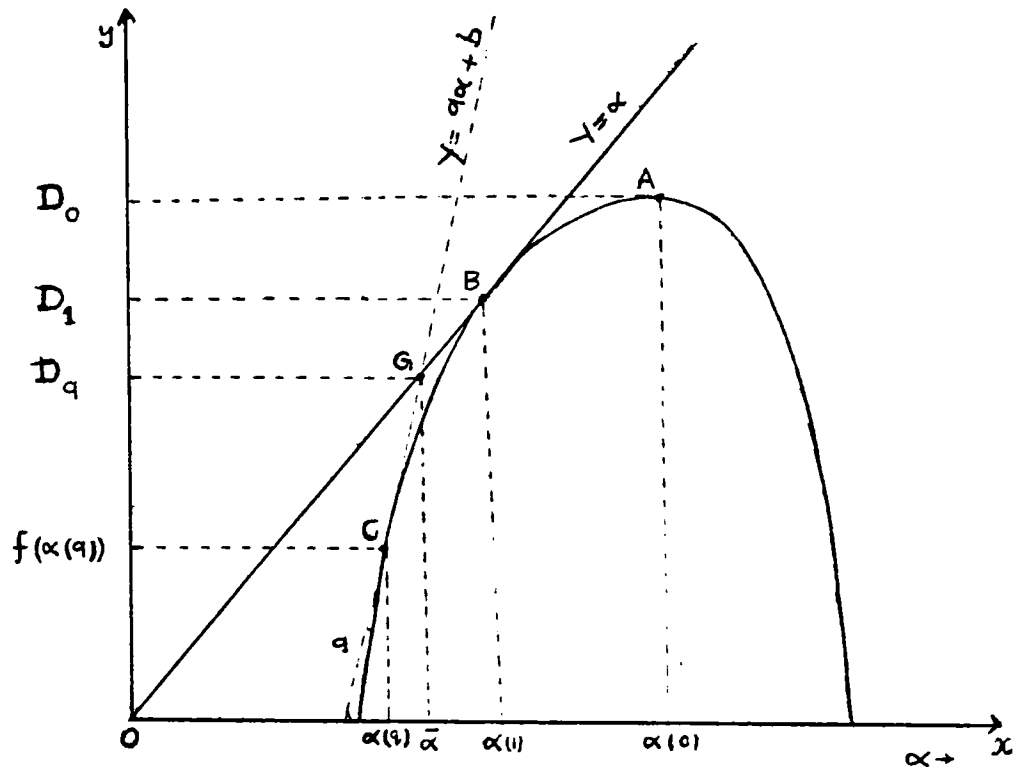$$\bar{\alpha} = f(\alpha(q)) + q(\bar{\alpha} - \alpha(q)).$$

Solving for $\bar{\alpha}$, one finds D_q as

$$\bar{\alpha} = D_q = \frac{1}{(q-1)}\,(q\alpha(q) - f(\alpha(q))),$$

the height of its intersection with the bisector.

For simple fractals it follows that

$$D_q = \alpha = f(\alpha), \quad \forall_q \qquad (1.40)$$

1.4 Universality Property of One Hump Maps

One hump maps are relations of the form

$x_{n+1} = f_\lambda(x_n) = 1 - \lambda|x_n|^z$ with the control parameter λ driving the system to various regimes from periodic to aperiodic ones and z denotes the different universality classes. Such maps are called maps of an interval onto itself [40,48]. This is because, if we take x_n from a finite interval I, then the iterate x_{n+1} belongs to the same interval. That is, the function f maps the interval I into itself. Also the function f is noninvertible, since

given x_{n+1}, one cannot solve $x_{n+1} = f(x_n)$ for x_n.

In the study of 1-d maps, [23,49-54] we are basically interested in the eventual behaviour of iterates of the map for a given initial point x_o. The iterates eventually tend to x^*; then x^* is a fixed point of the map

$$x^* = f_\lambda (x^*) \tag{1.41}$$

Suppose, we start from a nearby point

$$x_o = x^* + \epsilon_o \tag{1.42}$$

with $|\epsilon_o| \ll 1$

Then

$$x_{n+1} = f_\lambda (x_n) = x^* + \epsilon_n \tag{1.43}$$

if $\epsilon_o, \epsilon_1 \ldots \epsilon_n$ converge to zero, then x^* is stable against small perturbations. We have

$$f(x^* + \epsilon_{n-1}) = f(x^*) + f'(x^*) \epsilon_{n-1} + O(\epsilon_{n-1}^2) \tag{1.44}$$

In linear stability analysis, we retain terms upto the first order in the expansion. Thus

$$x^* + \epsilon_n = x^* + f'(x^*) \epsilon_{n-1} \tag{1.45}$$

or

$$\epsilon_n = f'(x^*) \epsilon_{n-1} = f'^n(x^*) \epsilon_o \tag{1.46}$$

The iterates of ϵ_o die away if $|f'(x^*)| < 1$. In other words, the fixed point x^* is stable at $\lambda = \lambda_o$ if

$$-1 < f'_{\lambda_0}(x_0) < 1 \qquad\qquad (1.47)$$

The most favourable case for stability occurs when $|f'(x^*)| = o$. This is called a superstable point. On the other hand, the stability is marginal if $|f'(x^*)|=1$. This point corresponds to the bifrucation point where x^* becomes unstable and two new fixed points x_1^* and x_2^* arise as λ exceeds the limit associated with the fixed point x^*. The process by which this transition occurs is period-doubling. These points satisfy,

$$x_1^* = f_\lambda(x_2^*) \qquad\qquad (1.48)$$

$$x_2^* = f_\lambda(x_1^*) \qquad\qquad (1.49)$$

The stability condition for a 2-cycle is

$$\left| \frac{d}{dx} f^2(\lambda; x) \right|_{x=x_1^*} < 1 \qquad\qquad (1.50)$$

ie

$$\left| f'_\lambda(f_\lambda(x_1^*) \, f'_\lambda(x_2^*)) \right| = \left| f'_\lambda(x_2^*) f'_\lambda(x_1^*) \right| < 1 \qquad (1.51)$$

Generalising this equation to hold for the stability for a period-p cycle with cycle elements x_1^*, x_2^*, ... x_p^* we have

$$f_\lambda^{p\,\prime}(x_i^*) = \prod_{i=1}^{p} f'_\lambda(x_i^*) \qquad\qquad (1.52)$$

The stability of the cycle is determined by the condition

$$- 1 < \prod_{i=1}^{p} f'_\lambda(x_i^*) < 1 \qquad (1.53)$$

One hump maps are found to possess stable periodic cycles of all periodicities for finite intervals of the control parameter. A given periodic cycle may have several stability zones. In determining the occurrence of a periodic p cycle , the solution of the equation $f_\lambda^p(x^*) = x^*$, presents difficulty. A qualitative geometrical analysis is often resorted to for this purpose. In this approach the function $f_\lambda(x)$ is plotted against x at the required parameter value and a line y=x with unit slope is drawn through the origin. For a given x_0 , the iterates are obtained by repeatedly drawing line segments vertically from the y = x line to the map and then hori-zontally from the map to the y=x line. Thus iterations are found by passing from the map to the y=x line, in a successive manner. While considering higher periodic cycles 2^n of the map, it is necessary to take higher iterates of the map. That is, f^{2^n} should be plotted against n. Then each point of the 2^n cycle becomes a fixed point of f at some suitable value of λ, which is a 2^n cycle for the original map. The chaotic regime starts at the accumulation point of this bifurcation and ends at the largest parameter value that the map has. This type of

bifurcation where each stable fixed point, when it becomes unstable, gives rise to two new fixed points is a pitchfork bifurcation.

1.5 Tangent bifurcations and intermittency

Beyond the accumulation point λ_∞, different types of behaviour are observed: There are infinitely many periodic windows in the chaotic regime. A periodic window occurs after a stable periodic orbit has been created by a tangent bifurcation. In order to get some feeling with regard to tangent bifurcations, consider the creation of a period-3 window at $\lambda = \lambda_3$. The third iterate of the one hump map has 7 extrema, of which three are tangent to the bisector $y = x$. For $\lambda > \lambda_3$, $f^3(x)$ passes through the line producing three pairs of new fixed points, of which three are stable and three unstable. These periodic orbits with period p undergo period-doubling producing subharmonic sequences $p.2^k$, leading to an aperiodic regime at λ_{p_∞}. For $\lambda < \lambda_3$ the map tends to chaos via intermittency which occurs towards the left end of the periodic window, while period-doubling leading to chaos occurs at the right end of the window. The periodic interval decreases as we move away from λ_3 and time of chaotic interval increases.

In addition, there exist parameter values, for which 2^k disjoint sub intervals open inside the chaotic region. These disjoint intervals, called chaotic bands, are periodically visited by the iterates, the motion inside being chaotic. These bands follow an inverse bifurcation sequence ending at λ_∞ from above with an infinite number of single orbits.

So far we assumed that period-doubling bifurcations and tangent bifurcations with the associated intermittency are the only possible phenomena responsible for the interesting changes resulting from the tuning of the parameter. Apart from these, it was found numerically that there are some sudden changes called crisis that occur due to the collision of the unstable fixed point with a chaotic attractor [46,55], as a system parameter reaches a critical value. This phenomenon has been observed in a number of experimental systems [56-57]. Crisis is connected with fast qualitative variation of the chaotic regime. Boundary crisis leads to the sudden disappearance of a chaotic attractor. As a result of internal crisis the size and attractor regions of the stochastic attractor suddenly vary.

1.6 Feigenbaum universality and renormalisation group approach

Universality is of two kinds: structural and metric.

The universal property that depends on there being only one local maximum, but not on the nature of the maximum is called structural universality [47]. Close to the local maximum $x = x_c$, if the nonlinear function f can be expanded in the form,

$$f(x) = f_{max} - A(x-x_c)^z + \ldots \tag{1.54}$$

those properties which are shared by maps with one and the same value of z, characterise metric universality. Feigenbaum established that the values of the scaling indices α and δ are universal in the sense that they are independent of the details of the map, but depend only on the order of the local maximum z [8,9].

It was found that universal features reside in the chaotic region as well [46,58]. For $\lambda > \lambda_\infty$ the attractor is composed of chaotic bands, which undergo a sequence of reverse bifurcations or band mergings. At each point of reverse sequence, band splitting occurs. The associated scaling goes as:

$$\bar{\lambda}_k - \lambda_{k;\,q} = C\,\delta^{-k}\gamma^{-q}$$

and
$$\lambda_{k;\,q} - \lambda_\infty = (A - C\gamma^{-q})\,\delta^{-k} \tag{1.55}$$

with $\bar{\lambda}_k$ the parameter value at which the band merging takes place. The value of γ is a universal number for the same universality class and for $z = 2$ it is found to be

$\gamma = 2.94805$. The statement (1.55) is a two fold scaling law. That is, for fixed period q, the doubling of fundamental orbits ie $q^{2^{k-1}} - q^{2^k}$ follows the rate δ, while for fixed $k, q^{2^k} - (q+1)^{2^k}$ follows the rate γ.

Associated with the reverse multifurcation sequence are the two universal scaling constants ψ and Θ defined by [58],

$$\psi = \lim_{k \to \infty} \frac{\lambda_\infty - \lambda_k}{\lambda_\infty - \bar{\lambda}_k} \tag{1.56}$$

$$\Theta = \lim_{k \to \infty} \frac{\lambda_{k+1} - \lambda_k}{\bar{\lambda}_{k+1} - \lambda_k} \tag{1.57}$$

where $\{\bar{\lambda}_k\}$ is the sequence of superstable 2^k cycles, convergent to λ_∞ from below. Furthermore, from ψ and Θ a universal constant may be defined:

$$\frac{\Theta}{\psi} = \lim_{k \to \infty} \frac{\lambda_{k+1} - \lambda_k}{\bar{\lambda}_{k+1} - \lambda_k} \tag{1.58}$$

may be found which does not depend on the reverse sequence at all. For $z = 2$, ψ and Θ have the values $\Theta = -0.31731$ and $\psi = -0.18781$.

The renormalisation group (RG) technique is a powerful mathematical technique used in problems having scaling properties. The notions of universality and scaling

invariance associated with the period-doubling sequence in one dimensional maps [8,60-64] invites the technique of RG. Below we briefly discuss the main steps involved in this approach.

In the RG approach, successive bifurcations are mapped to the preceeding ones by a change in scale of the physical variable and control parameter. We define a function space with $x_c = 0$ and $f(x_c) = 1$, for all maps which belong to the same universality class, characterised by the scaling exponents α and δ. The transformations under the RG, in the period-doubling sequence with periodic cycles of period 2^n, are: (1) repeatedly constructing the map with itself, (2) restricting to an appropriate domain, (3) and changing the coordinates to magnify the subdomain to the original domain.

These transformations are carried out by the doubling operator T defined by

$$Tf(\lambda_n; x) = -\alpha f(\lambda_{n+1}; f(\lambda_{n+1}, \frac{x}{-\alpha})) \qquad (1.59)$$

$$T^2 f(\lambda_n; x) = (-\alpha)^2 f^2(\lambda_{n+2}; f^2(\lambda_{n+2}; \frac{x}{(-\alpha)^2})) \qquad (1.60)$$

Repeated compositions and rescalings lead to a limit that is independent of the starting function f:

$$\lim_{k \to \infty} (-\alpha)^k f^{2^k}(\lambda_{n+k}; \frac{x}{(-\alpha)^k}) = g(x) \qquad (1.61)$$

From the composition law

$$f^n(\lambda; x) = f(\lambda; f(\lambda, \ldots f(\lambda; x))) \qquad (1.63)$$

of f^n we have

$$f^{2^k}(\lambda_{n+k}; \frac{x}{(-\alpha)^k}) = f^{2^{k-1}}(\lambda_{n+k}; f^{2^{k-1}}(\lambda_{n+k}; \frac{x}{(-\alpha)^k}))$$

$$(1.63)$$

Taking the $k \to \infty$, limit on both sides of the last equation results in the RG equation of Feigenbaum [9]:

$$g(x) = -\alpha g(g(\frac{x}{-\alpha})) \qquad (1.64)$$

with the restriction $g(o) = 1$, $g'(o) = o$.

The Feigenbaum RG equation given by (1.64) determines a fixed point $g(x)$ in the function space of all unimodal maps giving α:

$$\alpha = \frac{-1}{g(1)} \qquad (1.65)$$

Thus by introducing the fixed point function $g(x)$ through the RG transformation we have transformed the original

fixed point problem for a unimodal function to a fixed point problem in the space of all possible unimodal functions. The fixed function $g(x)$ is a saddle type fixed point in the function space of unimodal functions. The structure of T is such that it maps functions with a 2^{n+1} superstable cycle to that with 2^n superstable cycle. T is unstable only in one direction $h(x)$ corresponding to the unstable separatrix. Along other directions, the iterates tend to the fixed point function.

Considering small perturbations around $g(x)$ we have,

$$g_i(x) = g(x) + \mu_i h(x) \qquad (1.66)$$

Then using (1.64) and expanding to first order about $g(x)$ we obtain

$$g_{i-1}(x) = -\alpha g(g(x/\alpha) + \mu_i h(x/\alpha)$$

$$= -\alpha [\quad g(g(x/\alpha)) + \mu_i g(h(x/\alpha)) \qquad (1.67)$$

$$+ \mu_i g' (g(x/\alpha))h(x/\alpha) + 0 (\mu_i^2) + ...]$$

Substituting from (1.66) we have

$$g(x) + \mu_{i-1} h(x) = g(x) - \alpha\mu_i [g(h(x/\alpha)) + g'(g(x/\alpha))$$

$$h(x/\alpha)] \qquad (1.68)$$

Taking the limit $i \to o$, $\mu_i \to o$,

$$\mu_i = \frac{1}{\delta^i} \text{ with } \delta > 1 \qquad (1.69)$$

Hence

$$h(x) = \frac{-\alpha}{\delta} [h(g(x/\alpha)) + g'(g(x/\alpha)) h(x/\alpha)] \qquad (1.70)$$

which is the eigenvalue equation for δ in the function space.   Thus we have a nonlinear functional equation (1.64), the eigenvalue of which gives the scale factor α.   Its linearisation has led to an eigenvalue equation with eigenvalue δ.

CHAPTER II

PADÉ IMPROVED CALCULATION OF α and δ
VALUES OF ONE HUMP MAPS

2.1 Introduction

The one dimensional iterative map forms the
simplest deterministic system which gives rise to
chaotic behaviour. It also reveals many interest-
ing phenomena as the system becomes chaotic. In
addition to its rich structure, the iterative map
also appears naturally in many branches of physics
such as condensed matter physics [82, 106],fluid
dynamics [4], accelerator physics [3] etc. Feigen-
baum made the important discovery that all single
hump one dimensional maps with quadratic maxima
have the same universal behaviour near the infinite
bifurcation limit characterised by the scale factors
α and δ that are related through the functional
renormalisation group equations (1.64) and (1.70)
[8,9]. For any map, the evaluation of α and δ is
necessary to decide to which universality class the
map belongs. Several numerical procedures were
reported for the evaluation of these constants [63-67].
The usual method is to expand the universal function
$\overline{g}(x)$ into a power series and iterate it using renor-
malisation group equations until the coefficients

repeat. This method being purely numerical in nature, lacks good convergence and leads to errors. An analytic attempt in this direction was made by Virendra Singh using a perturbative approach [68] and further developed in ref. [69].

Eventhough the perturbative method is understood to be a good analytical tool, still better convergence to the results can be attained by employing Padé approximants [70] in the asymptotic series expansions. Detailed calculations for different orders of accuracy have been carried out for quadratic, quartic and sextic cases and the results are herein reported.

2.2 Perturbative scheme

We start with a résumé of the perturbative method [45,46] which aims at analytically solving the functional renormalisation group equations (1.64) and (1.70). Here α is determined by the functional equation

$$g(x) = - \alpha g(g(x/\alpha)) \qquad (2.1)$$

while δ is given by

$$- \alpha [g'(g(x))h(x) + h g(x)] = \delta h(\alpha x) \qquad (2.2)$$

Both $g(x)$ and $h(x)$ are expanded into power series in $|x|^z$ where z is the order of the local maximum of the map.

Then

$$g(x) = 1 + \sum_{n=1}^{\infty} P_n |x|^{nz} \qquad (2.3)$$

subject to the normalisation

$$g(o) = 1 \text{ and } g'(o) = o$$

$g(x)$ and α do, of course, depend on the order of the local maximum. In the neighbourhood of the extremum at $x = o$, $g(x)$ is positive for any z and so $g(g(x))$ can also be expanded into a similar power series:

$$g(g(x)) = 1 + \sum_{r=1}^{\infty} P_r + \left(P_1 \sum_{r=1}^{\infty} rz P_r\right) |x|^z$$

$$+ \left(P_2 \sum_{r=1}^{\infty} rz\, P_r + P_1^2 \sum_{r=1}^{\infty} \frac{rz(rz-1)}{2!} P_r\right) |x|^{2z}$$

$$+ \dots \qquad (2.4)$$

The perturbative method depends on the proper redefinition of the coefficients P_n:

$$P_n = \frac{S_n |\alpha|^z}{\alpha^n} \qquad (2.5)$$

Equations (2.3) and (2.4) are written in terms of the redefined coefficients S_n. Substituting in (2.1) and equating like powers of x on both sides of the resulting equation we get

$$\frac{1}{\alpha} + 1 + |\alpha|^{z} \sum_{r=1}^{\infty} \frac{S_r}{\alpha^r} = 0 \tag{2.6}$$

$$\frac{1}{z} + \sum_{r=1}^{\infty} \frac{r S_r}{\alpha^{r-1}} = 0 \tag{2.7}$$

and

$$S_n \left[1 - \frac{1}{|\alpha|^{z(n-1)}} \right] + \sum_{\ell \geqslant 2}^{n} \sum_{r \geqslant 1}^{\infty} \binom{rz}{\ell} \frac{S_r}{\alpha^{r-1}}$$

$$x \sum_{m_1 \geqslant 1, m_2 \geqslant 1 \ldots m_\ell \geqslant 1} \frac{S_{m_1} S_{m_2} S_{m_3} \ldots S_{m_\ell} \delta_{m_1 + m_2 \cdots m_\ell, n}}{|\alpha|^{z(n-\ell)}}$$

$$= 0 \; (\text{for } n = 2,3,4 \ldots) \tag{2.8}$$

These equations, however, are highly nonlinear and coupled, and to solve these equations, the coefficients S_n are expanded in inverse powers of α:

$$S_n(\alpha) = \sum_{m=0}^{\infty} \frac{S_{nm}}{\alpha^m} \tag{2.9}$$

Substituting this expansion in (2.7) and (2.8) and equating like powers of $\frac{1}{\alpha}$ we arrive at the following set of equations:

$$S_{10} = -1/z;$$

$$S_{11} + 2S_{20} = 0;$$

$$S_{12} + 2S_{21} + 3S_{30} = 0;$$

$$S_{13} + 2S_{22} + 3S_{31} + 4S_{40} = 0;$$

$$S_{14} + 2S_{23} + 3S_{32} + 4S_{41} + 5S_{50} = 0;$$

$$S_{15} + 2S_{24} + 3S_{33} + 4S_{42} + 5S_{51} + 6S_{60} = 0;$$

$$S_{16} + 2S_{25} + 3S_{34} + 4S_{43} + 5S_{52} + 6S_{61} + 7S_{70} = 0;$$

(for n = 1)

$$S_{20} + \frac{z(z-1)}{2!} S_{10}^3 = 0;$$

$$S_{21} + \frac{z(z-1)}{2!} 3S_{10}^2 S_{11} + \frac{2z(2z-1)}{2!} S_{20} S_{10}^2 = 0;$$

$$S_{22} + \frac{z(z-1)}{2!} (3S_{10}^2 S_{12} + 3S_{10} S_{11}^2) + \frac{2z(2z-1)}{2!}$$

$$\times (S_{10}^2 S_{21} + 2S_{20} S_{11} S_{10}) + \frac{3z(3z-1)}{2!} S_{30} S_{10}^2 = 0;$$

$$S_{23} + \frac{z(z-1)}{2!} (3S_{10}^2 S_{13} + 6S_{10} S_{11} S_{12} + S_{11}^3) + \frac{2z(2z-1)}{2!}$$

$$\times (2S_{20} S_{10} S_{12} + S_{20} S_{11}^2 + 2S_{21} S_{10} S_{11} + S_{22} S_{10}^2)$$

$$+ \frac{3z(3z-1)}{2!} (S_{10}^2 S_{31} + 2S_{30} S_{10} S_{11}) + \frac{4z(4z-1)}{2!} S_{40} S_{10}^2 = 0;$$

$$S_{24} - S_{20} + \frac{z(z-1)}{2!}(3S_{10}^2 S_{14} + 6S_{10}S_{11}S_{13} + 3S_{10}S_{12}^2 + 3S_{11}^2 S_{12})$$

$$+ \frac{2z(2z-1)}{2!}(2S_{20}S_{10}S_{13} + 2S_{20}S_{11}S_{12} + 2S_{21}S_{10}S_{12} + S_{21}S_{11}^2$$

$$+ 2S_{22}S_{10}S_{11} + S_{23}S_{10}^2) + \frac{3z(3z-1)}{2!}(2S_{31}S_{10}S_{11} + S_{30}S_{11}^2$$

$$+ S_{32}S_{10}^2 + 2S_{30}S_{10}S_{12}) + \frac{4z(4z-1)}{2!}(2S_{40}S_{10}S_{11} + S_{41}S_{10}^2)$$

$$+ \frac{5z(5z-1)}{2!} S_{50}S_{10}^2 = 0;$$

$$S_{25} - S_{21} + \frac{z(z-1)}{2!}(3S_{10}^2 S_{15} + 6S_{10}S_{11}S_{14} + 3S_{11}^2 S_{13} + 6S_{10}S_{12}S_{13}$$

$$+ 3S_{11}S_{12}^2) + \frac{2z(2z-1)}{2!}(2S_{20}S_{10}S_{14} + 2S_{20}S_{11}S_{13} + S_{20}S_{12}^2$$

$$+ 2S_{21}S_{10}S_{13} + 2S_{21}S_{11}S_{12} + 2S_{22}S_{10}S_{12} + S_{22}S_{11}^2 + 2S_{23}S_{10}S_{11}$$

$$+ S_{24}S_{10}^2) + \frac{3z(3z-1)}{2!}(2S_{30}S_{10}S_{13} + 2S_{30}S_{11}S_{12} + 2S_{31}S_{10}S_{12}$$

$$+ S_{31}S_{11}^2 + 2S_{32}S_{10}S_{11} + S_{33}S_{10}^2) + \frac{4z(4z-1)}{2!}(2S_{40}S_{10}S_{12}$$

$$+ S_{40}S_{11}^2 + 2S_{41}S_{10}S_{11} + S_{42}S_{10}^2) + \frac{5z(5z-1)}{2!}(2S_{50}S_{10}S_{11}$$

$$+ S_{51}S_{10}^2) + \frac{6z(6z-1)}{2!} S_{60}S_{10}^2 = 0; \qquad \text{(for } n=2\text{)}$$

$$S_{30} + \frac{z(z-1)(z-2)}{3!} S_{10}^4 = 0;$$

$$S_{31} + \frac{z(z-1)(z-2)}{3!} 4S_{10}^3 S_{11} + \frac{2z(2z-1)(2z-2)}{3!} S_{20}S_{10}^3 = 0;$$

$$S_{32} + \frac{z(z-1)(z-2)}{3!}(4S_{10}^3 S_{12} + 6S_{10}^2 S_{11}^2) + \frac{2z(2z-1)(2z-2)}{3!}$$

$$\times (3S_{20}S_{10}^2 S_{11} + S_{21}S_{10}^3) + \frac{3z(3z-1)(3z-2)}{3!}S_{30}S_{10}^3 = 0;$$

$$S_{33} + \frac{z(z-1)(z-2)}{3!}(4S_{10}^3 S_{13} + 12S_{10}^2 S_{11}S_{12} + 4S_{10}S_{11}^3)$$

$$+ \frac{2z(2z-1)(2z-2)}{3!}(3S_{20}S_{10}^2 S_{12} + 3S_{20}S_{10}S_{11}^2 + 3S_{21}S_{10}^2 S_{11}$$

$$+ S_{22}S_{10}^3) + \frac{3z(3z-1)(3z-2)}{3!}(S_{31}S_{10}^3 + 3S_{30}S_{10}^2 S_{11})$$

$$+ \frac{4z(4z-1)(4z-2)}{3!}S_{40}S_{10}^3 = 0;$$

$$S_{34} + \frac{z(z-1)(z-2)}{3!}(4S_{10}^3 S_{14} + 12S_{10}^2 S_{11}S_{13} + 12S_{10}S_{11}^2 S_{12}$$

$$+ 6S_{10}^2 S_{12}^2 + S_{11}^4) + \frac{2z(2z-1)(2z-2)}{3!}(3S_{20}S_{10}^2 S_{13}$$

$$+ 6S_{20}S_{10}S_{11}S_{12} + S_{20}S_{11}^3 + 3S_{21}S_{10}^2 S_{12} + 3S_{21}S_{10}S_{11}^2$$

$$+ 3S_{22}S_{10}^2 S_{11} + S_{23}S_{10}^3) + \frac{3z(3z-1)(3z-2)}{3!}(3S_{30}S_{10}^2 S_{12}$$

$$+ 3S_{30}S_{10}S_{11}^2 + 3S_{31}S_{10}^2 S_{11} + S_{30}S_{10}^3) + \frac{4z(4z-1)(4z-2)}{3!}$$

$$\times (3S_{40}S_{10}^2 S_{11} + S_{41}S_{10}^3) + \frac{5z(5z-1)(5z-2)}{3!}S_{50}S_{10}^3$$

$$+ \frac{z(z-1)}{2!}2S_{20}S_{10}^2 = 0;$$

(for n = 3)

$$S_{40} + \frac{z(z-1)(z-2)(z-3)}{4!}S_{10}^5 = 0;$$

$$S_{41} + \frac{z(z-1)(z-2)(z-3)}{4!}5S_{10}^4 S_{11} + \frac{2z(2z-1)(2z-2)(2z-3)}{4!}S_{20}S_{10}^4 = 0;$$

$$S_{42} + \frac{z(z-1)(z-2)(z-3)}{4!}(5S_{10}^4 S_{12} + 10S_{10}^3 S_{11}^2)$$

$$+ \frac{2z(2z-1)(2z-2)(2z-3)}{4!}(4S_{20}S_{10}^3 S_{11} + S_{21}S_{10}^4)$$

$$+ \frac{3z(3z-1)(3z-2)(3z-3)}{4!}S_{30}S_{10}^4 = 0;$$

$$S_{43} + \frac{z(z-1)(z-2)(z-3)}{4!}(5S_{10}^4 S_{13} + 20S_{10}^3 S_{11}S_{12} + 10S_{10}^2 S_{11}^3)$$

$$+ \frac{2z(2z-1)(2z-2)(2z-3)}{4!}(4S_{20}S_{10}^3 S_{12} + 6S_{20}S_{10}^2 S_{11}^2 + 4S_{21}S_{10}^3 S_{11}$$

$$+ S_{22}S_{10}^4) + \frac{3z(3z-1)(3z-2)(3z-3)}{4!}(4S_{30}S_{10}^3 S_{11} + S_{31}S_{10}^4)$$

$$+ \frac{4z(4z-1)(4z-2)(4z-3)}{4!}S_{40}S_{10}^4 = 0;$$

(for n = 4)

$$S_{50} = 0;$$

$$S_{51} + \frac{2z(2z-1)(2z-2)(2z-3)(2z-4)}{5!}S_{20}S_{10}^5 = 0;$$

$$S_{52} + \frac{2z(2z-1)(2z-2)(2z-3)(2z-4)}{5!}(5S_{10}^4 S_{11}S_{20} + S_{21}S_{10}^5)$$

$$+ \frac{3z(3z-1)(3z-2)(3z-3)(3z-4)}{5!}S_{30}S_{10}^5 = 0;$$

(for n = 5)

$$S_{60} = 0;$$

$$S_{61} + \frac{2z(2z-1)(2z-2)(2z-3)(2z-4)(2z-5)}{6!}S_{20}S_{10}^6 = 0;$$

(for n = 6)

Using these coefficients we can solve the equation for α:

$$\frac{1}{\alpha} + 1 + \alpha^z \sum_{r=1}^{\infty}\sum_{m=0}^{\infty}\frac{S_{rm}}{\alpha^{r+m}} = 0 \qquad (2.10)$$

To evaluate δ, we start from the functional renormalisation group equation (2.2). Then the function h(x) is also expanded into a power series in $|x|^z$:

$$h(x) = 1 + \sum_{n=1}^{\infty} h_n |x|^{nz} \qquad (2.11)$$

Using this along with (2.3) and (2.4), and equating coefficients of $|x|^{nz}$, a system of equations to be solved for δ [72] is obtained:

$$- \alpha \left[1 + \sum_{r \geqslant 1}^{\infty} h_r + |\alpha|^z \sum_{r \geqslant 1}^{\infty} \frac{rz S_r}{\alpha^r} \right] = \delta, \qquad (2.12)$$

$$- \alpha \left[\sum_{r \geqslant 1}^{\infty} \binom{rz}{1} h_r \frac{S_1}{\alpha} + \sum_{r \geqslant 1}^{\infty} 2 \binom{rz}{2} \frac{|\alpha|^{z-1} S_r S_1}{\alpha^r} \right.$$

$$\left. + h_1 \sum_{r \geqslant 1}^{\infty} \binom{rz}{1} \frac{S_r}{\alpha^r} \right] = \delta h_1, \quad \text{(for } n = 1\text{)} \qquad (2.13)$$

$$- \alpha \left[\sum_{\ell \geqslant 1}^{n} \sum_{r \geqslant 1}^{\infty} \left(\binom{rz}{\ell} \frac{h_r}{\alpha^n} + (\ell+1) \binom{rz}{\ell+1} \frac{S_r}{\alpha^{n-z+r}} \right) \right.$$

$$\times \sum_{m_1 \geqslant 1, m_2 \geqslant 1, \ldots, m_\ell \geqslant 1} \frac{S_{m_1} S_{m_2} \cdots S_{m_\ell}}{\alpha^{z(n-\ell)}} \delta_{m_1 + m_2 + \cdots m_\ell, n}$$

$$+ \sum_{n' \geqslant 1}^{n-1} \sum_{\ell \geqslant 1}^{n-n'} \sum_{r \geqslant 1}^{\infty} \left(h_{n'}(\ell+1) \binom{rz}{\ell+1} \frac{S_r}{\alpha^{n-n'-z+r}} \right)$$

$$\times \sum_{m_1 \geqslant 1, m_2 \geqslant 1, \ldots m_\ell \geqslant 1} \frac{S_{m_1} S_{m_2} \cdots S_{m_\ell}}{\alpha^{z(n-\ell)}} \delta_{m_1 + m_2 + \cdots m_\ell, n'}$$

$$+ h_n \sum_{r \geqslant 1}^{\infty} \frac{rzS_r}{\alpha^{r+(n-1)z}} \Bigg] = \delta h_n \text{ (for } n=2,3,4\ldots) \qquad (2.14)$$

The above set of equations can be cast into the form of a matrix eigenvalue equation

$$D\ h = \delta h \qquad\qquad (2.15)$$

where h is the column matrix $[1,h_1,h_2\ldots]$. The largest real eigenvalue of the coefficient matrix D furnishes the relevant δ.

Using the already determined S_{nm} coefficients, a few elements of the D matrix in the equation for δ in (2.15) for general z are given below.

$$D_{11} = - \Bigg[\alpha + z\alpha^z \Big\{ S_{10} + \frac{1}{\alpha}(S_{11}+2S_{20}) + \frac{1}{\alpha^2}(S_{12}+2S_{21}+3S_{30})$$

$$+ \frac{1}{\alpha^3}(S_{13}+2S_{22}+3S_{31}+4S_{40}) + \frac{1}{\alpha^4}(S_{14}+2S_{23}+3S_{32}$$

$$+ 4S_{41}+5S_{50}) + \frac{1}{\alpha^5}(S_{15}+2S_{24}+3S_{33}+4S_{42}+5S_{51}+6S_{60})$$

$$+ \frac{1}{\alpha^6}(S_{16}+2S_{25}+3S_{34}+4S_{43}+5S_{52}+6S_{61}+7S_{70}) \Big\} \Bigg] ,$$

$$D_{12} = - \alpha,$$

$$D_{13} = - \alpha,$$

$$D_{14} = - \alpha,$$

$$D_{21} = -z\alpha^{z-1}\left[(z-1)S_{10}^2 + \frac{1}{\alpha}\left\{(z-1)2S_{10}S_{11} + (2z-1)\right.\right.$$

$$\left.\times 2S_{20}S_{10}\right\} + \frac{1}{\alpha^2}\left\{(z-1)(2S_{10}S_{12}+S_{11}^2)+(2z-1)\right.$$

$$\left.\times (2S_{20}S_{11}+2S_{10}S_{21}) + (3z-1)3S_{30}S_{10}\right\}$$

$$+ \frac{1}{\alpha^3}\left\{(z-1)(2S_{10}S_{13}+2S_{11}S_{12})+(2z-1)\right.$$

$$\times (2S_{12}S_{20}+2S_{21}S_{11}+2S_{22}S_{10})+(3z-1)$$

$$\left.\times (3S_{30}S_{11}+3S_{31}S_{10})+(4z-1)4S_{40}S_{10}\right\}+ \frac{1}{\alpha^4}$$

$$\times\left\{(z-1)(2S_{10}S_{14}+2S_{11}S_{13}+S_{12}^2)+(2z-1)\right.$$

$$\times (2S_{20}S_{13}+2S_{21}S_{12}+2S_{22}S_{11}+2S_{23}S_{10})$$

$$+ (3z-1)(3S_{30}S_{12}+3S_{31}S_{11}+3S_{32}S_{10})+(4z-1)$$

$$\left.\left.\times 4\quad (S_{40}S_{11}+S_{41}S_{10})+(5z-1)(5S_{50}S_{10})\right\}\right] ,$$

$$D_{22} = -z\left[2S_{10}+ \frac{1}{\alpha}(2S_{11}+2S_{20})+\frac{1}{\alpha^2}(2S_{12}+2S_{21}+3S_{30})\right] ,$$

$$D_{23} = -2z\left[S_{10}+ \frac{S_{11}}{\alpha}+ \frac{S_{12}}{\alpha^2}\right] ,$$

$$D_{24} = -3z\left[S_{10}+ \frac{S_{11}}{\alpha}+\frac{S_{12}}{\alpha^2}\right] ,$$

$$D_{31} = - \frac{z(z-1)}{\alpha^2} S_{20}S_{10}- z\alpha^{z-2}\left[\frac{(z-1)(z-2)}{2!} S_{10}^3+ \frac{1}{\alpha}\right.$$

$$\times\left\{\frac{(z-1)(z-2)}{2!}3S_{10}^2S_{11}+\frac{(2z-1)(2z-2)}{2!} 2S_{20}S_{10}^2\right\}$$

$$+ \frac{1}{\alpha^2}\left\{\frac{(z-1)(z-2)}{2!}(3S_{10}^2 S_{12} + 3S_{10}S_{11}^2)\right.$$

$$+ \frac{(2z-1)(2z-2)}{2!} \times 2 \quad (2S_{20}S_{10}S_{11} + S_{21}S_{10}^2)$$

$$+ \frac{(3z-1)(3z-2)}{2!} 3S_{30}S_{10}^2\bigg\} + \frac{1}{\alpha^3}\left\{\frac{(z-1)(z-2)}{2!}\right.$$

$$\times (3S_{10}^2 S_{13} + 6S_{10}S_{11}S_{12} + S_{11}^3) + \frac{(2z-1)(2z-2)}{2!}$$

$$\times 2 \quad (2S_{20}S_{10}S_{12} + S_{20}S_{11}^2 + 2S_{21}S_{10}S_{11} + S_{22}S_{10}^2)$$

$$+ \frac{(3z-1)(3z-2)}{2!} \times 3 \quad (2S_{30}S_{10}S_{11} + S_{31}S_{10}^2)$$

$$+ \frac{(4z-1)(4z-2)}{2!} 4S_{40}S_{10}^2\bigg\} + \frac{1}{\alpha^4}\left\{\frac{(z-1)(z-2)}{2!}\right.$$

$$\times (3S_{10}^2 S_{14} + 6S_{10}S_{11}S_{13} + 3S_{11}^2 S_{12} + 3S_{10}S_{12}^2)$$

$$+ \frac{(2z-1)(2z-2)}{2!} \times 2 \quad (2S_{20}S_{10}S_{13} + 2S_{20}S_{11}S_{12}$$

$$+ 2S_{21}S_{10}S_{12} + S_{21}S_{11}^2 + 2S_{22}S_{10}S_{11} + S_{23}S_{10}^2)$$

$$+ \frac{(3z-1)(3z-2)}{2!} \times 3 \quad (2S_{30}S_{10}S_{12} + S_{30}S_{11}^2$$

$$+ 2S_{31}S_{10}S_{11} + S_{32}S_{10}^2) + \frac{(4z-1)(4z-2)}{2!} \times 4$$

$$\times (2S_{40}S_{10}S_{11} + S_{41}S_{10}^2) + \frac{(5z-1)(5z-2)}{2!}5S_{50}S_{10}^2\bigg\}\bigg],$$

$$D_{32} = -\bigg[\frac{z(z-1)}{2!} S_{10}^2 + \frac{1}{\alpha}\bigg\{(z-1)zS_{10}^2\bigg\} + \frac{1}{\alpha^2}\bigg\{\frac{z(z-1)}{2!} 2S_{10}S_{11}$$

$$+ z(z-1)2S_{10}S_{11} + 2z(2z-1)S_{20}S_{10}\bigg\}\bigg],$$

$$D_{33} = -\left[\frac{2z(2z-1)S_{10}^2}{2!}\frac{1}{\alpha} + \frac{1}{\alpha^2}\left\{\frac{2z(2z-1)}{2!}2S_{10}S_{11}\right\}\right],$$

$$D_{34} = -\left[\frac{3z(3z-1)}{2!}\left(\frac{S_{10}^2}{\alpha} + \frac{2S_{10}S_{11}}{\alpha^2}\right)\right],$$

$$D_{41} = -z\alpha^{z-2}\left[\frac{(z-1)(z-2)(z-3)S_{10}^4}{3!}\frac{1}{\alpha} + \frac{1}{\alpha^2}\left\{4S_{10}^3S_{11}\right.\right.$$

$$\times \frac{(z-1)(z-2)(z-3)}{3!} + \frac{(2z-1)(2z-2)(2z-3)}{3!}2S_{20}S_{10}^3\right\}$$

$$+ \frac{1}{\alpha^3}\left\{\frac{(z-1)(z-2)(z-3)}{3!}(4S_{10}^3S_{12}+6S_{10}^2S_{11}^2)\right.$$

$$+ \frac{(2z-1)(2z-2)(2z-3)}{3!} \times 2 \; [3S_{20}S_{10}^2S_{11}+S_{21}S_{10}^3]$$

$$+ \frac{(3z-1)(3z-2)(3z-3)}{3!}3S_{30}S_{10}^3\right\} + \frac{1}{\alpha^4}\left\{\frac{(z-1)(z-2)(z-3)}{3!}\right.$$

$$\times (4S_{10}^3S_{13}+12S_{10}^2S_{11}S_{12}+4S_{10}S_{11}^3)$$

$$+ \frac{(2z-1)(2z-2)(2z-3)}{3!} \times 2 \; (3S_{20}S_{10}^2S_{12}+3S_{20}S_{10}S_{11}^2$$

$$+ 3S_{21}S_{10}^2S_{11}+S_{22}S_{10}^3) + \frac{(3z-1)(3z-2)(3z-3)}{3!} \times 3$$

$$\times (3S_{30}S_{10}^2S_{11}+S_{31}S_{10}^3) + \frac{(4z-1)(4z-2)(4z-3)}{3!}$$

$$\times 4S_{40}S_{10}^3\left.\right\}\right],$$

$$D_{42} = -\left[\frac{z(z-1)(z-2)S_{10}^3}{3!}\frac{1}{\alpha^2} + \frac{z(z-1)(z-2)S_{10}^3}{2!}\frac{1}{\alpha^{z-2}}\right],$$

$$D_{43} = -\left[\frac{2z(2z-1)(2z-2)}{3!}\frac{S_{10}^3}{\alpha^2}\right],$$

$$D_{44} = -\left[\frac{3z(3z-1)(3z-2)}{3!}S_{10}^3\right].$$

The universal constant δ is identified as the largest D matrix in (15). The S_{nm} coefficients as well as α for quadratic maps were obtained by Singh[71]. The equation for δ was obtained as described above by [72] who evaluated α and δ for a quartic map.

2.3 Padé approximants and their use:

A Padé approximant [70] defined as the ratio of the polynomials constructed from the coefficients of the Taylor series expansion of a function, constitutes a particular type of rational fraction approximation to the value of a function. The [L/M] Padé approximant to a series A(x) is defined by

$$[L|M] = \frac{\sum\limits_{j=0}^{L} P_j (\frac{1}{\alpha})^j}{\sum\limits_{j=0}^{M} Q_j (\frac{1}{\alpha})^j} \qquad (2.16)$$

where $P_L(x)$ is a polynomial of degree atmost L and $Q_M(x)$ a polynomial with degree atmost M, with the normalisation $Q_0=1$. The series $A(x) = \sum\limits_{j} a_j x^j$ determines the coefficients of $P_L(x)$ as $Q_M(x)$. We have for polynomials $P_L(x)$ and $Q_M(x)$

$$P_L(x) = P_0 + P_1 x + \ldots + P_L x^L \qquad (2.17)$$

$$Q_M(x) = 1 + Q_1 x + \ldots + Q_M x^M. \qquad (2.18)$$

Using the fact that

$$A(x) - \frac{P_L(x)}{Q_M(x)} = O(x^{L+M+1}) \qquad (2.19)$$

we get, by equating equal powers of x,

$$a_o = P_o$$

$$a_1 + a_o q_1 = P_1$$

$$\ldots,$$

$$a_{L+M} + a_{L+M-1} q_1 + \ldots a_L q_M = o$$

with $a_n = o$ for $n < o$ and $q_j = o$ for $j > M$.

The Padé approximant to any series is unique. Because of this property we can effectively replace a power series by its corresponding Padé approximant rather than work with truncated ones. Another important property of the Padé approximant is its invariance, which ensures better con-vergence. Padé approximants have provided a means of solving a wide variety of problems: problems in fluid mechanics and certain problems in theoretical physics like calculation of critical indices, the low lying boson resonances in elementary particle physics etc. [71].

The series occuring in the equation for α in (2.11) as well as those giving the matrix elements D_{ij} are conver-gent but highly asymptotic. The selection of the truncation

point is crucial, because of this asymptotic nature. The accuracy as well as convergence can be improved by replacing the series by its Padé approximant [L/M]. Thus the equation for α is written as

$$\frac{1}{\alpha} + 1 + |\alpha|^z \ [L/M] \ = 0 \qquad\qquad (2.20)$$

Equating the series in (2.10) to (2.16), the coefficients P_j and Q_j are obtained to any required order. Eq. (2.20) is solved by means of the Newton-Raphson method to yield α. We find that this results in improved convergence. The efficiency of the approach is illustrated by working out three specific cases: $z = 2, 4$ and 6.

The elements of the D matrix can also be expressed, as power series in $\frac{1}{\alpha}$. We write, using Padé, the power series for the matrix element D_{ij} as,

$$D_{11} = -\alpha - \alpha^{z+1} \ [L/M]_{11}$$

$$D_{21} = -\alpha^{z-1} \ [L/M]_{21} \qquad \text{etc.} \qquad (2.21)$$

We consider terms upto D_{44}, and the largest eigenvalue of the resulting 4x4 matrix is computed as $\hat{\delta}$. This is done for several orders of the Padé approximant [L/M]. The convergence to numerical values is found to be excellent . The numerical values of the S_{nm} coefficients together with the α and δ values are presented in Tables 2.1 through 2.5.

Table 2.1 S_{nm} Coefficients for z = 2

n \ m	0	1	2	3	4	5	6
1	-0.500000	-0.2500000	0.0000000	-0.2500000	0.0000000	0.1250000	0.7812500
2	0.125000	0.0000000	0.0312500	-0.1250000	-0.3593750	0.2656250	
3	0.000000	0.0937500	0.2187500	0.1796875			
4	0.000000	-0.0078125	-0.0156256	-0.0722656			
5	0.000000	0.0000000	0.0000000				
6	0.000000	0.0000000					
7	0.000000						

Table 2.2 S_{nm} Coefficients for $z = 4$

n \ m	0	1	2	3	4	5	6
1	-0.2500000	-0.1875000	0.0468750	-0.0039062	0.0000000	-0.1875000	0.0298461
2	-0.0937500	0.0468750	0.0527343	-0.1171875	-0.0911865	-0.1835632	
3	-0.0156250	0.0351562	0.1074218	0.1855468	0.2403564		
4	0.0009765	-0.0219765	0.0531005	-0.1071166			
5	0.0000000	0.0051269	0.0097045				
6	0.0000000	-0.0006408					
7	0.0000000						

Table 2.3 S_{nm} Coefficients for z = 6

n \ m	0	1	2	3	4	5	6
1	−0.1666667	−0.1388888	−0.0462962	−0.0077160	−0.0006430	0.5390303	0.4311199
2	0.0694444	0.4629200	−0.0289351	0.0887345	−0.2055469	−0.0277543	
3	−0.0154320	0.0192901	0.0842335	0.0180755	−0.0777722		
4	0.0019290	−0.0184863	−0.0535836	−0.0777722			
5	−0.0001260	0.0064296	0.0271824				
6	0.0000035	−0.0013544					
7	0.0000000						

Table 2.4. α Values for z = 2,4 and 6 using Padé approximants. The numerical values are given for comparison [45].

Padé approximants [L/M]	z values		
	2	4	6
[1/1]	2.538017	1.720754	1.490768
[2/1]	2.923075	1.752354	1.518001
[2/2]	2.490066	1.712548	1.490806
[3/1]	2.318146	1.775863	1.497601
[3/2]	2.461060	1.740472	1.497176
[3/3]	2.523401	1.704381	1.482000
[4/4]	2.494272	1.667823	1.469210
[5/5]	2.494229	1.662815	1.467280
Numerical values	2.502	1.6908	1.468

Table 2.5 δ values for z = 2,4 and 6 using Padé approximants. The numerical values are given for comparison [45]·

Padé approximants [L/M]	z values		
	2	4	6
[1/1]	4.640784	7.450940	9.297613
[2/1]	4.483893	7.316797	9.260879
[2/2]	4.773389	7.268263	9.170148
[3/1]	4.261563	7.726422	9.810719
[3/2]	4.581424	7.349393	9.626893
[3/3]	4.669775	7.296393	9.299577
[4/4]	4.664557	7.283927	9.299474
Numerical value	4.669	7.284	9.2996

Table 2 .6 Distance to nearest pole from the origin

R_L^M in the complex plane of diagonal Padé

approximants P_L^M corresponding to z=2,4 and 6.

P_L^M	R_L^M values for		
	z=2	z=4	z=6
[1/1]	No poles	0.166667	0.222217
[2/2]	1.118034	0.361249	0.319311
[3/3]	1.226683	0.811874	0.815977
[4/4]	1.326701	1.086010	1.068047
[5/5]	1.337311	1.115285	1.098317

2.4 Discussion

The appearance of poles in the region of convergence limits the convergence behaviour. Usually the poles tend to cluster about the essential singularity. To get an idea about the size of the region in which P^L_M is a good approximation to the series we computed the singularities of P^L_M in the complex plane for diagonal Padé approximants. The distance of the nearest pole from the origin for $z = 2, 4$ and 6 for successive [L/M] are shown in Table 2.6. It is found that the closet poles are very accurately located by low order Padé approximants. The poles shift as higher and higher orders of the approximant are considered. Moreover, the root of the numerator cancells the root of the denominator for $L = 5$ in (2.20), meaning thereby that the corresponding Padé approximant is a good replacement to the series. Thus the perturbative scheme together with Padé approximants provide a reliable analytical technique for computing α and δ for one dimensional maps.

CHAPTER III

UNIVERSAL CONSTANTS AND $f(\alpha)$ SPECTRUM OF CIRCLE MAPS

3.1 Introduction

For 1-d maps of the form considered in Ch.II, the system becomes chaotic after an infinite sequence of period-doubling bifurcations. A dissipative system with attracting two torus in phase-space and a flow on the torus described by two incommensurate frequencies may undergo transition to chaos as some control parameter exceeds its critical value. That is, in phase space, a two torus attractor turns into a strange attractor. This route to chaos, called quasi-periodic, occurs in low aspect ratio systems [74,82,103]. Usually, the actual transition is preceeded by mode locking in which the ratio of the two basic frequencies sticks at a rational value for some range of parameter values, where the observed flow is periodic.

To describe quasi-periodicity, the model system must possess an attracting invariant two torus, the Poincaré section of which approximates an unfolded circle. A model system rich enough to undergo the quasiperiodic transition to chaos is the map of an annulus onto itself [83-88]:

$$T \begin{pmatrix} \Theta \\ r \end{pmatrix} = \begin{pmatrix} \Theta + \Omega - \dfrac{K}{2\pi} \sin 2\pi\Theta \\ br - \dfrac{K}{2\pi} \sin 2\pi\Theta \end{pmatrix} \qquad (3.1)$$

with constant Jacobian b. The long time behaviour of this planar map will be modelled by maps of a circle onto itself:

$$\Theta_{n+1} = f(\Theta_n) = \Theta_n + \Omega - \frac{K}{2\pi} \sin(2\pi\Theta_n) \quad \text{(mod 1)} \qquad (3.2)$$

Here Θ_n represents the position on the circle at the nth iteration. K accounts for nonlinearity and Ω is the parameter that determines the rate at which points travel around the circle, called the winding number, which is defined as,

$$\rho = \lim_{n \to \infty} \frac{f^n(\Theta) - \Theta}{n} \qquad (3.3)$$

The winding number represents the ratio of the two frequencies in the quasi-periodic regime. When the frequencies are commensurate, ρ is rational and when the frequencies are incommensurate, ρ is irrational, the attractor of which is an entire invariant curve. Irrational numbers may be approximated by means of rationals, and a quasi-periodic orbit may be well approached by a sequence of periodic orbits [95,98-101]. Any irrational number [0,1] can be uniquely represented by a continued fraction expansion:

$$\sigma = \cfrac{1}{n_1 + \cfrac{1}{n_2 + \cfrac{1}{n_3 + \cdots}}} \qquad (3.4)$$

where the n_i are positive integers. A rational number is expressed by a finite continued fraction expansion and an irrational one by a nonterminating continued fraction. The truncations of the infinite continued fractions give a systematic approximation to an irrational number. The rational approximants were constructed using Fibonacci numbers that satisfy the recursion relation [77,85], $F_{n+1} = F_n + F_{n-1}$, with the initial condition $F_o = F_1 = 1$. The nth order approximation to ρ is given by the ratio of Fibonacci numbers

$$\rho_n = \frac{F_n}{F_{n+1}} \tag{3.5}$$

When this sequence is followed upto $n \to \infty$, the transition to chaos occurs. The particular quasiperiodic orbit we will focus on is the one with inverse golden mean winding number whose continued fraction representation corresponds to all the n_i being unity.

For $|K| < 1$, the attractor of the map (3.2) consists of a torus and exhibits mode looking. The mode locked intervals increase in size when the nonlinearity K is increased, forming domains called Arnold tongues[85,86] in the (Ω, K) plane which cover roughly triangular regions in a plot of K versus Ω as shown below. Between the tongues the motion is quasiperiodic.
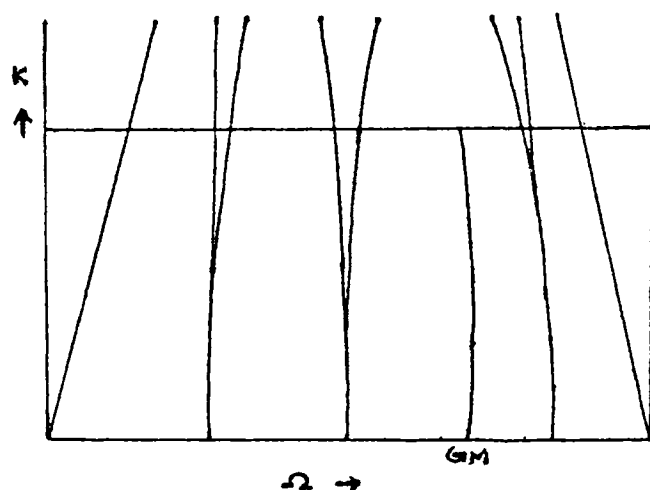
Each tongue represents a region in parameter space associated with a particular rational winding number, and for $K \leq 1$ the tongues bend away from each other and do not overlap. When $|K|=1$, the successive iterates converge to a periodic cycle for almost every Ω, and the Arnold tongues consume the entire range of Ω. That is the circle map is a diffeomorphism for $|K|<1$ and acquires a cubic inflection point at $|K|=1$. The universality class of the map is determined by its power law behaviour near this critical point. For $|K|>1$, the map is non-invertible. The tongues begin to overlap leading to hysteresis effect and chaos. Inside the tongues, there are period-doubling cascades leading gradually to chaotic motion. Outside the tongues, the remaining quasi-periodic orbits disappear abruptly, giving rise to further chaotic motion.

The circle map provides a generic model for the response of nonlinear oscillators to periodic perturbations [97], the

dynamics of Josephson Junctions [91], and charge density waves in condensed matter physics [94]. Using numerical techniques, it was shown that the quasiperiodic route to chaos is universal for certain classes of maps, and critical exponents have been obtained in these cases. Studies of the transition in Rayleigh-Bénard convection were found to be in agreement with theoretical predictions for both local and global properties [88-93].

It is found that there exist two interesting classes of scaling behaviour for the circle map, one for $|K| < 1$ and the other for $|K| = 1$ [77,79]. Let Ω_n denote the value of Ω such that there is a cycle with winding number ρ_n passing through $\Theta = 0$; Ω_n is the accumulation point of the sequence. It was found that for both cases,

$$\Omega_n - \Omega_\infty \approx \delta^{-n} \tag{3.6}$$

δ characterises the convergence rate of successive parameter differences. The distance from $\Theta = 0$ to the nearest point of the cycle, given by $f^{F_n}(\Theta) - F_{n-1}$ converges geometrically as

$$f^{F_n}(\Theta) - F_{n-1} \approx \alpha^{-n} \tag{3.7}$$

with $\Omega = \Omega_n$. Here α characterises the convergence rate of successive orbital differences. The scaling exponents α and

δ take on two distinct sets of values [77], which in the subcritical case $|K|<1$, is $\alpha = -\varphi^{-1}$ and $\delta = -\varphi^{-2}$. In the critical case, these indices assume nontrivial values $\alpha = -1.28857$, $\delta = -2.83360$. For the critical case, to give a more complete description of the fine structure of quasiperiodic scaling, additional subdominant exponents have been considered and it was found that the scale factors for the circle map are closer to each other than those in the period doubling route [102].

The renormalisation group analysis for the transition from quasiperiodicity to chaos [77,84] is based on approaching the golden mean rotation number by ratios of Fibonacci numbers. The great utility of renormalisation group in dynamical systems has been to reduce the questions of existence and universality to a geometric problem in function space. Here the transformation is defined on an open set of maps, that does not contain the winding number. As a result, the universal features follow from co-ordinate change that reduces the fixed point function to a rotation.

Defining a map

$$f^n(x) = f^{F_{n+1}}(x) - F_n \qquad (3.8)$$

obeying the composition rule,

$$f^{n+1} = f^n \cdot f^{n-1}$$

$$f^{n+1} = f^{n-1} \cdot f^n \qquad (3.9)$$

one finds that for $\Omega = \Omega_\infty$ and for $|K| \ll 1$

$$f^n(x) = \alpha^{-n} \bar{f} (\alpha^n x), \qquad (3.10)$$

which, for $|K| = 1$, is a linear map $f(x) = -1+x$ with $\alpha = -\frac{1}{\rho}$. For $|K|=1$, f is a universal and nontrivial analytic function in x^3. The function f satisfies the recurrence relations,

$$\bar{f}(x) = \alpha \bar{f} (\alpha \bar{f}(\alpha^{-2} x)) \qquad (3.11)$$

$$\bar{f}(x) = \alpha^2 \bar{f} (\alpha^{-1} \bar{f}(\alpha^{-1} x)) \qquad (3.12)$$

Choosing a value for α, we define

$$f_n(x) = \alpha^n f^n (\alpha^{-n} x) \qquad (3.13)$$

which obeys the recurrence relations,

$$f_{n+1}(x) = \alpha f_n (\alpha f_{n-1}(\alpha^{-2} x)) \qquad (3.14)$$

$$f_{n+1}(x) = \alpha^2 f_{n-1} (\alpha^{-1} f_n (\alpha^{-1} x)) \qquad (3.15)$$

In this formulation, one must specify both f_n and f_{n-1} in order to produce f_{n+1}. That is, if F is a space of functions, then the recursion relations (3.14) and (3.15)

are usually transformations on FxF back into itself.

However, if we choose as our initial condition,

$$f_1(\alpha^{-1} f_1(\alpha x)) = \alpha^{-1} f_1(\alpha(f_o(x)))$$ (3.16)

the above two recursion relations (3.14) and (3.15) become equivalent.

With the choice $g(x) = \alpha f(x)$, one obtains the following fixed point equations, in the limit $n \to \infty$,

$$g(x) = \alpha_{qp} \, g(g(x/\alpha_{qp}^2))$$ (3.17)

$$g(x) = \alpha_{qp}^2 \, g(\alpha_{qp}^{-2} \, (g(x/\alpha_{qp})))$$ (3.18)

for the constaints $g(o)=1$ and $g'(o)=o$. The solutions to these eouations and the linearised version yield the relevant scaling parameters α and $\hat{\delta}$, which are exponents in the x space and parameter space respectively. The scale factors α and δ do depend on the rotation number and the order of the inflection point.

Although there are two functional group equations, under appropriate boundary conditions one of them alone determines $g(x)$ completely. The first equation has a self-determining interval (0,1) while the second equation determines $g(x)$ in $(-\alpha g^{-1}(o), o)$. By considering perturbations

about the fixed point,

$$g_r(x) = g(x) + \epsilon h(x),$$
(3.19)

we have

$$g_r(g_r(x)) = g_r(g(x) + \epsilon h(x))$$

$$= g(g(x)) + \epsilon\{hg(x) + g_r'g(x)h(x)\}$$

But by (3.14)

$$g(\alpha^2 x) = \alpha g(g(x))$$

$$\alpha[g'(g(x)) h(x) + hg(x)] = \delta h(\alpha^2 x)$$
(3.20)

The equations (3.14), (3.15) and (3.20) can be used to evaluate α and δ for a given z value. Numerical determination of α and δ shows that there exist universality classes characterised by scale factors α and δ for different z values [79].

3.2 Universal parameters for circle maps

The perturbative method is herein extended to the study of the universality of α and δ as well as g(x) for the circle map. Detailed calculations for different orders of accuracy are presented for the sine circle map. To account for different universality classes, a polynomial form of

circle map is chosen, and using the perturbative scheme, the values of α and δ for varying orders of accuracy in the Padé scheme for specific z values are calculated. Also the behaviour of the universal function $g(x)$ with x is discussed. Using the perturbative technique, the corresponding fractal dimensions D_q and the f-α spectrum of the chaotic attractor associated with the quasiperiodic route, are analysed.

The functional equations (3.14) and (3.15) are replaced by infinite dimensional vector equations. In the universal function $g(x)$

$$g(x) = 1 + \sum_{n=1}^{\infty} C_n |x|^{nz} \tag{3.21}$$

it is convenient to redefine the coefficients C_n by

$$C_n \, \alpha^n = S_n |\alpha|^{2z} \tag{3.22}$$

Employing (3.21) and (3.22) in (3.17) and equating the coefficients of $|x|^{nz}$ on both sides, we get

$$\frac{1}{z} = \sum_{m=1}^{\infty} \frac{mS_m}{\alpha^{m-1}} \tag{3.23}$$

$$\frac{1}{\alpha} - 1 - |\alpha|^{2z} \sum_{m=1}^{\infty} \frac{S_m}{\alpha^m} = 0 \tag{3.24}$$

and

$$S_n \left[1 - \frac{1}{\alpha^{2z(n-1)}} \right] = \sum_{\ell \geq 2}^{n} \sum_{r \geq 1}^{\infty} \binom{rz}{\ell} \frac{S_r}{\alpha^{r-1}}$$

$$\times \sum_{m_1 \geq 1, m_2 \geq 1, \ldots m_\ell \geq 1} \frac{S_{m_1} S_{m_2} \ldots S_{m_\ell} \delta_{m_1+m_2+\ldots m_\ell, n}}{|\alpha|^{2z(n-\ell)}} \qquad (3.25)$$

To solve these equations, the coefficients S_n are expanded:

$$S_n(\alpha) = \sum_{m=0}^{\infty} \frac{S_{nm}}{\alpha^m} \qquad (3.26)$$

Substituting (3.26) in (3.25) and (3.24) a series of equations similar to those given in Ch II are obtained for the coefficients S_{nm}. The calculated values of the S_{nm} coefficients for z=3 and k=1 are given in Table 3.1. Using the S_{nm} coefficients in (3.24) we get the equation for α:

$$\frac{1}{\alpha} - 1 = |\alpha|^{2z} \sum_{r=1}^{\infty} \sum_{m=0}^{\infty} \frac{S_{rm}}{\alpha^{r+m}} \qquad (3.27)$$

Expanding h(x) also as a power series we have

$$h(x) = 1 + \sum_{n=1}^{\infty} h_n |x|^{nz} \qquad (3.28)$$

Using (3.28), (3.21),(3.26) and (3.22) in (3.20) and equating coefficients of $|x|^{nz}$ on both sides we get the following

Table 3.1. S_{nm} Coefficients for z = 3

n \ m	0	1	2	3	4	5	6
1	0.333333	−0.2222222	0.0370370	0.000000	0.000000	0.000000	−1.1358024
2	0.1111111	−0.0370370	−0.0740740	0.1316822	−0.2043895	0.3045267	
3	0.0123456	0.0493827	−0.1152263	0.1883859	0.0740740		
4	0.000000	0.0205761	−0.0425240	0.0941293			
5	0.0000000	0.0027434	−0.0036579				
6	0.0000000	0.0001524					
7	0.000000						

system of equation for δ:

$$\alpha\left[1+ \sum_{m\geq 1}^{\infty} h_m + |\alpha|^{2z} \sum_{m\geq 1}^{\infty} \frac{mzS_m}{\alpha^m}\right] = \delta \tag{3.29}$$

$$\alpha\left[\sum_{m\geq 1}^{\infty} \binom{mz}{1} h_m \frac{S_1}{\alpha} + \sum_{m\geq 1}^{\infty} 2\binom{mz}{2} \frac{S_m S_1}{\alpha^m} |\alpha|^{2z-1}\right.$$

$$\left. + h_1 \sum_{m\geq 1}^{\infty} \binom{mz}{1} \frac{S_m}{\alpha^m}\right] = \delta h_1$$

$$\alpha\left[\sum_{\ell\geq 1}^{\infty} \sum_{m\geq 1}^{\infty} \left(\binom{mz}{\ell} \frac{h_m}{\alpha^m} + (\ell+1)\binom{mz}{\ell+1} \frac{S_m}{\alpha^{n-2z+m}}\right)\right.$$

$$\times \sum_{m_1\geq 1; m_2\geq 1 \ldots m_\ell \geq 1} \frac{S_{m_1} S_{m_2} \ldots S_{m_\ell} \delta_{m_1+m_2+\ldots m_\ell,n}}{|\alpha|^{2z(n-\ell)}}$$

$$+ \sum_{n'\geq 1}^{n-1} \sum_{\ell\geq 1}^{n-n'} \sum_{m\geq 1}^{\infty} \left(h_{n'} (\ell+1)\binom{mz}{\ell+1} \frac{S_m}{\alpha^{n-n'-2z+m}}\right)$$

$$\times \sum_{m_1\geq 1; m_2\geq 1 \ldots m_\ell \geq 1} \frac{S_{m_1} S_{m_2} \ldots S_{m_\ell} \delta_{m_1+m_2+\ldots m_\ell,n}}{|\alpha|^{2z(n-\ell)}}$$

$$\left. + h_n \sum_{m\geq 1}^{\infty} \frac{mz\, S_m}{\alpha^{m+(n-1)2z}}\right] = \delta h_n$$

$$(\text{for } n=2,3,4,\ldots)$$

These equations can be written in the form of a matrix eigenvalue equation (2.15). The elements of the D matrix are computed using the expansion in (3.22) and the S_{nm} coefficients in Table 3.1. The largest real eigenvalue

gives the values of $\overset{C}{\delta}$. Due to the asymptotic nature of the equations for α and δ, alternative methods to sum the resulting asymptotic series have to be chosen. It is found that there is definite advantage if we use Padé approximants to sum the resulting series, due to its faster convergence property.

The calculations are performed for the specific case z=3 and k=1 of the circle map. The results obtained for various orders of Padé approximant for the sine circle map with cubic inflection point are collected in Table 3.2. For this specific case the universal function g(x) is found:

$$g(x) = 1-0.952659x^3 - 0.3478276x^6 + 0.3349593x^9$$
$$- 0.142136x^{12} + 0.00558223x^{15} + \ldots \qquad (3.32)$$

The function g(x) obtained in (3.32) can be substituted on the R.H.S. of (3.18) to get the universal function in the interval $(\frac{-1}{\alpha^2},o)$. The behaviour of the universal function g(x) versus x in the interval $(\frac{-1}{\alpha^2},1)$ is represented in Fig 3.1. It is found that the iterates crowd around $\frac{-1}{\alpha^2}$ and 1.

3.3 Universal constants for general z

In the quasiperiodic route to chaos modelled by the circle map, it is found that the universal behaviour depends on the degree of inflection z. To study this form of
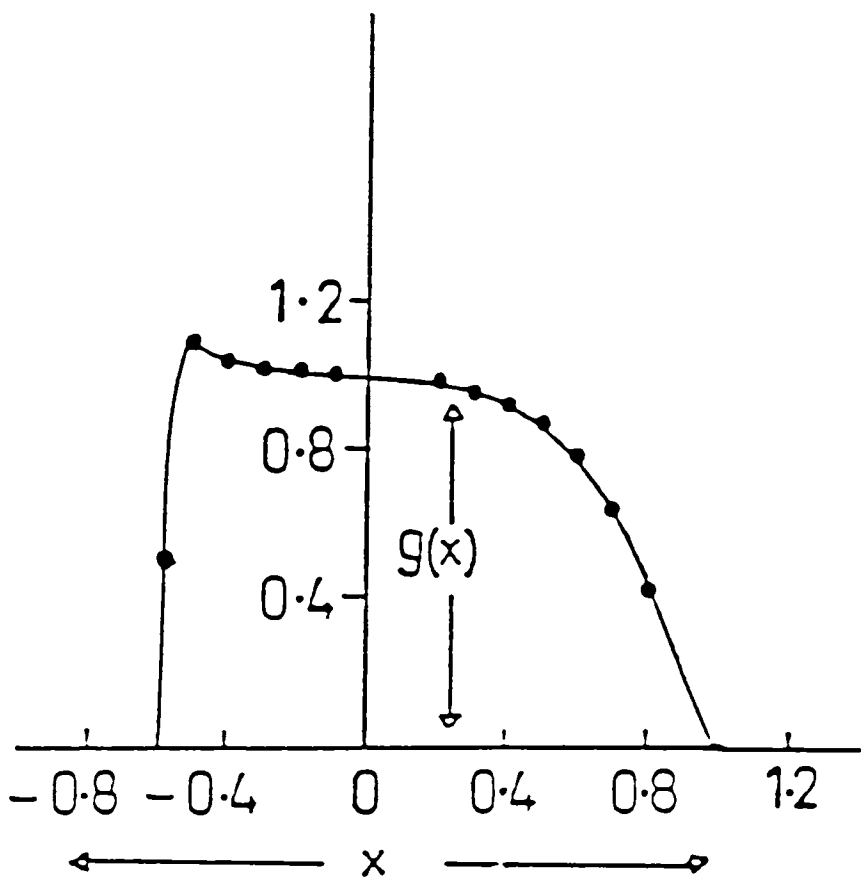
Fig. 3.1The universal function $g(x)$ vs. x in the interval $(-1/x^2, 1)$.

universality, we take a polynomial form of the circle map [79]:

$$\Theta_{n+1} = \Theta_n + \Omega - \frac{K}{2\pi} f(\Theta_n) \qquad (3.33)$$

where

$$f(\Theta_n) = 2\pi\Theta_n - 2^{z-1} \Theta_n |\Theta_n|^{z-1}, \quad \Theta\in[-1/2, \ 1/2]$$

For z=3, this map has a cubic inflection point, and, therefore, belongs to the same universality class as the sine circle map. For (3.33), details regarding the variation of fractal dimension with z have been worked out numerically by Delburgo and Kenny [96]. The universal indices α and δ associated with this route have been obtained numerically by Hu [29] for different universality classes.

The renormalisation group equations in this context are formally the same as those for the sine circle map. The perturbative method yields the following system of equations for the S_{nm} coefficients for general z:

$$S_{10} = \frac{1}{z}$$

$$S_{20} = z(z-1)S_{10}^3$$

$$S_{11} = -2S_{20}$$

$$S_{21} = \frac{z(z-1)}{2!} 3S_{10}^2 S_{11} + \frac{2z(2z-1)}{2!} S_{20}S_{10}^2$$

$$S_{30} = \frac{z(z-1)(z-2)}{3!} S_{10}^4$$

$$S_{12} = -(2S_{21}+3S_{30})$$

$$S_{31} = \frac{z(z-1)\ (z-2)}{3!}4S_{10}^{3}S_{11}+ \frac{2z(2z-1)(2z-2)}{3!}\ S_{20}S_{10}^{3}$$

$$S_{22} = \frac{z(z-1)}{2!}\ (3S_{10}^{2}S_{12}+3S_{10}S_{11}^{2})+ \frac{2z(2z-1)}{2!}(S_{10}^{2}S_{21}+2S_{20}S_{11}S_{10})$$

$$+ \frac{3z(3z-1)}{2!}\ S_{30}S_{10}^{2}$$

$$S_{40} = \frac{z(z-1)(z-2)(z-3)}{4!}\ S_{10}^{5}$$

$$S_{13} = -(2S_{22}+3S_{31}+4S_{40})$$

$$S_{41} = \frac{z(z-1)(z-2)(z-3)}{4!}\ 5S_{10}^{4}S_{11}+ \frac{2z(2z-1)(2z-2)(2z-3)}{4!}S_{20}S_{10}^{4}$$

$$S_{42} = \frac{z(z-1)(z-2)(z-3)}{4!}(5S_{10}^{4}S_{12}+10S_{10}^{3}S_{11}^{2})+\frac{2z(2z-1)(2z-2)(2z-3)}{4!}$$

$$\times \left(4S_{20}S_{10}^{3}S_{11}+S_{21}S_{10}^{4}\right)+ \frac{3z(3z-1)(3z-2)(3z-3)}{4!}S_{30}S_{10}^{4}$$

$$S_{50} = 0$$

$$S_{51} = \frac{2z(2z-1)(2z-2)(2z-3)(2z-4)}{4!}S_{20}S_{10}^{5}$$

$$S_{52} = \frac{2z(2z-1)(2z-2)(2z-3)(2z-4)}{5!}(5S_{10}^{4}S_{11}S_{20}+S_{21}S_{10}^{5})$$

$$+ \frac{3z(3z-1)(3z-2)(3z-3)(3z-4)}{5!}\ S_{30}S_{10}^{5}$$

$$S_{61} = \frac{2z(2z-1)(2z-2)(2z-3)(2z-4)(2z-5)}{6!}\ S_{20}S_{10}^{6}$$

$$S_{32} = \frac{z(z-1)(z-2)}{3!}\left(4S_{10}^{3}S_{11}^{2}+6S_{10}^{2}S_{11}^{2}\right)+ \frac{2z(2z-1)(2z-2)}{3!}$$

$$\times (3S_{20}S_{10}^{2}S_{11}+S_{21}S_{10}^{3}) + \frac{3z(3z-1)(3z-2)}{3!}\ S_{30}S_{10}^{3}$$

$$S_{33} = \frac{z(z-1)(z-2)}{3!}(4S_{10}^{3}S_{13}+12S_{10}^{2}S_{11}S_{12}+4S_{10}S_{11}^{3})$$

$$+ \frac{2z(2z-1)(2z-2)}{3!}(3S_{20}S_{10}^{2}S_{12}+3S_{20}S_{10}S_{11}^{2}+3S_{21}S_{10}^{2}S_{11}$$

$$+ S_{22}S_{10}^{3})$$

$$+ \frac{3z(3z-1)(3z-2)}{3!}(S_{31}S_{10}^3 + 3S_{30}S_{10}^2 S_{11}) + \frac{4z(4z-1)(4z-2)}{3!} S_{40}S_{10}^3$$

$$S_{23} = \frac{z(z-1)}{2!}(3S_{10}^2 S_{13} + 6S_{10}S_{11}S_{12} + S_{11}^3) + \frac{2z(2z-1)}{2!}$$

$$(2S_{20}S_{10}S_{12} + S_{20}S_{11}^2 + 2S_{21}S_{10}S_{11} + S_{22}S_{10}^2) + \frac{3z(3z-1)}{2!}(S_{10}^2 S_{31}$$

$$+ 2S_{30}S_{10}S_{11}) + \frac{4z(4z-1)}{2!} S_{40}S_{10}^2$$

$$S_{14} = -(2S_{23} + 3S_{32} + 4S_{41} + 5S_{50})$$

$$S_{43} = \frac{z(z-1)(z-2)(z-3)}{4!} (5S_{10}^4 S_{13} + 20S_{10}^3 S_{11}S_{12} + 10S_{10}^2 S_{11}^3)$$

$$+ \frac{2z(2z-1)(2z-2)(2z-3)}{4!} (4S_{20}S_{10}^3 S_{12} + 6S_{20}S_{10}^2 S_{11}^2$$

$$+ 4S_{21}S_{10}^3 S_{11} + S_{22}S_{10}^4)$$

$$+ \frac{3z(3z-1)(3z-2)(3z-3)}{4!} (4S_{30}S_{10}^3 S_{11} + S_{31}S_{10}^4)$$

$$+ \frac{4z(4z-1)(4z-2)(4z-3)}{4!} S_{40}S_{10}^4$$

$$S_{34} = \frac{z(z-1)(z-2)}{3!}(4S_{10}^3 S_{14} + 12S_{10}^2 S_{11}S_{13} + 12S_{10}S_{11}^2 S_{12} + 6S_{10}^2 S_{12}^2 + S_{11}^4)$$

$$+ \frac{2z(2z-1)(2z-2)}{3!}(3S_{20}S_{10}^2 S_{13} + 6S_{20}S_{10}S_{11}S_{12} + S_{20}S_{11}^3$$

$$+ 3S_{21}S_{10}^2 S_{12} + 3S_{21}S_{10}S_{11}^2 + 3S_{22}S_{10}^2 S_{11} + S_{23}S_{10}^3)$$

$$+ \frac{3z(3z-1)(3z-2)}{3!}(3S_{30}S_{10}^2 S_{12} + 3S_{30}S_{10}S_{11}^2 + 3S_{31}S_{10}^2 S_{11}$$

$$+ S_{30}S_{10}^3)$$

$$+ \frac{4z(4z-1)(4z-2)}{3!}(3S_{40}S_{10}^2 S_{11} + S_{41}S_{10}^3)$$

$$+ \frac{5z(5z-1)(5z-2)}{3!} S_{50}S_{10}^3$$

etc.

The scale factor α_{qp} given by (3.27) is

$$\frac{1}{\alpha_{qp}} - 1 = |\alpha|_{qp}^{2z} \sum_{r=1}^{\infty} \sum_{m=o}^{\infty} \frac{S_{rm}}{\alpha_{qp}^{r+m}} \qquad (3.34)$$

and

$$g(x) = 1 + |\alpha|_{qp}^{2z} \left(\frac{1}{z\alpha_{qp}} - \frac{(z-1)x^z}{z^2\alpha_{qp}^2} + \frac{(z-1)x^{2z}}{2z^2\alpha_{qp}^2} + \cdots \right) \qquad (3.35)$$

For any z value, the first few coefficients S_{nm} work out to be

$$S_{10} = \frac{1}{z} \ ; \quad S_{11} = \frac{(z-1)}{z^2}; \quad S_{20} = \frac{(z-1)}{2z^2} \qquad (3.36)$$

Then (3.34) becomes

$$\frac{1}{\alpha_{qp}} - 1 = |\alpha|_{qp}^{2z} \left(\frac{1}{z\alpha_{qp}} + \frac{(z-1)}{2z^2\alpha_{qp}^2} + \cdots \right) \qquad (3.37)$$

The asymptotic series in (3.34) is replaced by the corresponding Padé approximant [L/M]. In an actual calculation, the [L/M] are determined to different orders and the converging value of α_{qp} is used in further applications. Fig. 3.2 shows the α_{qp} values thus obtained for different z. The computed results along with their numerical values are given in Table 3.3 . We find that the agreement to numerical values is quite good, except for z≠2.
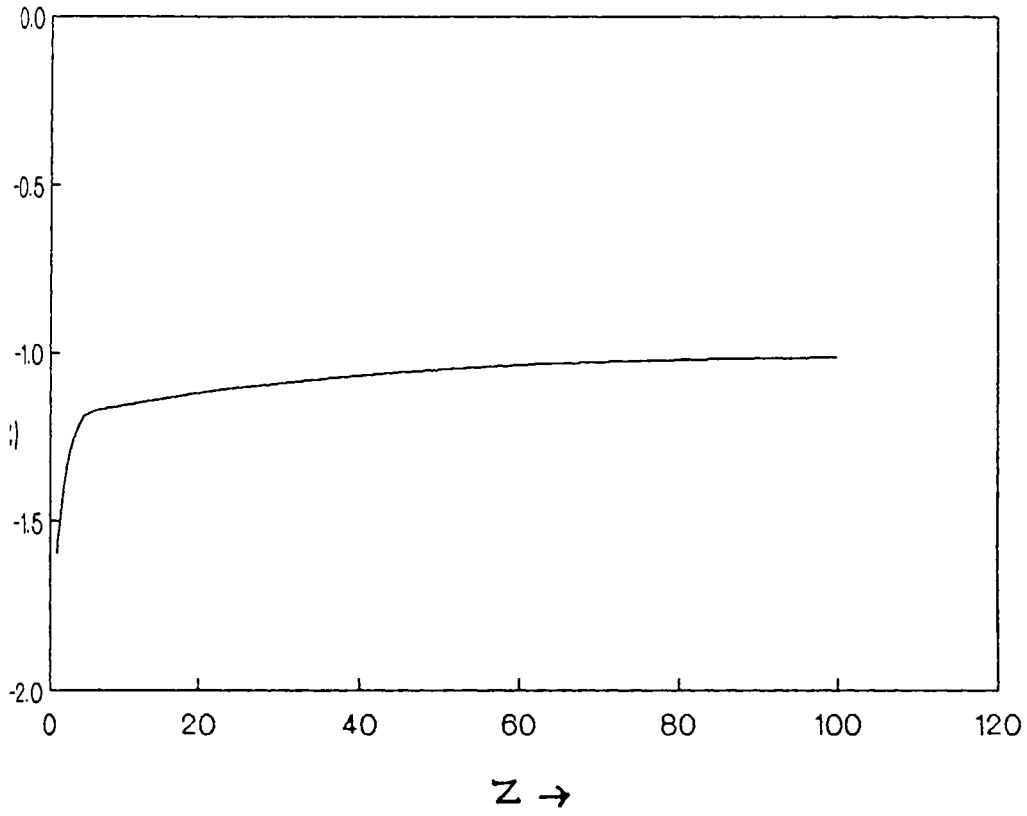
Fig.3.2   The $\alpha_{qp}(z)$ values for maps with different z values

Table 3.2.   Values of α_{qp} and δ for z = 3 and k = 1, using Padé approximants

[L/ M]	α_{qp}	δ
[1/1]	− 1.327866	− 2.832372
[2/2]	− 1.319653	− 2.827951
[3/3]	− 1.307812	− 2.782274
[4/4]	− 1.299829	− 2.821394
[5/5]	− 1.299681	− 2.821381
Numerical value	− 1.28857	− 2.83360

Table 3.3. α_{qp} versus z

z	α_{qp}(calculated)	Numerical value
1.1	−1.595027	−
2	−1.40421	−1.388
3	−1.28857	−1.288
4	−1.23110	−1.2314
5	−1.19024	−
6	−1.1603	−1.19
50	−1.0211	−
100	−1.01140	−

A good replacement of the series by the Padé approximant is possible only if we locate the exact region of poles. We calculated the location of poles for each Padé approximated series. We can infer from this that, for z=2, the slight variation from numerical value may be due to the location of pole situated around the α_{qp} value, whereas for high z values, the poles are found to be shifting as higher and higher approximants are considered.

The elements of D matrix for general z are

$$D_{11} = \alpha + z\alpha^{2z} \left(S_{10} + \frac{1}{\alpha}(S_{11} + 2S_{20}) + \frac{1}{\alpha^2}(S_{12} + 2S_{21} + 3S_{30}) + \cdots \right)$$

$$D_{12} = \alpha$$

$$D_{13} = \alpha$$

$$D_{14} = \alpha$$

$$D_{21} = z\alpha^{2z-1} [(z-1)S_{10}^2 + \frac{1}{\alpha}((z-1)2S_{10}S_{11} + (2z-1)2S_{20}S_{10})$$

$$+ \frac{1}{\alpha^2}((z-1)(2S_{10}S_{12} + S_{11}^2) + (2S_{20}S_{11} + 2S_{10}S_{21})(2z-1)$$

$$+ (3z-1)3S_{30}S_{10}) + \frac{1}{\alpha^3}((z-1)(2S_{10}S_{13} + 2S_{11}S_{12})$$

$$+ (2z-1)(2S_{12}S_{20} + 2S_{21}S_{11} + 2S_{22}S_{10}) + (3z-1)$$

$$\times (3S_{30}S_{11} + 3S_{31}S_{10}) + (4z-1)4S_{40}S_{10}) + \frac{1}{\alpha^4}((z-1)$$

$$(2S_{10}S_{14} + 2S_{11}S_{13} + S_{12}^2) + (2z-1)(2S_{20}S_{13} + 2S_{21}S_{12}$$

$$+ 2S_{22}S_{11} + 2S_{23}S_{10}) + (3z-1)(3S_{30}S_{12} + 3S_{31}S_{11} + 3S_{32}S_{10})$$

$$+ (4z-1)x4 \ (S_{40}S_{11}+S_{41}S_{10}) +(5z-1) \ (5S_{50}S_{10}))]$$

$$D_{22}= z \ [2S_{10}+ \frac{1}{\alpha}(2S_{11}+2S_{20}) + \frac{1}{\alpha^2}(2S_{12}+2S_{21}+3S_{30})]$$

$$D_{23}= 2z[S_{10}+ \frac{S_{11}}{\alpha}+\frac{S_{12}}{\alpha^2}$$

$$D_{24}= 3z[S_{10}+ \frac{S_{11}}{\alpha} + \frac{S_{12}}{\alpha^2}]$$

$$D_{31}= \frac{z(z-1)}{\alpha^2} \ S_{20}S_{10}+ \ z\alpha^{2z-2} \ [\ \frac{(z-1)(z-2)S_{10}^3}{2!}$$

$$+ \frac{1}{\alpha}(\ \frac{(z-1)(z-2)}{2!}3S_{10}^2S_{11}+ \ \frac{(2z-1)(2z-2)}{2!} \ 2S_{20}S_{10}^2)$$

$$+ \frac{1}{\alpha^2}(\ \frac{(z-1)(z-2)}{2!} \ (3S_{10}^2S_{12}+3S_{10}^2S_{11})$$

$$+ \frac{(2z-1)(2z-2)}{2!} \ x \ 2 \quad (2S_{20}S_{10}S_{11}+S_{21}S_{10}^2)$$

$$+ \frac{(3z-1)(3z-2)}{2!} \ 3S_{30}S_{10}^2)+ \frac{1}{\alpha^3} \frac{(z-1)(z-2)}{2!} \ (3S_{10}^2S_{13}$$

$$+ 6S_{10}S_{11}S_{12}+S_{11}^3)+ \frac{(2z-1)(2z-2)}{2!} \ x2 \ (2S_{20}S_{10}S_{12}$$

$$+ S_{20}S_{11}^2+2S_{21}S_{10}S_{11}+S_{22}S_{10}^2) + \frac{(3z-1)(3z-2)}{2!}$$

$$x \ 3 \ (2S_{30}S_{10}S_{11}+S_{31}S_{10}^2) + \frac{(4z-1)(4z-2)}{2!} \ 4S_{40}S_{10}^2)$$

$$+ \frac{1}{\alpha^4}(\frac{(z-1)(z-2)}{2!} (3S_{10}^2 S_{14} + 6S_{10} S_{11} S_{13} + 3S_{11}^2 S_{12}$$

$$+ 3S_{10} S_{12}^2) + \frac{(2z-1)(2z-2)}{2!} \times 2 \quad (2S_{20} S_{10} S_{13} + 2S_{20} S_{11} S_{12}$$

$$+ 2S_{21} S_{10} S_{12} + S_{21} S_{11}^2 + 2S_{22} S_{10} S_{11} + S_{23} S_{10}^2)$$

$$+ \frac{(3z-1)(3z-2)}{2!} \times 3 \quad (2S_{30} S_{10} S_{12} + S_{30} S_{11}^2 + 2S_{31} S_{10} S_{10}^2$$

$$+ S_{32} S_{10}^2) + \frac{(4z-1)(4z-2)}{2!} \times 4 \quad (2S_{40} S_{10} S_{11} + S_{41} S_{10}^2)$$

$$+ \frac{(5z-1)(5z-2)}{2!} 5S_{50} S_{10}^2)]$$

$$D_{32} = [\frac{z(z-1)}{2!} S_{10}^2 + \frac{1}{\alpha} ((z-1) zS_{10}^2) + \frac{1}{\alpha^2}(\frac{z(z-1)}{2!} 2S_{10} S_{11}$$

$$+ z(z-1)2S_{10} S_{11} + 2z(2z-1)S_{20} S_{10})]$$

$$D_{33} = [\frac{2z(2z-1)}{2!} \frac{S_{10}^2}{\alpha} + \frac{1}{\alpha^2} (\frac{2z(2z-1)}{2!} 2S_{10} S_{11})],$$

$$D_{34} = [\frac{3z(3z-1)}{2!} (\frac{S_{10}^2}{\alpha} + \frac{2S_{10} S_{11}}{\alpha^2})] ,$$

$$D_{41} = z\alpha^{z-2} [\frac{(z-1)(z-2)(z-3)}{3!} \frac{S_{10}^4}{\alpha}$$

$$+ \frac{1}{\alpha^2}(\frac{(z-1)(z-2)(z-3)}{3!} 4S_{10}^3 S_{11} + \frac{(2z-1)(2z-2)(2z-3)}{3!} 2S_{20} S_{10}^3)$$

$$+ \frac{1}{\alpha^3}(\frac{(z-1)(z-2)(z-3)}{3!} (4S_{10}^3 S_{12} + 6S_{10}^2 S_{11}^2)$$

$$+ \frac{(2z-1)(2z-2)(2z-3)}{3!} \times 2 \quad (3S_{20} S_{10}^2 S_{11} + S_{21} S_{10}^3$$

$$+ \frac{(3z-1)(3z-2)(3z-3)}{3!} 3S_{30}S_{10}^3) + \frac{1}{\alpha^4}((z-1)(z-2)$$

$$\times \frac{(z-3)}{3!}(4S_{10}^3S_{13}+12S_{10}^2S_{11}S_{12}+4S_{10}S_{11}^3)$$

$$+ \frac{(2z-1)(2z-2)(2z-3)}{3!} x2 (3S_{20}S_{10}^2S_{12}+3S_{20}S_{10}S_{11}^2$$

$$+ 3S_{21}S_{10}^2S_{11}+S_{22}S_{10}^3) + \frac{(3z-1)(3z-2)(3z-3)}{3!}$$

$$x3 (3S_{30}S_{10}^2S_{11}+S_{31}S_{10}^3) + \frac{(4z-1)(4z-2)(4z-3)}{3!}$$

$$x4S_{40}S_{10}^3)]$$

$$D_{42}=[\frac{z(z-1)(z-2)}{3!} \frac{S_{10}^3}{\alpha^2} + \frac{z(z-1)(z-2)}{2!} \frac{S_{10}^3}{\alpha^{2z-2}}]$$

$$D_{43}=[\frac{2z(2z-1)(2z-2)}{3!} \frac{S_{10}^3}{\alpha^2}] ,$$

$$D_{44}=[\frac{3z(3z-1)(3z-2)}{3!} S_{10}^3] .$$

The D matrix has only one eigenvalue greater than unity which is the acceptable value of δ. The computed results for various values of z are presented in Table 3.4. Here also the convergence to numerical values is excellent. Fig. 3.3 gives the variation of $\delta(z)$ with z. From Figs. 3.2 and 3.3 it is seen that $\alpha_{qp}(z)$ versus z is a decreasing function, while $\delta(z)$ is a monotonic increasing function, as expected, in agreement with numerical findings.

Using the S_{nm} coefficients given in (3.36), the universal function g(x) is obtained:

$$g(x) = 1 +|\alpha|_{qp}^{2z}(\frac{1}{z\alpha_{qp}} - \frac{(z-1)|x|^2}{z^2\alpha_{qp}^2} +\frac{(z-1)}{2z^2\alpha_{qp}^2}|x|^{2z} + ...) \qquad (3.38)$$
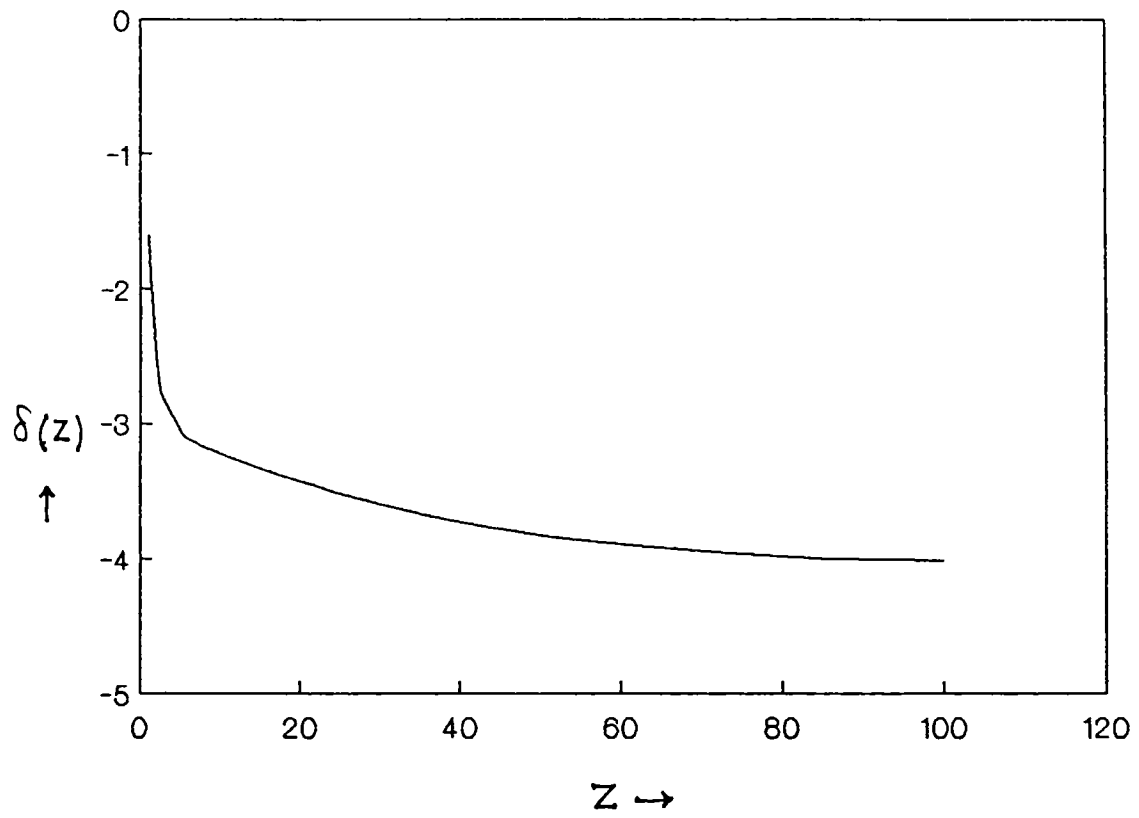
Fig. 3.3 $\delta(z)$ as a function of degree of inflection z

The behaviour of g(x) versus x for various z values in the interval (0,1) is sketched in Fig. 3.4. From the figure it is clear that the curves tend to converge to a common value for small x values, while they get separated for large x values.

3.4 Multifractals in circle maps

The circle maps of the form described in the preceding section, which follow a quasiperiodic route to chaos possess unusual scaling properties at the transition K=1. The corresponding universal behaviour is characterised by the function g(x) that satisfies the two renormalisation group equations. The iterates of g(x) form a nearly self similar cantor set. For (3.33) the details regarding the variation of fractal dimension with z have been worked and by Delburgo and Kenny [96]. They derived an approximate formula

$$D \simeq 1 - [\frac{(z-1)}{3}][\frac{1}{z}]^{z/(z-1)}$$ for the fractal dimension

associated with the critical circle map with an arbitrary order inflection point. Recently it was shown by Ji-Cang and Hu[87] that the singularity spectrum f(α) and the generalised dimension D_q of the critical invariant circle on an area-perserving twist map depend on z, and there is a cross-over phenomenon when z changes.
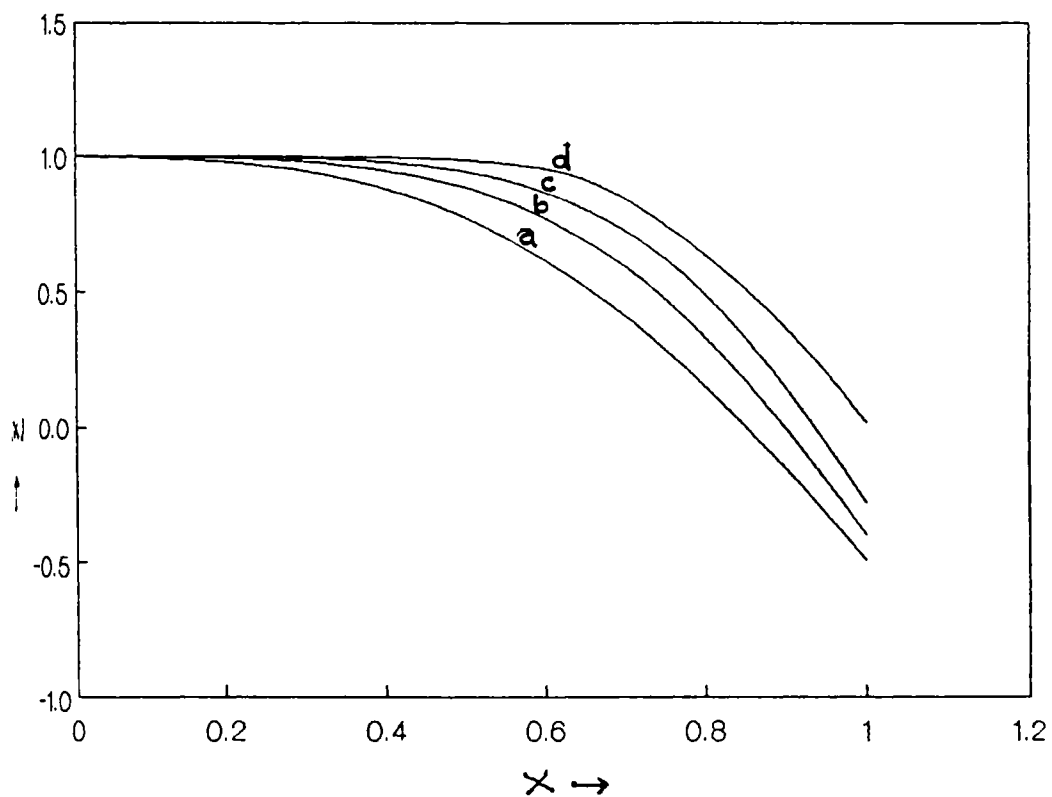
Fig. 3.4 The universal function g(x) computed using (3.38)
for a) z=2, b) z=3, c) z=5, d) z=7

Here we present the analytic expressions arrived at using the universal function $g(x)$ obtained by solving equations (3.16) and (3.17). The generalised dimension D_q as well as $f(\alpha)$ spectrum has been studied numerically by Per Bak [100] for $z = 3$. Applying the perturbative procedure the fractal dimensions D_q and the f-α spectrum are obtained.

The attractor consists of a set of points, and is seen to follow the construction of a Cantor set. At each stage, the probabilities P_i are equal while the lengths ℓ_i of the subset are different. This set consists of two sub sets: the even and the odd ones. From the normalisation condition $g(o)=1$, we find the first few iterates starting from $x_o=o$, as given by (3.34):

$$x_1 = 1$$
$$x_2 = \frac{1}{\alpha_{qp}}$$
$$x_3 = g(\frac{1}{\alpha_{qp}})$$
$$x_4 = \frac{1}{\alpha} g(\alpha_{qp}) \qquad\qquad (3.39)$$

The whole set lies in the interval $(\frac{1}{\alpha_{qp}}, 1)$. It is possible to rescale the set such that the new set (x_i') lies in the interval $(0,1)$. Using the rescaling rule [104]

$$x_1' = \frac{|x_i + |\frac{1}{\alpha_{qp}}||}{1 + |\frac{1}{\alpha_{qp}}|} \qquad\qquad (3.40)$$

The rescaled iterates are

$$x'_1 = 1$$

$$x'_2 = 0$$

$$x'_3 = \frac{g(\frac{1}{\alpha_{qp}}) - \frac{1}{\alpha_{qp}}}{1 - \frac{1}{\alpha_{qp}}} \quad \text{and}$$

$$x'_4 = \frac{\frac{1}{\alpha}g(\alpha_{qp}) - \frac{1}{\alpha_{qp}}}{1 - \frac{1}{\alpha_{qp}}} \tag{3.41}$$

Considering the first four iterates as given by (3.41), we find that the set consists of two subsets that are scaled by S_1 and S_2 respectively. The subsets are

$$S_1 = \frac{1}{x'_1 - x'_3} = \frac{1}{\ell_1}$$

$$S_2 = \frac{1}{x'_4 - x'_2} = \frac{1}{\ell_2} \tag{3.42}$$

In the first stage of the construction of the Cantor set the lengths ℓ_1 and ℓ_2 are given by

$$l_1 = x'_1 - x'_3$$

$$l_2 = x'_4 - x'_2 \tag{3.43}$$

Since the probabilities p_i are equal we have

$$S_1^{\tau} + S_2^{\tau} = 2^q \tag{3.44}$$

as the equation for computing c for different values of q.

The generalised dimensions D_q and the f-α values are computed using the method [22,32] reviewed in Chapter 1.

For any specific value of q chosen (3.44) is solved by a root finding procedure to get $\tau(q)$. Then

$$\alpha = \frac{\partial \tau}{\partial q} = \frac{2^q \ln 2}{S_1^\tau \ln S_1 + S_2^\tau \ln S_2} \tag{3.45}$$

f(α) is computed using the relation

$$f = \alpha q - \tau \tag{3.46}$$

The generalised dimensions D_q are then computed using:

$$\tau = (q-1)D_q \tag{3.47}$$

The D_q versus q curves for a few z values are shown in Fig. 3.5. It is clear that as z increases the change from -q to q becomes sharper. The D_q values tend to converge on the +q side while they are far apert on the -q side. In Fig. 3.6 the D_q values plotted against z are shown. Here we find that for any q, D_q varies continuously with z. D_q gets spread over a wide range, and the values are asymmetric about D_o, while for large q values, D_q gets closer and closer. The D_q values are very close for both negative and positive.

Using (3.45) and (3.46) we calculate α and the f-α curve for a few specific z values (See Fig. 3.7). As is evident from the D_q versus q curve, the f-α values crowd near the $D_{\pm\infty}$ region for large z while they are distributed uniformly over the curve for small α values and far apart for large α values. Moreover, the values of $D_{\pm\infty}$ region are not much different for different z values, while they differ

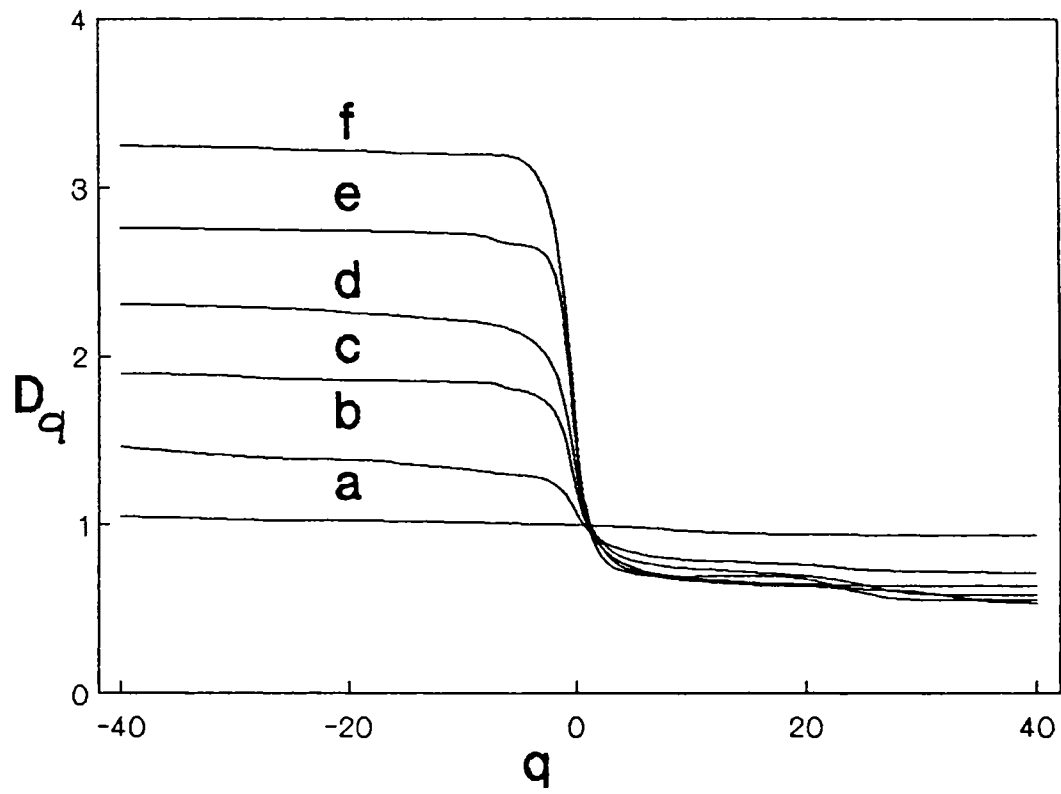Fig. 3.5 Plot of fractal dimensions D_q vs. q for typical z values

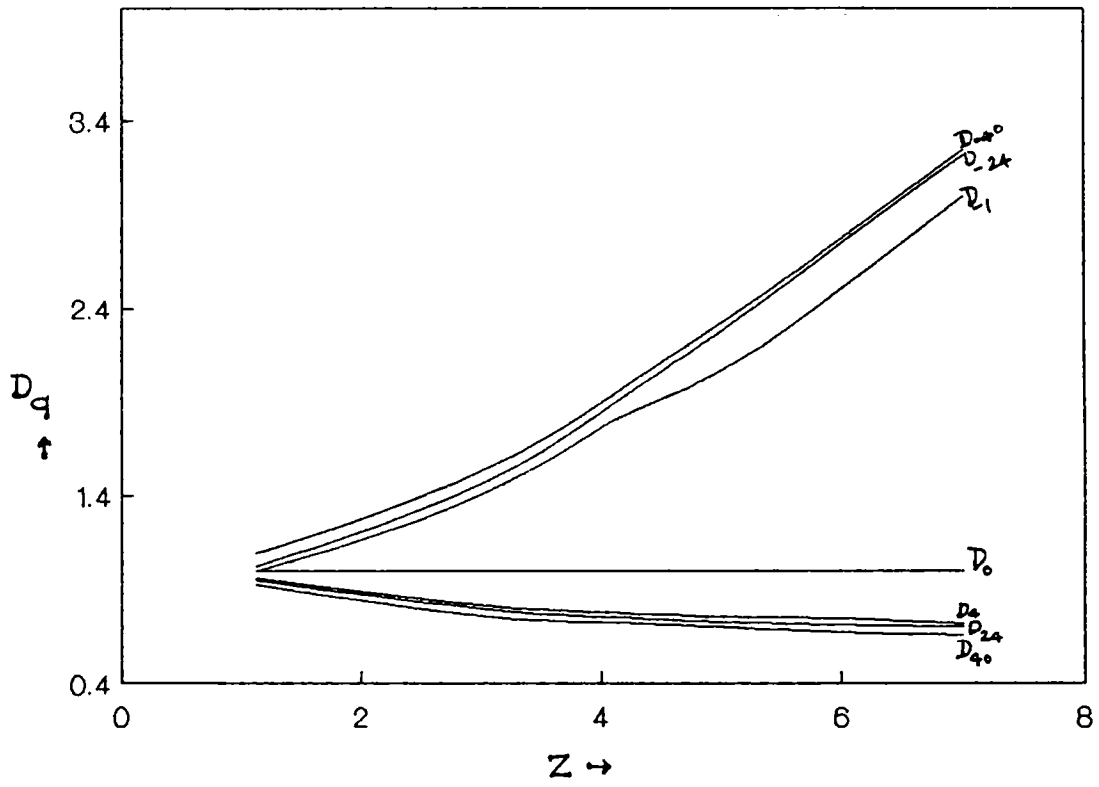a) z=1.1, b) z=2, c) z=3, d) z=4, e) z=5, f) z=6

Fig. 3.6 Dependence of fractal dimensions D_q on
          the degree of inflection point
          z of the map.

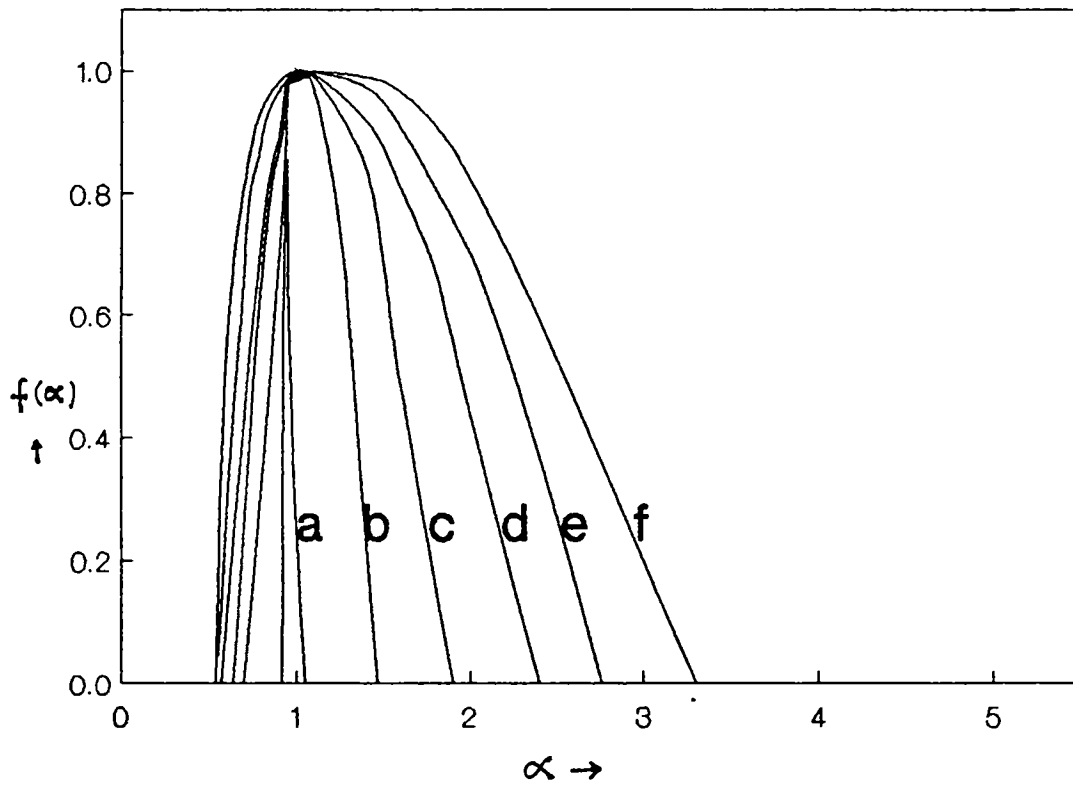Fig.3.7 The f against α curve for typical z values
a) z=1.1, b) z=2, c) z=3, d) z=4, e) z=5
f) z=6

considerably for the $D_{-\infty}$ region, revealing a difference in
different attractors which corresponds to rarefied regions.
There are usual physical situations where the experimentally
observed f-α curve agrees with that of the sine circle map
for small α values [101] but differs near large α values.
We conjecture that for such systems the discretised map may
be some polynomial circle map which may be different from
that for z = 3.

For large z values, say 50 and 100 as shown separately
in Fig. 3.8 , the f-α curves are flat at the top portion
with the exponents crowding along the flat region, leading
to the conclusion that as z increases, the points on the
attractor show a tendency towards a more or less uniform
distribution with the scaling exponents avoiding the most
rarefied and concentrated regions. This is in contrast to
the behaviour of the Feigenbaum attractor in 1-d maps where-
as our earlier calculations show that with increase in z,
the exponents crowd near the ends, revealing an increasing
tendency for bunching.

The end points of the f-α curves give the D_{∞} values
(α_{min}) and $D_{-\infty}$ values (α_{max}). In the context of quasiperiodic
route to chaos, these are given by [36]

$$D_{\infty} = \frac{\ell n \ w^*}{\ell n \ \alpha_{qp}^{-z}} \quad \text{and} \quad D_{-\infty} = \frac{\ell n \ w^*}{\ell n \ \alpha_{qp}^{-1}} \qquad (3.48)$$

where ϱ^* is the Golden Mean winding number

$$\varrho^* = \frac{\sqrt{5}-1}{2} \qquad\qquad (3.49)$$

By means of a set of computed α_{qp} values, we calculate D_∞ and $D_{-\infty}$ from (3.48). The results agree with those taken from the graph. The relevant results of our computation are collected in Table 3.4. For large z values, say 50 and 100, the calculated D_∞ and $D_{-\infty}$ values are used to complete the f-α curves in Fig. 3.8, where the variation of $D_{\pm\infty}$ with z is shown. From this we find that $D_{-\infty}$ is a monotonically increasing function of z while D_∞ decreases with z. It is clear from (3.48) that

$$\alpha_{max} = z\ \alpha_{min} \qquad\qquad (3.50)$$

Our graphical values also establish this relation as is evident from Table 3.3. This is a universal relation that is true for any z value. From an experimentally observed f-α curve, using (3.50), one can fix the value of z and hence the map of relevance. The fact that the same relation holds for the period-doubling rate in 1-d maps [86], gives added significance to the result.
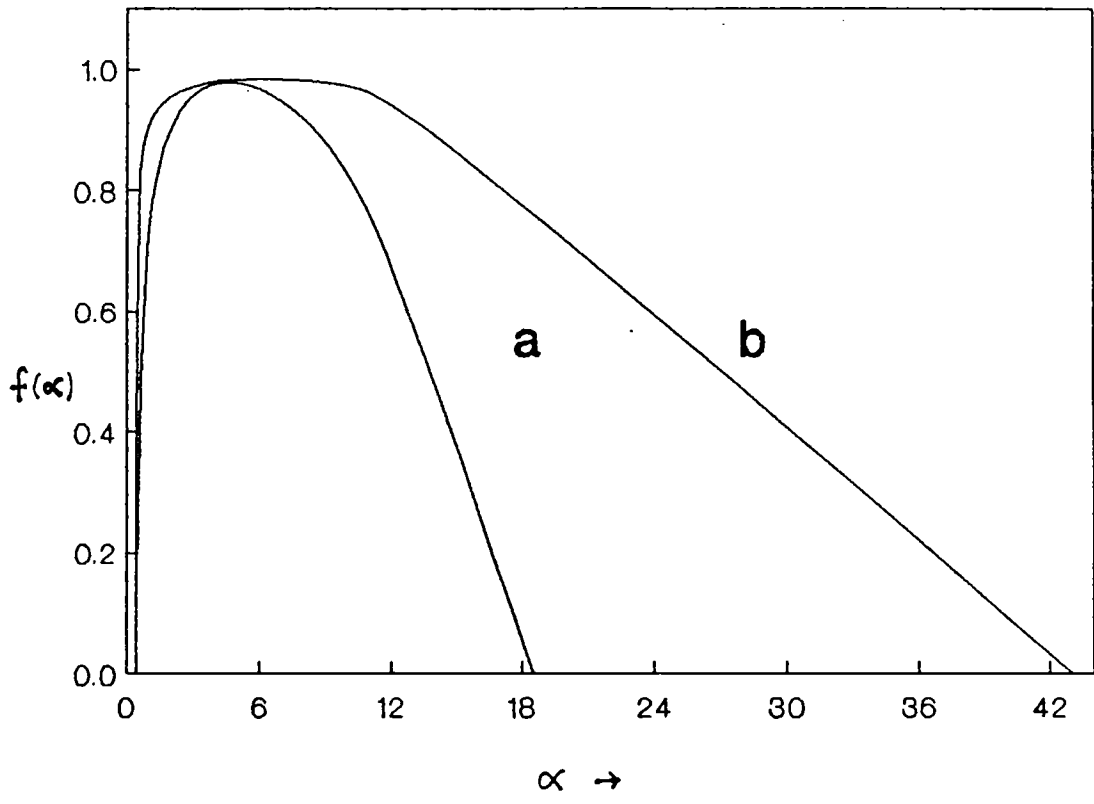
Fig. 3.8   The f against α curve for typical z values

a) z=50, b) z=100

Table 3.4. $\delta(z)$ versus z

z	δ (calculated)	δ (numerical)
1.1	-1.60804	-
2	-2.70671	-2.707
3	-2.83350	-2.833
4	-2.94576	-2.946
5	-3.04017	-3.040
6	-3.19190	-
50	-3.98979	-
100	-4.01414	-

Table 3.5. $D_{+\infty}$ values computed graphically
(Numerical values are given for comparison)

z	$D_{+\infty}$		$D_{-\infty}$	
	Calculation	graph	Calculation	graph
1.1	0.936975	0.940	1.0306734	1.04
2	0.7089859	0.706	1.4660502	1.47
3	0.6325329	0.64	1.8982408	1.8
4	0.578794	0.572	2.314572	2.4
6	0.460973	0.53	3.2366341	3.3
50	0.460973	0.458	22.11329	-
100	0.4399172	0.44	43.98728	-

3.5 Discussion

It is observed that for the polynomial circle map, $\alpha(z)$ is a decreasing function of z while $\delta(z)$ is an increasing function of z. The asymptotic limit of $\alpha(z)$ obtained analytically tends towards -1, while that of $\delta(z)$ to -4, in agreement with the numerical result. The fact that this rigorous bound holds for the quasiperiodic route is an interesting result, since in the period doubling route also such a bound is known to exist [59,60].

The perturbation method furnishes the singularity spectrum $f(\alpha)$ and the generalised dimension D_q for a general circle map with the order of inflection z, and it applies to any z. For z=3, the f-α curve has been determined earlier universally [36,97]. This method being purely analytic in nature, avoids lengthy computations and applies to any z. The accuracy of the method can be further enhanced by employing higher order terms in the construction of the attractor in (3.37). From the calculated values of $D_{\pm\infty}$ a universal relation connecting $D_{\pm\infty}$ with z is also established in analogy with the period-doubling route. The asymptotic values of the dimensions D_q are very small for small z values while they are far apart for large z values.
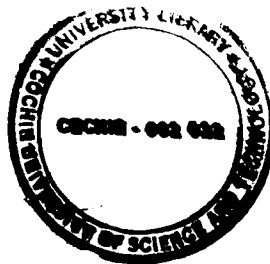
Thus this perturbative method coupled with the Padé
technique has the advantage that an analytic $g(x)$ is used
with the accuracy being determined by the number of terms
in $g(x)$.   It yields the best values in a small number of
steps.

CHAPTER IV

SYMMETRIES IN DISSIPATIVE SYSTEMS

4.1 Introduction

Symmetry holds considerable fascination for modern physics. The appeal of symmetry seems to transcend its usefulness and importance in crystallography, quantum theory, elementary particle physics and so forth.

By symmetry we mean the invariance of an object under a specified type of transformation. If an object or a physical process remains unchanged under a given operation such as translation, rotation or reflection, the particular operation is called a symmetry operation or symmetry. A self-contained set of symmetries forms a symmetry group. Symmetries can be broadly classified into external and internal types. An external symmetry corresponds to invariance under an operation such as rotation, translation or reflection that is thought to be, or actually, carried out outside the object while an internal symmetry implies invariance under transformations in an internal abstract space. Examples of internal symmetry are electric charge, isospin, strangeness, and hypercharge rotations defined for elementary particles.

One of the remarkable phenomena in dissipative dynamics is pattern formation, which is normally associated with the presence of instabilities. Various physical as well as nonphysical systems, including biological ones, belong to this category. A familiar example exhibiting this mechanism is that of thermal convection of a fluid between two infinite plates subject to a temperature gradient. Beyond a critical temperature difference between the upper and lower surfaces, the initial passive state gets destabilised and is replaced by a roll pattern or hexagonal pattern, discovered by Bénard [10]. The actual pattern that is formed depends on the vessel geometry. When the heating is continued further and further, the liquid may undergo a sequence of instabilities leading to oscillatory rolls and finally to chaos. One possible way of looking at these instabilities is that they are caused by symmetry breaking. It is interesting to note that the phenomena of breaking and restoration of symmetries appear in the bifurcation diagrams of many dynamical systems [114].

As mentioned in Ch. I, a dissipative system is modelled by a first order autonomous system of differential equations,

$$\dot{x} = F_{\lambda}(x), \tag{4.1}$$

where λ is the control parameter, and by analogy with phase transition theory, the phase space vector x will be called

the order parameter vector. In the present investigation
we deal with the case where both x and F belong to $\mathbb{R}^n$.

A symmetry of the system (4.1) is a mapping

$$x \rightarrow x', \quad F_\lambda(x) \rightarrow F_\lambda'(x') \tag{4.2}$$

that leaves (4.1) invariant:

$$\dot{x}' = F_\lambda'(x') \tag{4.3}$$

for a fixed value of λ. In this work we consider time-
dependent translations, rotations and scale transformations
of the phase space.

If Σ denotes translation, rotation or a combination
thereof, its effect on x is defined by

$$x \xrightarrow{\Sigma} x', \quad F_\lambda(x) \xrightarrow{\Sigma} F_\lambda(x') \tag{4.4}$$

Since Σ is continuously implementable an infinitesimal
version can always be considered.

$$x \xrightarrow{\delta\Sigma} x+\delta x, \quad F_\lambda(x) \xrightarrow{\delta\Sigma} F_\lambda(x+\delta x) \tag{4.5}$$

For fixed x, an infinitesimal symmetry operation of this
kind is a fluctuation. A fluctuation δx is said to be a
normal mode fluctuation if it can be represented in the
form

$$\delta x = \delta x_o \exp(\omega_f t) \tag{4.6}$$

where ω_f is called the fluctuation or normal mode exponent.

If $\omega_f \geq 0$ the corresponding symmetry Σ is said to be spontaneously broken at the reference point $x = \xi$; if $\omega_f < 0$, Σ remains unbroken at ξ. Also, it is clear that $\omega_f = \omega_f(\xi, \lambda)$ and consequently, this criterion is only of local significance. But when the stability of a specified kind of symmetry is considered in a finite region, certain regularities may be revealed in the distribution of the particular type of stability. The phrase, spontaneous symmetry breaking (SSB), is herein used in the sense that, eventhough the original system of equations remains invariant, no stable trajectory is available through the point in question. In standard linear stability analysis fluctuations are considered about a critical point x_c, defined by $\dot{x}_c = 0$. A critical point will be asymptotically stable or unstable depending on the value of the control parameter.

We shall introduce some more jargon to enable us to discuss SSB. The point $x = 0$ is called the ordinary equilibrium or ordinary vacuum. Any other critical point $x_c = \xi$, $\dot{\xi} = 0$, is called a higher equilibrium or higher vacuum. It is often the case that fluctuations about a higher equilibrium do not possess all the symmetries exhibited by those around the ordinary equilibrium. In the Lorenz model, for instance, the order parameter is a three vector (x_1, x_2, x_3) and the Lorenz equations possess the inversion symmetry $(x_1, x_2) \rightarrow (-x_1, -x_2)$, $x_3 \rightarrow x_3$, besides translation and rotation invariances. However, this discrete symmetry is

maintained only with respect to fluctuations about
the ordinary equilibrium (0,0,0) but is broken in
other cases. This is a trivial example of SSB. Not
only these discrete symmetries, but continuous symme-
tries such as translation and rotation are broken
spontaneously (in the sense explained above) in certain
regions of phase space. Such regions can be identified
by means of linear stability analysis appropriate to
the symmetry in question.

4.2 Translation symmetry

If we assume translation invariance in phase space,
then (4.1) gives

$$\dot{x} + \dot{\epsilon} = F_\lambda \ (x+\epsilon) \tag{4.7}$$

for an infinitesimal displacement ϵ . Taylor-expanding
the r.h.s. about a particular point $x = \xi$ and using
(4.1) we get

$$\dot{\epsilon} = F_\lambda' \ (\xi) \cdot \epsilon \tag{4.8}$$

where F_λ' is the Jacobian matrix. Assuming a normal
mode solution,

$$\epsilon = \epsilon_o \ \exp(\omega_t t) \tag{4.9}$$

(4.8) yields

$$\omega_t \ \epsilon_o = F_\lambda' \ (\xi) \cdot \epsilon_o \tag{4.10}$$

The translational normal mode exponents ω_t are the roots of the characteristic equation

$$|F'_\lambda (\xi) - 1 \omega_t(\xi, \lambda)| = 0 \qquad (4.11)$$

When $\xi = x_c$, (4.11) coincides with the criterion employed in customary linear stability analysis. In the present context it is the consequence of a postulated translation symmetry in phase space. The modes $\omega_t(\xi, \lambda)$ in general correspond to transients. In the light of the criteria spelt out earlier, if there is at least one $\omega_t(\xi, \lambda)$ which is ≥ 0, translation invariance is said to be spontaneously broken at $x = \xi$.

4.3 Rotation symmetry

A rotation in an n-dimensional phase space is defined by

$$x \to x' : x' = Rx \qquad (4.12)$$

where R is a nonsingular matrix in $\mathbb{R}^n$. Let

$$R = 1 + \delta \qquad (4.13)$$

where δ is an antisymmetric matrix of infinitesimals $(\delta_1, \delta_2, \ldots, \delta_p)$ with $p = n(n-1)/2$.

Imposing rotational invariance for the system we have

$$\dot{x}' = F_\lambda(x') \qquad (4.14)$$

For a reference point $x = \xi$, an infinitesimal rotation

gives

$$\dot{\xi} + \delta\dot{\xi} + \dot{\delta}\xi = F_\lambda (\xi + \delta\xi) \qquad (4.15)$$

A rotational normal mode is described by the relation

$$\delta = \delta_o \exp (\omega_r t) \qquad (4.16)$$

where δ_o is an antisymmetric constant matrix.

Hence we find

$$\omega_r \delta_o \xi + \delta_o F_\lambda (\xi) = F'_\lambda (\xi) \delta_o \xi \qquad (4.17)$$

Comparing this equation with (4.10) for $\xi = x_c$,

it follows that

$$\omega_r(x_c) = \omega_t(x_c) \text{ and } \delta_o(x_c) = \epsilon_o \qquad (4.18)$$

modulo some normalisation constant. It is clear that at a critical point translational and rotational symmetries co-exist provided the corresponding ω values are all negative. At any other point the two symmetries need not coexist.

As (4.17) constitutes a system of linear homogeneous equations in the δ_o unknowns, a consistency condition can be written for the existence of nontrivial solutions. This turns out to be an algebraic equation for ω_r. Contrary to expectations, when $n \geq 2$ the degree of this equation is only $n-1$, an apparent consequence of the antisymmetry of the $\tilde{\delta}_o$ matrix. Just as in the case of translational invariance we say that at any point $x = \xi$ in phase space rotational invariance is spontaneously broken if at least one of the ω_r values is ≥ 0.

According to the characterization given in Ch.I,
two trajectories on a strange attractor which are
arbitrarily close initially, diverge exponentially
with time. From a symmetry point of view we may
assume that such a region corresponds to the overlap
of domains with non-negative ω_t and ω_r values, signal-
ling spontaneous breaking of translation and rotation
symmetries.

4.4 Scale symmetry

Scale invariance is a fundamental symmetry in linear
physics but its role in non-linear phenomena is not very
clear. For the sake of completeness, here we discuss
it in an elementary way. Let us consider a dissipative
system described by a homogeneous flow vector $F_i(x)$ in
phase space. A scale transformation is then of the
form

$$x_i \rightarrow \Sigma x_i$$
$$F_i \rightarrow \Sigma^{\Delta_i} F_i(\Sigma x_i)$$

(4.19)

where Σ is a constant scalar scale parameter and the
dependence of F_i on the control parameter is suppressed;
Δ_i is the scaling index for the function F_i. We wish
to remark that most non-linear models studied in the
literature do not satisfy the criterion of homogeneity.

An infinitesimal static scale transformation is taken in the form $\sigma = 1+\sigma$, where σ is infinitesimal. Then we have

$$\dot{x}_i = (1+\sigma)^{\Delta_i - 1} F_i[(1+\sigma)x]$$

or

$$\dot{x}_i = [1+(\Delta_i - 1)\sigma] F_i(x+\sigma x) \tag{4.20}$$

At a given point $x = \xi$, we obtain to $O(\sigma)$,

$$\Delta_i(\xi) \approx 1 - \sum_j F_{ij} \xi_i / F_i \tag{4.21}$$

where $F_{ij}(\xi) = \dfrac{\delta F_i(\xi)}{\delta \xi_j}$

The above notion of static scale transformations may be extended to include dynamic or time-dependent scale transformations:

$$x \rightarrow \Sigma(t) x$$
$$F(x) \rightarrow \Sigma^{\Delta}(t) F(\Sigma(t)x) \tag{4.22}$$

Here $\Sigma(t)$ is a time dependent matrix of order N and Δ is a (scalar) scaling index that is assumed to be independent of time. It may be noted that Δ is introduced for the entire system of n differential equations.

In the infinitesimal case let us set

$$\Sigma(t) = 1+\sigma(t) \tag{4.23}$$

where $\sigma(t)$ is a matrix of infinitesimal components. Then the dynamically scaled equations of motion read:

$$\frac{d}{dt} (1+\sigma(t))x = (1+\sigma(t))^{\triangle} F_\lambda (1+\sigma(t))x \qquad (4.24)$$

Replacing $(1+\sigma(t))$ by $1+\triangle\sigma(t)$ and choosing a specific point $x = \xi$ we find

$$\dot{\sigma}\xi + \sigma F_\lambda (\xi) = \triangle\sigma F_\lambda (\xi) + F'_\lambda (\xi)\sigma \xi \qquad (4.25)$$

To determine the local stability of a dynamically scaled trajectory passing through the point $x = \xi$, we use the normal mode ansatz:

$$\sigma(t) = \sigma_0 \exp(\omega_s t) \qquad (4.26)$$

yielding the equation

$$\omega_s \sigma_0 \xi + (1-\triangle)\sigma_0 F_\lambda(\xi) = F'_\lambda (\xi)\sigma_0 \xi \qquad (4.27)$$

At a critical point this becomes

$$F' (x_c)\sigma_0 x_c = \omega_s \sigma_0 x_c \qquad (4.28)$$

This equation defines the same eigenvalue problem as considered in the two preceding sections. Hence (4.18) is extended to include dynamic scaling besides translation and rotation invariances:

$$\epsilon_0 = \delta_0 x_c = \sigma_0 x_c \qquad (4.29)$$

upto normalizations. If follows trivially that σ_o tends
to be an antisymmetric matrix δ_o (modulo normalization)
as $x \to x_c$.

Thus we find that in systems which permit scale tran-
sformations, scale invariance coexists with translation
and rotation invariances at critical points. Thanks to
the antisymmetry of the σ_o and δ_o matrices, infinitesimal
rotation and infinitesimal dynamical scale transformations
are almost indistinguishable near a critical point.

It may be noted that the appearance of the matrix
$\Sigma(t)$ in the definition of dynamic scaling distinguishes
this kind of transformation from static scaling. $\Sigma(t)$
defines a time-dependent linear transformation of a very
special type, because of the particular transformation
rule postulated for $F(x)$ (See (4.22)). Under $\Sigma(t)$ the
flow functions $F_i(x)$ are also assumed to be transformed
in a non-trivial way. Here the resemblance to the static
scaling transformation (4.19) is only superficial.

In the next (and last) chapter a numerical study of
translation and rotation symmetries in Lorenz and Rössler
models is attempted using the formatism developed herein.

CHAPTER V

ANALYSIŞ OF TRANSLATION AND ROTATION SYMMETRIES
IN MODEL SYSTEMS EXHIBITING CHAOS

5.1 Introduction

Eventhough various routes to chaos in dissipative
systems have been identified and understood to a large
extent, little is known about the dynamics from a
symmetry point of view. An understanding of this
requires a knowledge of how translation and rotation
symmetries fare in phase-space. It is in this context
that we examine the dynamics of such models as Lorenz
and Rössler which exhibit complex behaviour. It should
be realised that even if various evolution centres are
localised, it can still be a consequence of spontaneous
breaking of rotation and translation symmetries at
particular points.

In this chapter, we carry out a detailed numerical
study of the Lorenz and Rössler models in a symmetry
framework. To start with, we compute the translational
and rotational normal mode exponents for varying control
parameter values, and a plot of these values versus the

control parameter indicates that the formation of
stable patterns depends on the spontaneous breaking
of rotation and translation symmetries. In order to
study the behaviour in detail, we make use of a
quantitative measure, namely the probability for the
occurrence of stable points for a fixed parameter value.

5.2 The Lorenz system

The Lorenz model, briefly mentioned in the preceed-
ing chapter, is a set of partial differential equations
[20], which appears to have aroused considerable interest
in recent years [112]. The system was proposed as a
simplified model for describing Bénard convection in a
fluid layer heated from below. Convective phenomena
that occur in the fluid can be explained in terms of
three nondimensionalised equations, one of which describes
the coupled transport of momentum of the fluid. The
velocity field $\vec{v}$ satisfies the Navier-Stokes equation

$$\frac{1}{S} [\frac{\partial \vec{v}}{\partial t} + \vec{v}. \; \vec{\nabla}\vec{v}] = -\vec{\nabla}p + \Theta\lambda + \nabla^2 v \qquad (5.1)$$

Here we define the Prandtl number $S = \frac{\nu}{D_T}$ where ν is the
kinetic viscosity of the fluid, D_T the thermal diffu-
sivity, P the hydrostatic pressure, $\vec{\lambda}$ the unit vector
along the vertical axis in the direction of gravity,
$\Theta(\vec{r},t)$ the temperature deviation.

The incompressibility of the fluid is expressed by

$$\vec{\nabla} . \vec{v} = 0 \qquad (5.2)$$

and the heat propagation through the temperature deviation $\Theta(\vec{t}, t)$:

$$\frac{\partial \Theta}{\partial t} + \vec{v} . \vec{\nabla} \Theta = R_a \vec{\lambda} . \vec{v} + \vec{\nabla}^2 \Theta \qquad (5.3)$$

where R_a is the Rayleigh number

$$R_a = \frac{\rho_o \, g\alpha d^3}{\eta \, D_T} \, \delta_T \; ; \qquad (5.4)$$

g is the accleration due to gravity, ρ_o the mean density, α the expansion coefficient, η the dynamic viscosity and d the thickness of the fluid. The equations describing the fluid motion have an equilibrium solution when the fluid is at rest and the temperature varies with time. When the Rayleigh number $R_a < R_{a_c}$ (Critical Rayleigh number), the fluid remains at rest, while if $R_a > R_{a_c}$, the fluid becomes unstable and convection develops. Convective rolls are created between two plates, with adjacent rolls rotating in opposite directions with velocity $\vec{v}$.

Lorenz reduced the dynamical behaviour of the convective fluid into the following form by a three mode truncation of the Navier-Stokes equations:

$$\dot{x}_1 = F_1 = - S(x_1 - x_2)$$

$$\dot{x}_2 = F_2 = - x_2 + x_1 x_3 + \gamma x_1$$

$$\dot{x}_3 = F_3 = x_1 x_2 - b x_3 \qquad\qquad (5.5)$$

Here x_1 is the amplitude of the convective motion, x_2 the temperature difference between ascending and descending currents and x_3 is the distortion of the vertical temperature profile from linearity. It is interesting to note that the same system of equations can be obtained for single mode lasers by truncating the Maxwell-Bloch equations [6,10,115]. The values of the parameter S and b are fixed. Usually S=10 and $b = \frac{8}{3}$ and γ is taken as the control parameter.

The system given by (5.5) is dissipative. The volume V of the small domain of phase-space, where each point moves according to (5.5), varies according to the law:

$$\dot{V} = \Omega V$$

$$\Omega = \frac{\partial \dot{x}_1}{\partial x_1} + \frac{\partial \dot{x}_2}{\partial x_2} + \frac{\partial \dot{x}_3}{\partial x_3} = - (S+b+1) \qquad (5.6)$$

That is, the volume is reduced by a factor of $e^{-(S+b+1)}$ in each unit of time. As mentioned in Ch. IV, the equations are invariant under the transformation $x_1 \rightarrow -x_1$, $x_2 \rightarrow -x_2$, $x_3 \rightarrow x_3$. Furthermore, the x_3 axis is invariant in the sense that any trajectory starting at, or passing through,

a point $(0,0,x_3)$ on the x_3 axis, remains on the x_3 axis, but all such trajectories approach the origin. The nature of the phase-space trajectories varies with γ. When $\gamma < 1$ the coordinate origin is globally attracting $x_1 \to 0$, $x_2 \to 0$, $x_3 \to 0$. That is, there is no convection. An obvious fixed point of the Lorenz system is the origin. For $\gamma = 1$, the linearised problem that determines the stability of the origin as a fixed point has a zero eigenvalue. Bifurcation occurs and as a result, the origin loses stability and for $\gamma > 1$, two symmetric fixed points appear:

$$x_1 = \pm\sqrt{(b(\gamma-1))} \; ; \; x_2 = \pm\sqrt{(b(\gamma-1))} \; ; \; x_3 = (\gamma-1) \tag{5.7}$$

That is, a pitchfork bifurcation occurs here as a consequence of invariance under inversion symmetry. Physically, they correspond to the onset of convection, each being associated with one of the two possible directions of rotation. The stability of the fixed point may be investigated by linearising the Lorenz equations about the fixed point and finding the eigenvalues of the resulting 3x3 matrix. For the linearised flow near the origin these eigenvalues are

$$\lambda = -b$$
$$\lambda_{1,2} = \frac{-1}{2}(S+1) \mp ((S-1)^2 + 4S\gamma)^{1/2} \tag{5.8}$$

One of these eigenvalues is positive whenever $\gamma > 1$, and so the origin is an unstable fixed point for $\gamma > 1$. For $\gamma < 1$ all

trajectories approach the origin and two of the eigenvalues
of the linearised flow about the origin are always negative,
indicating a two dimensional stable manifold of the origin-
the set of points where a starting trajectory approaches
the origin as $t \to \infty$. The one dimensional unstable manifold
of the origin for $\gamma > 1$, on the other hand, consists of points
approaching the origin as $t \to -\infty$. At $\gamma = 1$, the fixed points
(5.7) are born, and a trajectory starting on the unstable
manifold of the origin for $\gamma > 1$ heads for that fixed point
lying in the same half space. The trajectory spirals
towards the fixed point. As γ increases the spiral loops
get larger.

When γ is increased beyond $\gamma = \gamma' = 13.926$, the spiral
loops have become large enough so that they become attracted
to the fixed point in the opposite half space. At $\gamma = \gamma'$,
a trajectory starting out on the unstable manifold of the
origin is eventually attracted to the origin. That is,
the unstable manifold of the origin lies within its stable
manifold, giving rise to a homoclinic orbit - a trajectory
tending to the fixed point for both $t \to \infty$ and $t \to -\infty$. This
homoclinic orbit gives way to an unstable limit cycle.
At $\gamma = \gamma'' = 24.06$, the unstable manifold of the
origin spirals onto the unstable limit cycle rather than
a stable fixed point. Between $\gamma = \gamma''$ and $\gamma = \gamma_c = 24.71$
trajectories settle onto a chaotic attractor or one of the

stable fixed points, depending on the initial conditions. At $\gamma = \gamma_c$ the unstable limit cycle collapses onto the fixed points, and beyond $\gamma = \gamma_c$, all three fixed points are unstable; only the chaotic attractor remains. For $\gamma \in (24.74, 30.1)$ the strange attractor constitutes the only possible solution of the flow. For very large γ values all trajectories are attracted towards a stable limit cycle. Above $\gamma = 30.1$ and until $\gamma = 214$, the diagram of solutions becomes extremely complex with alternation of periodic and chaotic regimes. The windows of periodicity are infinite in number. They are the domains for different periodic attractors. Slightly before the actual beginning of the window of periodicity, an inverse cascade of bifurcations is observed. This inverse cascade is succeeded by a direct subharmonic cascade which ends with the basic limit cycle, the whole constituting the window of periodicity. The windows of periodicity for the Lorenz system are described by

$$99.524 < \gamma < 100.795$$
$$145 \quad < \gamma < 166$$
$$214.364 < \gamma$$

Here the last window of periodicity begins at $\gamma = 214.364$ terminating an inverse cascade which begins at $\gamma = 197.4$. The direct cascade ends at $\gamma = 313$, above which there remains only the corresponding basic limit cycle as stable attractor. In the limit of large γ values, the ultimate

attractor is a limit cycle.

5.3 Pattern of spontaneous symmetry breaking in the Lorenz model

The Lorenz model has been found to describe varied physical situations such as irregular spiking in lasers [6,116,117] and the dynamics of weakly unstable finite amplitude baroclininic waves. We have chosen this model to test the concepts introduced mainly because it is the most well studied system in the literature, and as such there exists a wealth of numerical data to guide us. It is also typical of different kinds of behaviour such as preturbulence, intermittency, period-doubling, strange attractor etc.

We have, from (4.11), for translational symmetry,

$$\begin{vmatrix} F_{11} - \omega & F_{12} & F_{13} \\ F_{22} & F_{22} - \omega & F_{23} \\ F_{31} & F_{32} & F_{33} - \omega \end{vmatrix} = 0 \quad (5.9)$$

with $F_{ij} = \dfrac{\partial F_i}{\partial x_j}$

Here

$$F_{11} = -S \quad , \quad F_{12} = S \quad , \quad F_{13} = 0 \quad ,$$
$$F_{21} = \gamma - x_3 \quad , \quad F_{22} = -1 \quad , \quad F_{23} = -x_1 \quad ,$$
$$F_{31} = x_2 \quad , \quad F_{32} = x_1 \quad , \quad F_{33} = -b \cdot$$

The eigenvalue equation for translational symmetry is

$$\omega^3 - A_1\omega^2 - A_2\omega + A_3 = 0 \qquad\qquad (5.10)$$

where

$$A_1 = - (F_{11} + F_{22} + F_{33})$$

$$A_2 = F_{22}F_{11} + F_{22}F_{33} + F_{33}F_{11} - F_{23}F_{32} - F_{21}F_{12} - F_{13}F_{31}$$

$$A_3 = F_{11}F_{23}F_{32} + F_{12}F_{21}F_{33} + F_{13}F_{31}F_{22} - F_{11}F_{22}F_{33}$$

$$- F_{12}F_{23}F_{31} - F_{13}F_{21}F_{32}$$

We have investigated translational symmetry in the phase-space of the Lorenz model for varying γ (Fig.5.1). It is found that one of the eigenvalues ω_t is always negative irrespective of the reference point in question, reflecting the dissipative nature of flow characterised by the global contraction of the phase-space. The other two eigenvalues ω_t do alone determine stability against translational symmetry breaking. Evidently, for this system at $\gamma=1$ one of the eigenvalues ω_t vanishes and retains positive value for γ value beyond unity. So one can draw the conclusion that, when the fixed point becomes unstable, translational symmetry in phase-space is broken. Extending the stability analysis for points other than fixed points in the x_1-x_2 plane for $x_3=\gamma-1$ we find that, beyond $\gamma=1$, the structure of stable and unstable regions
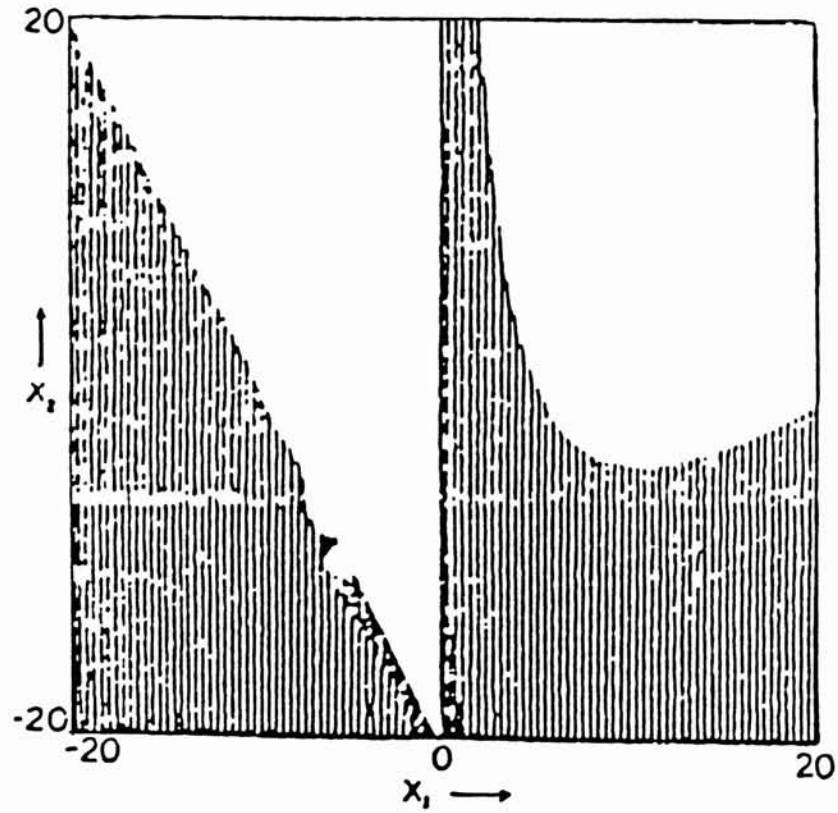
Fig.5-1 Stable and unstable regions in
the x_1-x_2 plane for translational
symmetry. The shaded regions
correspond to stable regions.

is independent of γ, leading to the conclusion that it is only the fixed point which does depend on γ.

We have pursued the analysis in the arbitrary $x_1 - x_2$ plane for arbitrarily fixed x_3 value, and it is seen that the patterns shift for high γ values (Fig.5.2). We have plotted ω values against γ abcissae. As is evident, one of the eigenvalues keeps on decreasing while the other two increase with γ [Fig. 5.3].

Turning to the rotation symmetry aspect, we have from eqn. (4.17),

$$F' \, \epsilon_0 \, x - \epsilon_0 \, F - \omega \, \epsilon_0 \, x = 0 \qquad\qquad (5.11)$$

where $F = F_\lambda$, and F' is the Jacobian of the F matrix introduced in the preceding chapter.

Substituting the following three parameter form for the infinitesimal rotation matrix

$$\epsilon_0 = \begin{pmatrix} 0 & \epsilon_3 & -\epsilon_2 \\ -\epsilon_3 & 0 & \epsilon_1 \\ \epsilon_2 & -\epsilon_1 & 0 \end{pmatrix} \quad , \quad |\epsilon_i| << 1 \, . \qquad (5.12)$$
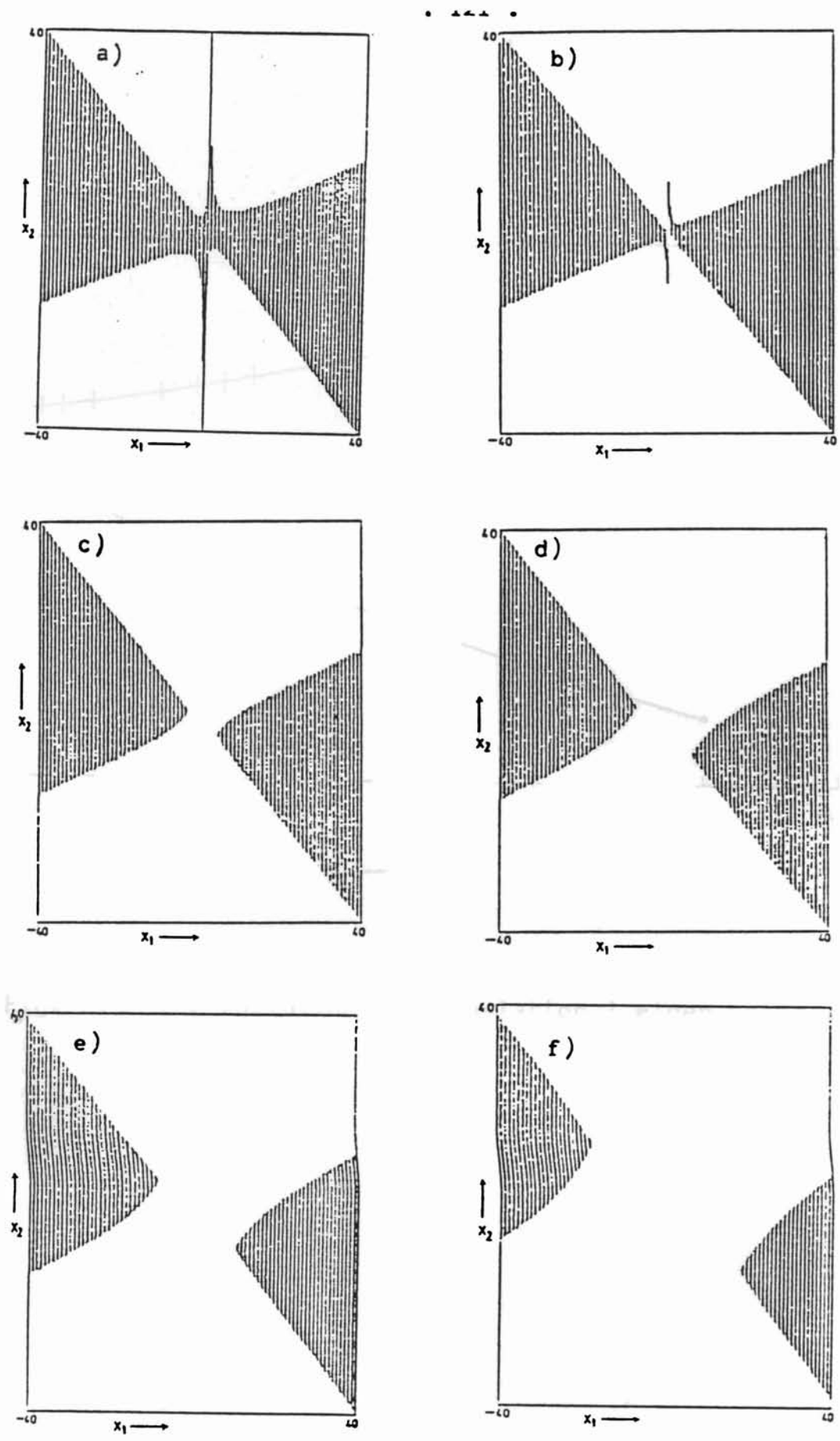
Fig. 5.2   Stable and unstable regions in the x_1-x_2 plane for
translational symmetry for fixed $x_3 = 27$ and for
varying γ. a) $\gamma=13$, b) $\gamma=28$, c) $\gamma=99.5$, d) $\gamma=100.5$
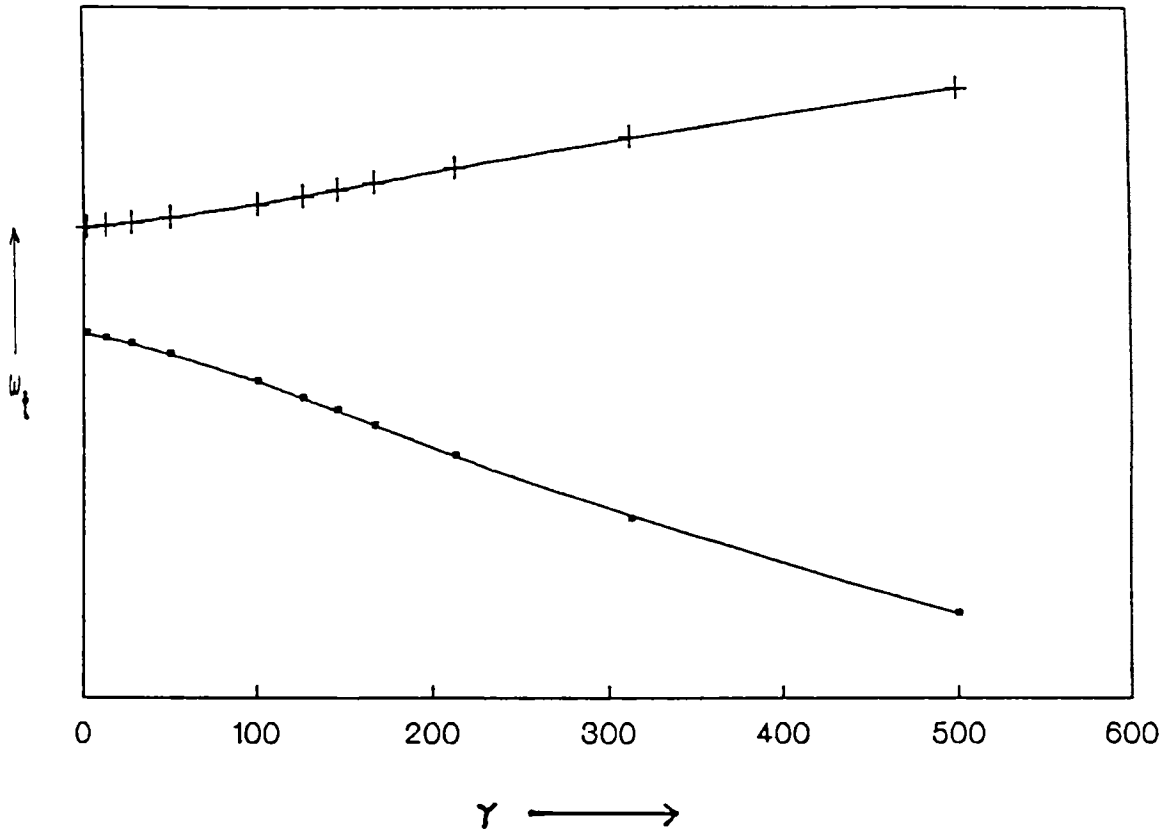e) $\gamma = 166.3$, f) $\gamma = 500$

Fig. 5.3 The variation of translational eigen value ω_t with γ.

We get

$$\begin{bmatrix} F_{11} & F_{12} & F_{13} \\ F_{21} & F_{22} & F_{23} \\ F_{31} & F_{32} & F_{33} \end{bmatrix} \begin{bmatrix} 0 & \epsilon_3 & -\epsilon_2 \\ -\epsilon_3 & 0 & \epsilon_1 \\ \epsilon_2 & -\epsilon_1 & 0 \end{bmatrix} \begin{bmatrix} x_1 \\ x_2 \\ x_3 \end{bmatrix} - \begin{bmatrix} 0 & \epsilon_3 & -\epsilon_2 \\ -\epsilon_3 & 0 & \epsilon_1 \\ \epsilon_2 & -\epsilon_1 & 0 \end{bmatrix} \begin{bmatrix} F_1 \\ F_2 \\ F_3 \end{bmatrix}$$

$$- \omega \begin{bmatrix} 0 & \epsilon_3 & -\epsilon_2 \\ -\epsilon_3 & 0 & \epsilon_1 \\ \epsilon_2 & -\epsilon_1 & 0 \end{bmatrix} \begin{bmatrix} x_1 \\ x_2 \\ x_3 \end{bmatrix} = 0 \qquad (5.13)$$

or equivalently,

$$(F_{12}x_3 - F_{13}x_2)\epsilon_1 + (F_{13}x_1 - F_{11}x_3 + F_3 + \omega x_3)\epsilon_2$$
$$+ (F_{11}x_2 - F_{12}x_2 - F_2 - \omega x_2)\epsilon_3 = 0 \qquad (5.14)$$

$$(F_{22}x_3 - F_{23}x_2 - F_3 - \omega x_3)\epsilon_1 + (F_{23}x_1 - F_{21}x_3)\epsilon_2 +$$
$$+ (F_{21}x_2 - F_{22}x_1 + F_1 + \omega x_1)\epsilon_3 = 0 \qquad (5.15)$$

and

$$(F_{32}x_3 - F_{33}x_2 + F_2 + \omega x_2)\epsilon_1 + (F_{33}x_1 - F_{31}x_3 - F_1 - \omega x_1)\epsilon_2 \qquad (5.16)$$
$$+ (F_{31}x_2 - F_{32}x_1)\epsilon_3 = 0$$

The characteristic equation is

$$\begin{vmatrix} F_{12}x_3 - F_{13}x_2 & F_{13}x_1 - F_{11}x_3 + F_3 + \omega x_3 & F_{11}x_2 - F_{12}x_1 - F_2 - \omega x_2 \\ F_{22}x_3 - F_{23}x_2 - F_3 - \omega x_3 & F_{23}x_1 - F_{21}x_3 & F_{21}x_2 - F_{22}x_1 + F_1 + \omega x_1 \\ F_{32}x_3 - F_{33}x_2 + F_2 + \omega x_2 & F_{33}x_1 - F_{31}x_3 - F_1 - \omega x_1 & F_{31}x_2 - F_{32}x_2 \end{vmatrix} = 0$$

$$(5.17)$$

Substituting for the F_i and F_{ij} elements this becomes

$$\begin{vmatrix} Sx_3 & Sx_3+F_3+\omega x_3 & -S((x_2+x_1)+F_2+\omega x_2) \\ -(x_3-x_1x_2+F_3+\omega x_3) & -(x_1^2+(\gamma-x_3)x_3) & (\gamma-x_3)x_2+x_1+F_1+\omega x_1 \\ x_1x_3+bx_2+F_2+\omega x_2 & -(bx_1+x_2x_3+F_1+\omega x_1) & x_2^2-x_1^2 \end{vmatrix}=0$$

(5.18)

When expanded this equation reads

$$\omega^2\left\{Ax_1^2+Ix_3^2+Ex_2^2+(B+D)x_1x_2+(G+C)x_1x_3+(F+H)x_2x_3\right\}$$

$$+ \omega\left\{x_1(AF-AH+BG-CD) + x_2(BF-CE-HD+EG)\right.$$

$$\left.+ x_3(BI-ID+GF-CH)\right\} + \left\{A(EI-FH)+B(GF-ID)\right.$$

$$\left.+ C(HD-EG)\right\} = 0 \qquad (5.19)$$

where $A = Sx_3$

$B = Sx_3 + F_3 + \omega x_3$

$C = -(S(x_2+x_1) + F_2+\omega x_2)$

$D = -(x_3-x_1x_2 +F_3 +\omega x_3)$

$E = -(x_1^2 + (\gamma-x_3)x_3)$

$F = (\gamma-x_3)x_2+x_1+F_1+\omega x_1$

$G = x_1x_3+bx_2+F_2+\omega x_2$

$H = -(bx_1+x_2x_3+F_1+\omega x_1)$

$I = x_2^2 - x_1^2$

We have studied rotational symmetry of the Lorenz
model by computing ω_r values for varying γ by choosing
the plane $x_3 = \gamma - 1$. It should be remarked that for high
γ values the structure of the patterns is independent of
γ, as there exists only one eigenvalue in this case. In
fact for high γ values, the pattern consisting of stable
and unstable regions in an arbitrary x_1-x_2 plane also has
this property of γ-independence. However, for small
values of γ the pattern depends on the choice of the x_1-x_2
plane. i.e., on the value that we fix for x_3. Generally
where $x_3 \sim \gamma$, more stable regions are found to develop
symmetrically and thereafter, there is a slow evolution
of the structure of stable and unstable regions as γ keeps
changing. In Fig. 5.4 we display this change for a few
chosen values of γ. However, before and after period-
doubling, or in the region of intermittency, there is no
marked or sudden change in the pattern. This is clear from
Fig. 5.4, e-f. The boundary separating stable and unstable
regions becomes more and more well defined as γ is increased.
A plot of rotational ω_r values versus γ is given in Fig.5.5.
One of the rotational eigenvalues is zero for all γ values.
At the parameter value where a strange attractor emerges,
there is a large variation in the rotational eigenvalue ω_r.

To express the evolution more quantitatively, as
evident from Fig. 5.6, we have computed the number N_s of
stable points in a unit square that correspond to negative
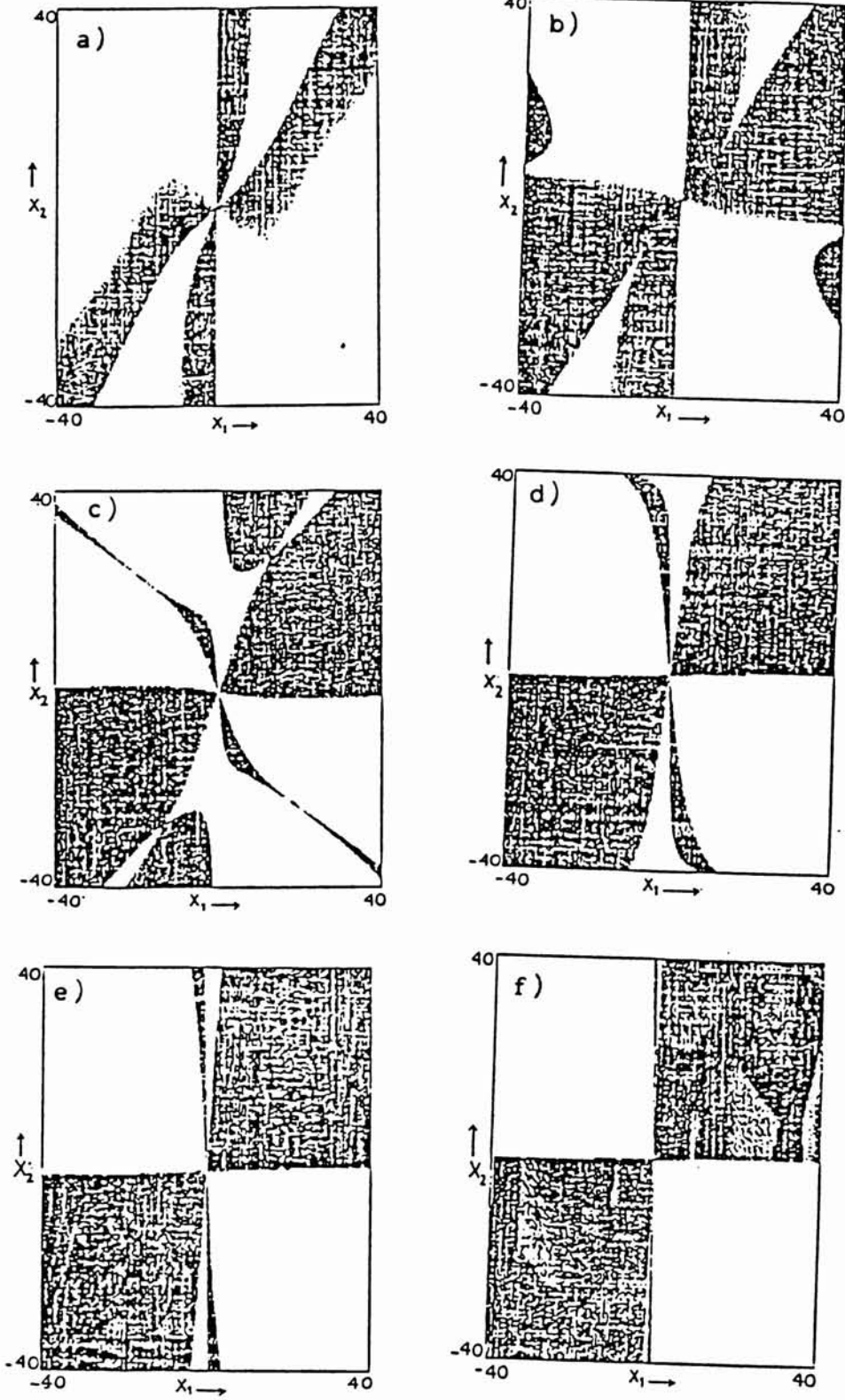
Fig. 5.4   Patterns showing rotationally stable and
           unstable regions in the x_1-x_2 plane for
           different values of γ.   Here $x_3=27$

           a) $\gamma = 13$ b) $\gamma = 28$ c) $\gamma = 50$

           d) $\gamma = 99.529$ e) $\gamma = 166.3$ f) $\gamma = 500$

Fig. 5.5   The variation of rotational eigen value
of ω_r with γ .

Fig. 5.6 The variation of P along the x_1 direction with $x_3 = 27$ and $x_2 = 10$ and for chosen values of γ :

a) = 13   b) =28   c) =99.5
d) = 166.3   e) =100.5   f) =500

values of ω_r. This number divided by the total number of points N considered within the square, i.e. $P = \dfrac{N_s}{N}$ represents the probability for the occurrence 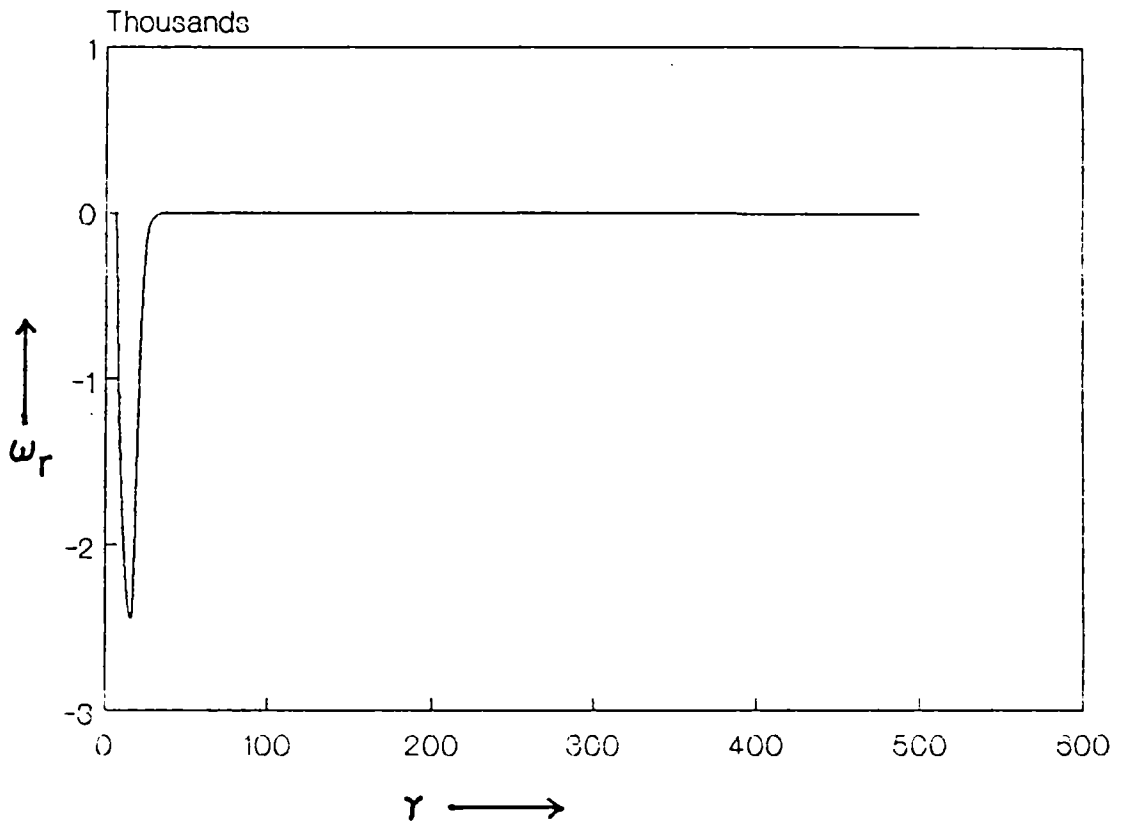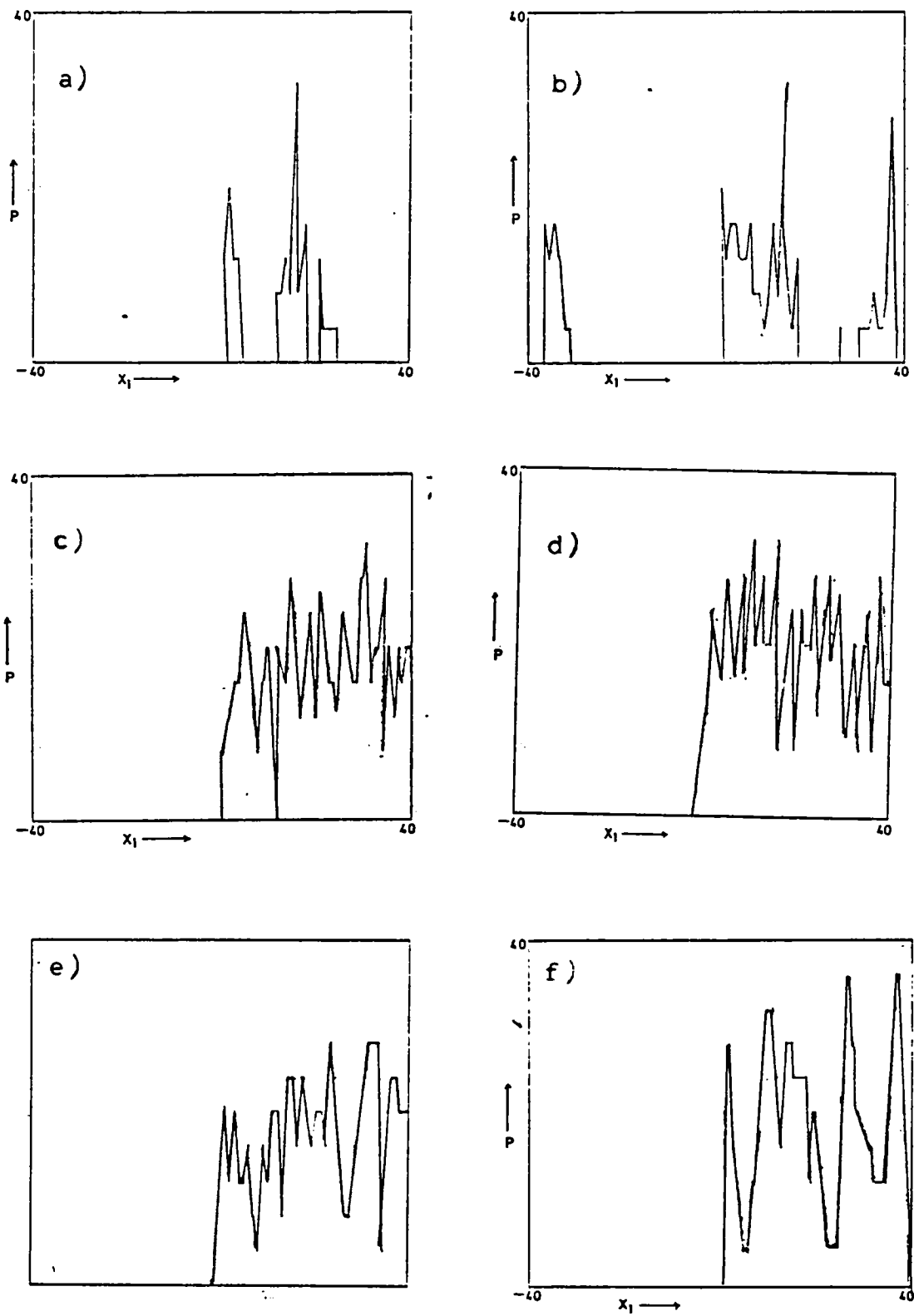of stable points. The variation of P with x_1, for $x_2 = 10$ and $x_3 = 27$ is plotted in Fig. 5.6 a-f for different γ values. The pictures clearly indicate that there is structure inside the stable region as revealed by a number of horizontal segments in the graph. For small values or γ where preturbulence and chaos exist, the variation of p depends crucially on the selection of the x_1-x_2 plane. However for γ values for which stable limit cycles exist, we find that horizontal regions are present in the curve of p versus x_1, indicating a decrease in the fluctuations of p (eg. $\gamma=50$, 100.5, 500). A comparison of the curves for $\gamma = 100.5$ and $\gamma = 99.5255$ should make this point clear. At $\gamma = 100.5$ a stable one cycle is known to exist, while $\gamma = 99.5255$ corresponds to the accumulation point of period-doubling bifurcations. We also note this in the region near $\gamma = 166.3$ where intermittent behaviour is observed. Thus rapid fluctuations in p from point to point in phase-space do not favour the formation of stable cycles.

5.4 Symmetries of Rössler Model

The Rössler system is represented by the following first order equations [113,118]:

$$F_1 = \dot{x}_1 = -(x_2+x_3)$$

$$F_2 = \dot{x}_2 = x_1 + \frac{1}{5}x_2 \qquad\qquad (5.20)$$

$$F_3 = \dot{x}_3 = \frac{1}{5} + x_3(x_1-\mu)$$

This is a prototype system of equations to the Lorenz
model of turbulence that contains only one nonlinear term
in one variable. Many natural systems are governed by
this type of equations [119]. In this model the transi-
tion from simple to strange attractor proceeds via a
sequence of period-doubling bifurcations that converge
at some limiting parameter value. Beyond this value one
generally finds chaotic behaviour superimposed on a reverse
bifurcation sequence. For $\mu=2.6$ the attractor is a simple
limit cycle. For $\mu>2.6$ the limit cycle becomes unstable
and at $\mu= 3.5$ a period doubling bifurcation occurs. These
period-doubling bifurcations accumulate at $\mu=\mu_\infty = 4.2$ and
a transition to chaotic motion occurs at this point. The
strange attractor for $\mu>\mu_\infty$ appears as bands of chaotic
behaviour that lie between regular orbits. This attractor
has a simple sheet-like structure that has been stretched,
folded over once, and joined from right to left edge. The
Lorenz attractor is more complicated, consisting of two
such sheets, with the stretched edge of each sheet on the
right divided into two parts. The right edge of each
sheet joins both sheets on their left.

The fixed points of the Rössler system are

$$x_1 = \frac{\mu_{+}^{-}\sqrt{(\mu^2 - 4/25)}}{2}; \quad x_2 = \frac{-\mu\pm\sqrt{(\mu^2-4/25)}}{2/5}; \quad x_3 = \frac{\mu_{+}^{-}\sqrt{(\mu^2-4/25)}}{2/5}$$

(5.21)

In contrast with the Lorenz system, the Rössler model possesses fixed points for every value of μ. The origin is not a fixed point. A translation symmetry analysis for the Rössler model has been carried out. As in the Lorenz model the translation pattern is double-branched with the middle portion remaining blank for all μ values. As the chaotic regime is approached, the middle portion gets enlarged ie, stable regions decrease in size. Fig. 5.7.

The characteristic equation for the rotational normal exponent for the Rössler system is

$$\begin{vmatrix} -(x_2+x_3) & F_3+\omega x_3-x_1 & x_1-F_2-\omega x_2 \\ \frac{1}{5}x_3-F_3-\omega x_3 & -x_3 & x_2-\frac{1}{5}x_1+F_1+\omega x_1 \\ \mu x_2-x_1 x_2+F_2+\omega x_2 & (x_1-\mu)x_1-F_1-\omega x_1 & 0 \end{vmatrix} = 0$$

with

$$F_{11}= 0 \quad , \quad F_{12}= -1 \quad , \quad F_{13}= -1$$

$$F_{21}= 1 \quad , \quad F_{22}= \frac{1}{5} \quad , \quad F_{23}= 0 \quad ,$$

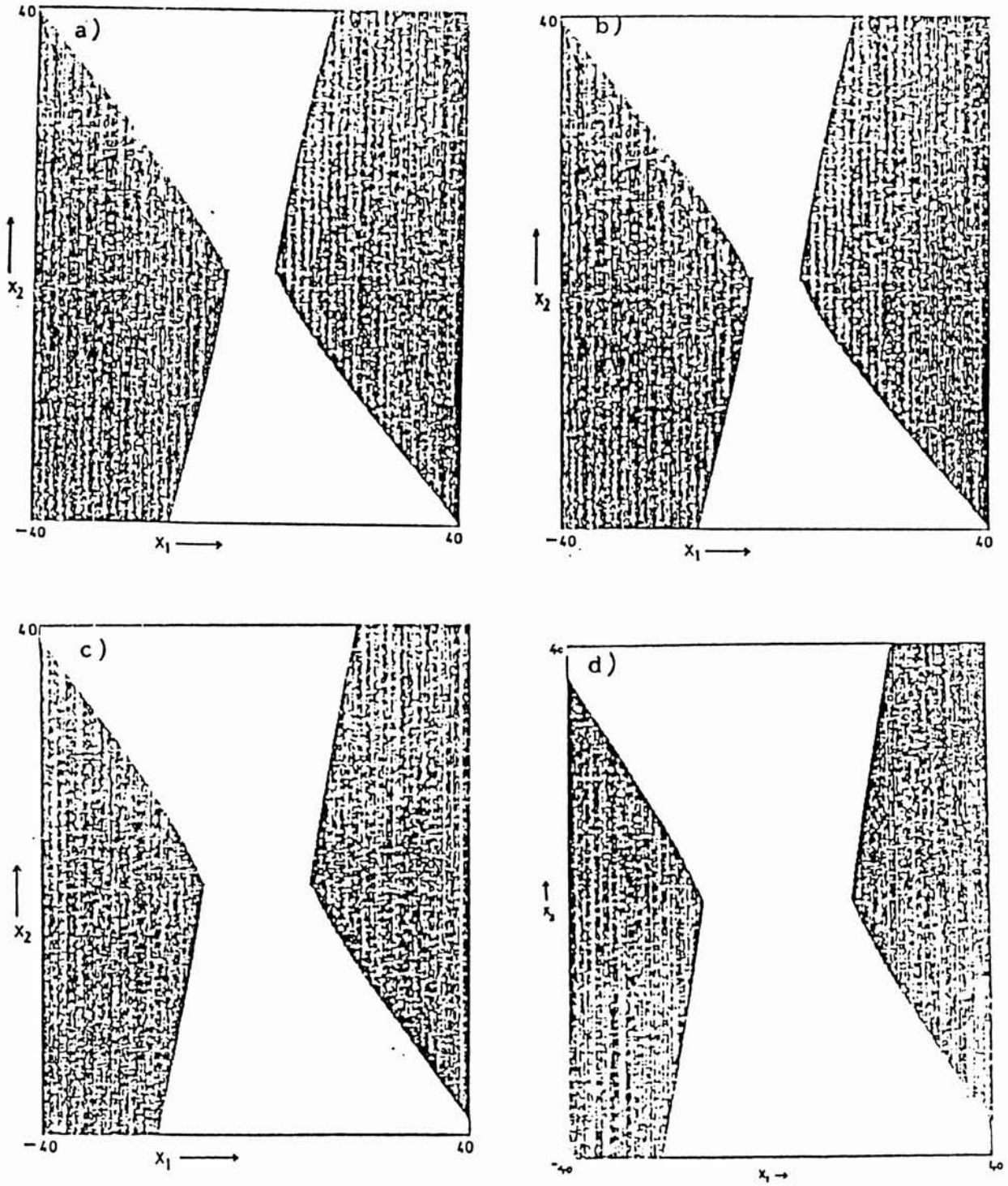$$F_{31}= 0 \quad , \quad F_{32}= 0 \quad , \quad F_{33}= (x -\mu)$$

Fig. 5.7 The variation of translationally stable and unstable region in the x_1-x_2 plane for different values of μ. Here $x_3=1$

a) $\mu = 1$ b) $\mu = 2.6$ c) $\mu = 4.2$

d) $\mu = 57$

We have computed the rotational ω_r values for different μ values for the fixed plane $x_3=1$. We find that the stable region decreases while the unstable region increases with increasing μ. However, there is no marked change before and after period-doubling and at the point $\mu>4.2$, where a strange attractor exists. One observes the slow evolution of stable and unstable regions with increasing μ, strengthening the view that the formation of stable limit cycles as well as their symmetry properties depend to a great extent on the pattern of stable and unstable regions. The variation of rotationally stable and unstable regions is depicted in Fig.5.8. A plot of rotational ω_r values versus μ also indicates a sudden change in ω_r value where a strange attractor exists, as is evident from Fig. 5.9.

We have also computed the number of stable points in a unit square that give rise to stable regions corresponding to negative ω_r for the Rössler attractor and hence the probability P. Here also it is seen in the P vs x_1 plot that as the chaotic region is approached, there is a fluctuating behaviour in contrast to the limit cycle region where we can observe more horizontal portions corresponding to stable regions. The variation of P in the x_1 direction for fixed x_3 and for a few chosen values of μ is sketched in Fig. 5.10.
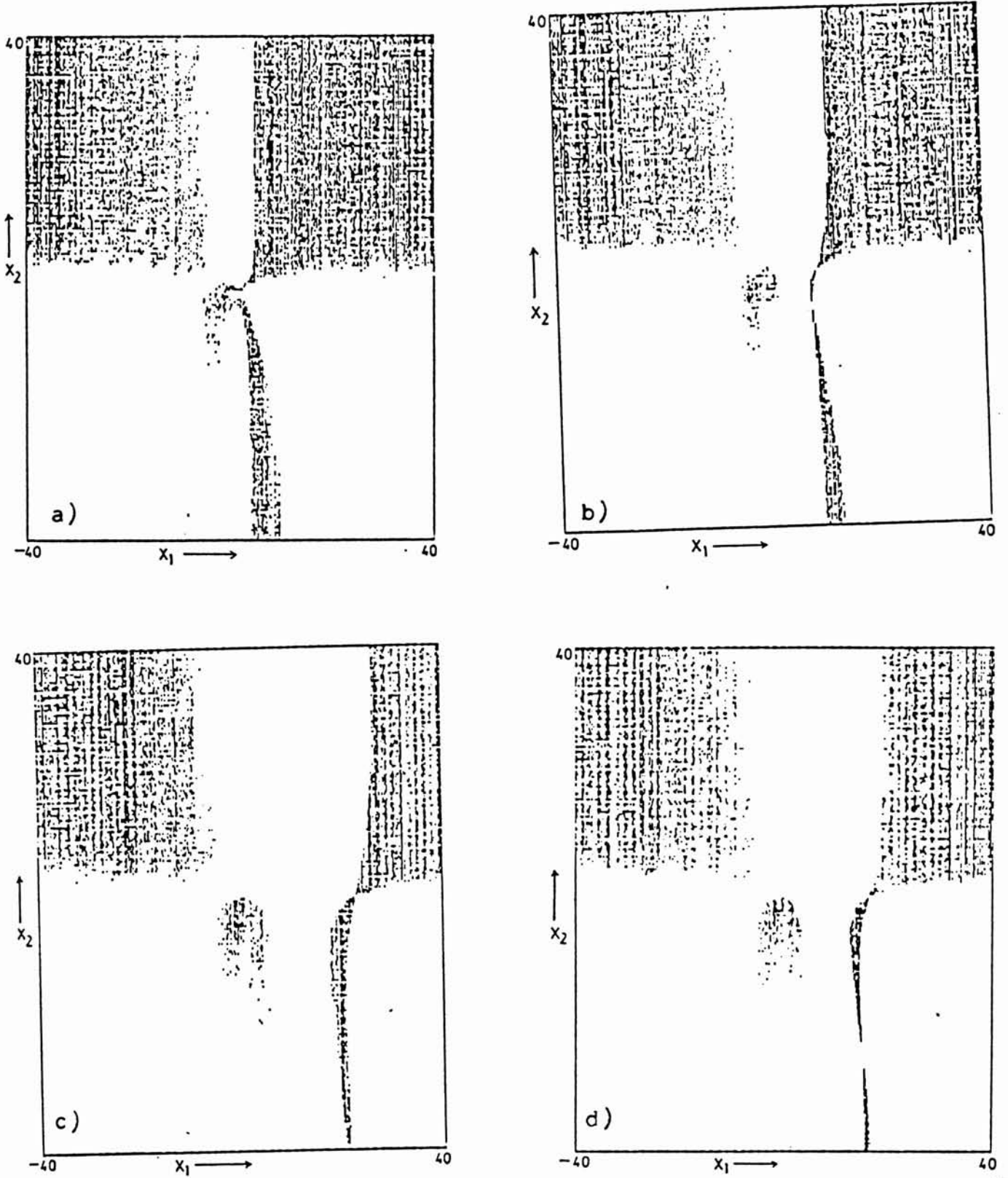
Fig. 5.8 Plot of rotationally stable and unstable regions in the $x_1 - x_2$ plane for different values of μ. Here $x_3 = 1$.

a) $\mu = 1$ b) $\mu = 2.6$ c) $\mu = 4.2$ d) $\mu = 5.7$
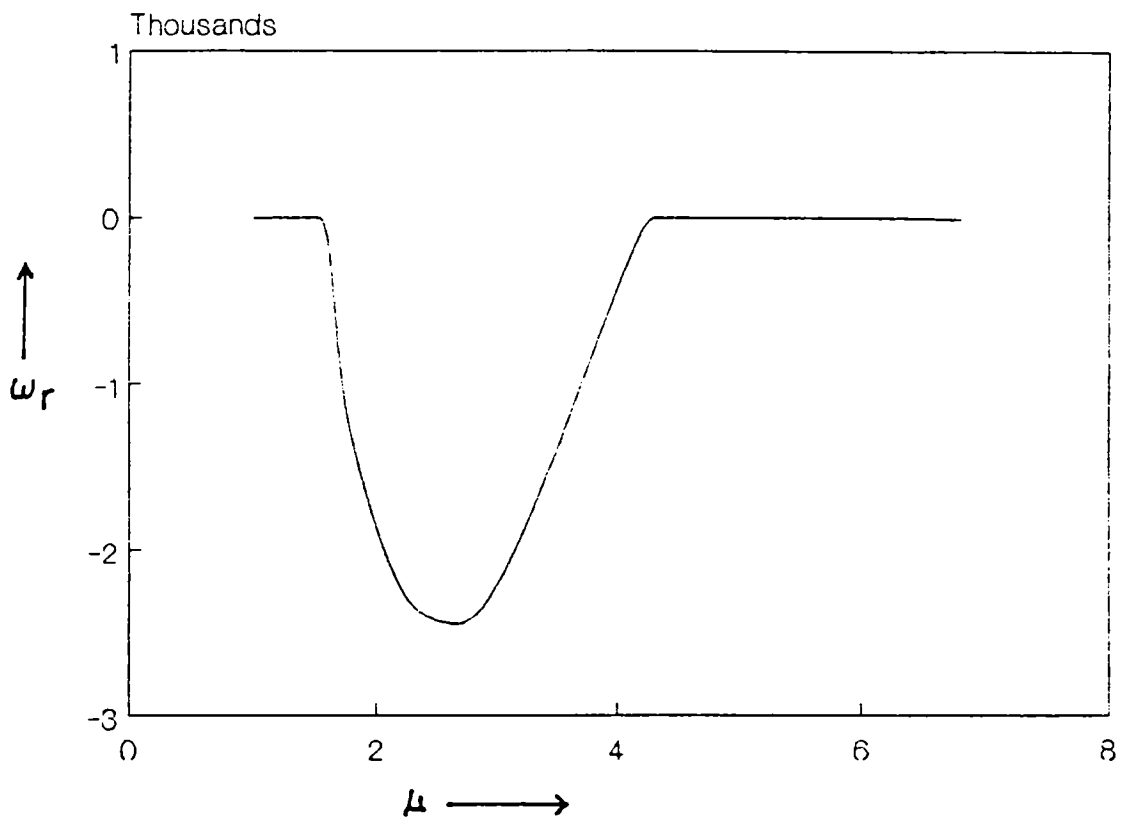
Fig. 5.9   The variation of rotational eigen-
           value ω_r with μ.
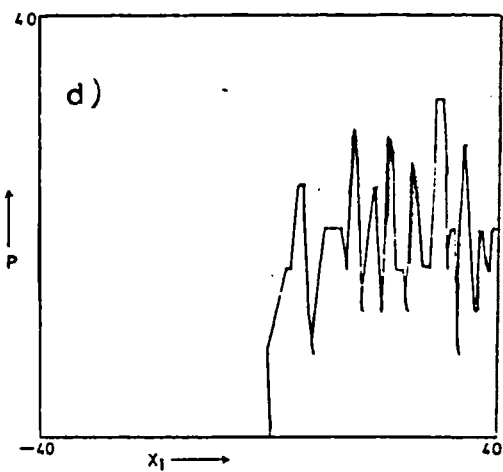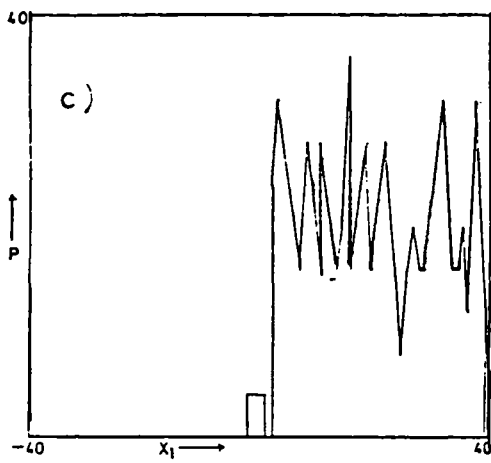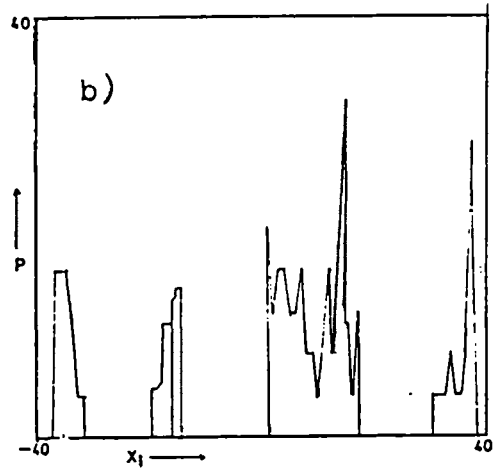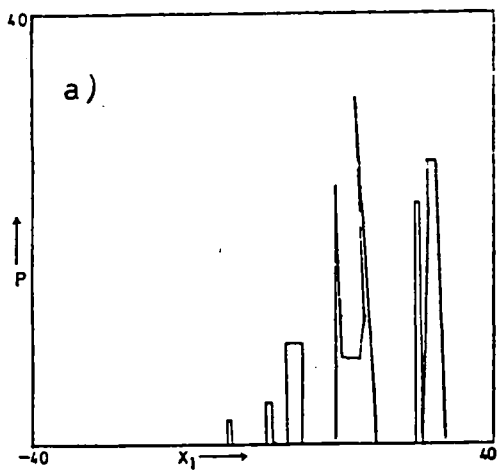
Fig. 5.10   The variation of P along the x_1 direction
with $x_3 = 1$ and for few chosen values of μ:

a) $\mu = 1$ b) $\mu = 2.6$ c) $\mu = 4.6$ d) $\mu = 5.7$

5.5 Discussion

The method of analysis carried out here helps the exploration of continuous symmetries of dissipative systems in phase space. We have demonstrated the possibility of employing a normal mode exponent as the local indicator of stability against the spontaneous breaking of a particular symmetry. Thus if the exponent is zero or positive at a point in phase space the given point is unstable and the particular symmetry at that point is said to be spontaneously broken. If a finite region not coincident with a strange attractor exhibits a fair degree of SSB, it may be associated with mild chaos on preturbutence.

The quantitative investigations herein reported lead to the following conclusions:

1) The distribution of translational and rotational stability regions in phase-space is parameter-dependent.

2) Translational symmetry patterns do not yield any clue to the onset of chaos.

3) There is some indication of the onset of chaos in the rotational symmetry pattern, as revealed by rapid fluctuations in the probability function P represented as a function of one of the phase-space variables.

4) The probability plot is seen to develop horizontal
   segmentation in a pronounced manner, indicating a
   constant probability in the vicinity of a limit cycle.
   Since a limit cycle is conventionally regarded as a
   stable, and highly symmetric asymptotic limit in the
   behaviour of a dynamical system, it is natural that
   the corresponding probability function manifests con-
   stant portions.

References

1   J. Guckenheimer and   'Nonlinear Oscillations Dynamical
    P.J. Holmes   Systems and Bifurcation of Vector
                            Fields (Springer, Berlin 1986)

2   Pierre Berge, Y.   'Order within Chaos'
    Pomeau and Christian   (John Wiley, New York 1984)
    Vidal

3   A.J. Litchenberg and   'Regular and Stochastic Motion'
    M.A. Liebermann   (Springer, New York 1983)

4   Hao-Bai-Lin   'CHAOS II (World Scientific,
                            Singapore 1990)

5   R. May   Nature 261, 459 (1976)

6   P.W. Milonni,   'Chaos in Laser Matter Inter-
    M.L. Shih and   actions' (World Scientific,
    J.R. Ackerhalt   Singapore 1987)

7   P.W. Milonni,   Phy. Rev. Lett. 50, 966 (1983)
    J.R. Ackerhatt and
    H.W. Galbraith

8   M.J. Feigenbaum   J. Stat. Phys. 19, 25 (1978)

9   M.J. Feigenbaum   J. Stat. Phys. 21, 665 (1979)

10 J.K. Bhatachargee   'Convection and Chaos in Fluids'
                            (World Scientific, Singapore
                            1987)

11 J. Ford   'Fundamental Problems in Statis-
                            tical Mechanics' Vol.3. ed: ECD
                            Cohen (North Holland, Amsterdam
                            1975) 215

12 W. Israel   Physica 106A,204 (1981)

13 W. Israel   Ann. Phys. 100 ,370 (1976)

14 J.P. Eckmann   Rev. Mod. Phys. 53, 643 (1981)

15 Y. Pomeau and   Comm.Math. Phys. 74, 189(1980)
    P.Manneville

16 J.H. Curry   Comm.Math. Phys. 60, 193 (1978)

17 D. Ruelle   The Math Intelligencer 2, 126 (1980)

18 U. Parlitz and   Phys. Lett. 107A, 351 (1985)
    W. Lauterborn

19 J.P. Eckmann,   Rev. Mod. Phys. 57, 617 (1985)
    D. Ruelle

20 E.N. Lorenz   J. Atmos. Sci. 20, 130 (1963)

21 W.H. Steeb and   'Chaos and Quantum Chaos'
    J.A. Louw   (World Scientific, Singapore, 1982)

22 Hao-Bai-Lin   'Elementary Symbolic Dynamics and
                            Chaos in Dissipative Systems'
                            (World Scientific, Singapore, 1989)

23 T.S.Akhromeyeva,   Phys. Rep. 176, 189 (1983)
    S.P. Kurdymo.v,
    G.G. Malinetski,
    and M.A.Samarski

24 M.J. Feigenbaum,
    M.H. Jensen and   Phy. Rev. Lett. 57 153 (1986)
    I. Proccacia

25 J.D. Farmer, E.   Physica 7D, 153 (1983)
    Ott and J.A.Yorke

26 G. Qui, D.Gang,   Phys. Lett 141A, 412 (1989)
    R. Li and X.Wen

27 Y. Ueda   J. Stat. Phys. 20, 181(1979)

28 N.H. Packard,   Phy. Rev. Lett. 45, 712 (1980)
    J.P.Crutchfield,
    J.D.Farmer and
    R.S. Shaw.

29 T. Kapitaniak and   Phys. Lett. 154A, 249 (1991)
    M.S. El Naschie

30 B.B. Mandelbrot   'Fractal Geometry of Nature'
                        (Freeman, New York, 1982)

31 P. Tabeling   Phy. Rev. 31A, 3460 (1985)

32 J. Guckenheimer   Phy. Rev. Lett. 51, 1438 (1983)
    and G. Buzyna

33 J. Farmer   Physica 4D, 366 (1982)

34 P. Grassberger   Physica 13D, 34 (1984)
    and I.Proceacia

35 H.G.E. Hentschel   Physica 8D, 435 (1983)
    and I.Procaccia

36 T.C.Halsey, M.H.
    Jensen, L.P.Kada-   Phy. Rev 30A, 1141 (1986)
    noff, I.Procaccia
    and B.I.Shraiman

37 Tamas Vicsek   'Fractal Growth Phenomena'
                        (World Scientific, Singapore, 1990)

38 G.Paladin and   Phys. Rep. 156 ,149 (1987)
    A.Vulpiani

39 E. Ott   Rev. Mod. Phys. 53,655 (1981)

40 H.G. Schuster   'Deterministic Chaos'
                        (VCH, Weinheim 1988)

41 P. Collet and J.P.   'Iterated Maps on the Interval
    Eckmann   as Dynamical Systems'
                             (Birkhaüser, Basel, 1980)

42 J.D. Farmer   Phy. Rev. Lett $\underline{55}$, 351 (1985)

43 R.L. Devaney   'An Introduction to Chaotic
                             Dynamical Systems' (Addison-Wiley,
                             New York 1989)

44 S.J. Chang and   Phy. Rev $\underline{30A}$, 1149 (1984)
    J. McCown

45 D.P. Siemens and   Physica $\underline{20D}$, 363 (1986)
    M. Butcher

46 T. Geisel, T. Nier-   Phys. Lett. $\underline{86A}$, 75 (1981)
    wetburg and J.Keller

47 N. Metropolis, M.L.   J. Comb. Theory $\underline{15}$, 25 (1978)
    Stein and P.R.Stein

48 W.Z.Zeng, B.L.Hao,   Comm. Theo. Phys. $\underline{3}$, 283 (1984)
    G.R.Wang and
    S.G. Chen

49 J.P.Eckmann and H.   Comm. Math. Phys. $\underline{128}$, 427 (1990)
    Epstein

50 B. Hu and J.M.Mao   Phy. Rev. $\underline{25A}$, 3259 (1982)

51 P.R. Hauser, C.   Phy. Rev. $\underline{30A}$, 2074 (1982)
    Tsallis and E.
    Curado

52 Y.Ge   Phys. Lett. $\underline{156A}$, 479 (1991)

53 M. Feigenbaum   Comm. Math. Phys. $\underline{77}$, 65 (1980)

54 A.S. Dimnitrev, A.I.   Phys. Lett. $\underline{155A}$, 494 (1991)
    Panas and S.O.
    Starker

55	C. Greboggi and E. Ott	Physica 7D, 181 (1983)
56	J.C. Sommerer, W.L.Ditto, C. Greboggi,E.Ott and M.L.Spano	Phys. Lett· 153A, 105 (1991)
57	F. Palmero and F.R. Romero	Phys. Lett. 156A, 272 (1991)
58	M. Lutzky	Phys. Lett· 128A, 332 (1988)
59	J.P.Vander Weele, H. Capel and R. Kluiving	Phys. Lett. 119A, 15 (1986)
60	J.P. Vander Weele, H. Capel and R. Kluiving	Physica 145A, 425 (1987)
61	K.I. Lin,W.S.Lo and K. Yang	Phys. Lett. 105A, 103 (1984)
62	M.C. de Souza Vieira, E.Lazo and C.Tsallis	Phy. Rev. 35A, 945 (1987)
63	R. Delbourgo and B.G. Kenny	Phy. Rev. 33A, 3292 (1986)
64	B. Hu	Phys. Rep. 91, 233 (1982)
65	B. Hu	J. Phys. 20A, 1809 (1987)
66	B. Hu and I.I. Satija	Phys. Lett. 98A, 143 (1983)
67	B.Hu and J.Rudnick	Phy. Rev. 34A, 2453 (1986)

| 68 | V. Singh | Pramana. J. Phys. $\underline{24}$, 31 (1985) |

69 G. Ambika and Pramana. J. Phys. $\underline{26}$, 465 (1986)

K. Babu Joseph

70 G.A. Baker Jr. 'Essentials of Padé Approximants'

(Academic, New York 1975)

71 E.B.Saff and 'Padé and Rational Approximants'

R.S. Varga (Academic, New York 1977)

72 A. Libchaber and J. Phys. Colloq. $\underline{41}$, C3-51 (1980)
J. Maurer

73 J. Testa, J.Perez Phy. Rev. Lett. $\underline{48}$, 714 (1982)

and C.Jeffries

74 S. Shenker Physica $\underline{5D}$, 405 (1982)

75 D. Rand, S.

Ostlund, J. Phy. Rev. Lett. $\underline{49}$, 132 (1982)

Sethna and

E. Siggia

76 S. Ostlund, D.

Rand, J.Sethna Physica $\underline{8D}$, 303 (1983)

and E. Siggia

77 M.J.Feigenbaum,

L.P.Kadanoff and Physica $\underline{5D}$, 370 (1982)

S. Shenker

78 M.H. Jensen, P. Phy. Rev. Lett. $\underline{50}$, 1637 (1983)

Bak and T.Bohr Phy. Rev. $\underline{30A}$, 1960 (1984)

79 B. Hu, A.Valinia Phys. Lett. $\underline{144A}$, 7 (1990)

and O. Piro

80 E.J.Ding and P.C. J. Stat. Phys. $\underline{46}$, 99 (1986)
Hemmer

81 E.G. Gwinn and R.M.   Phy. Rev. Lett. 57, 1060 (1986)
    Westervelt

82 G.A. Held and C.   Phy. Rev. Lett. 56, 1183 (1986)
    Jeffries

83 M.C. de Souza   J. Stat. Phys. 53, 1315 (1988)
    Vieira

84 J. Doyne, J.D.Farmer   Phy. Rev. 31A, 3520 (1985)
    and I.I. Satija

85 J.A. Glazier, M.H.   Phy. Rev. 34A, 1621 (1986)
    Jensen, A.Libchaber
    and J. Stavans

86 J. Stavans, F.Heslot   Phy. Rev. Lett. 55, 596 (1985)
    and A.Libchaber

87 Wen. Jer Tzeng, T.
    Chen Yu, B. Hu and   Phys. Lett. 155A, 117 (1991)
    Chin-Ku-Hu

88 A.S. Pikovsky and   Phys. Lett. 155A, 373 (1991)
    M.A. Zaks

89 Ji Cang Shi and   Phys. Lett. 155A, 267 (1991)
    M.A. Zaks

90 W. Gang and W. Wenzel   Phy. Rev. 43A, 6550 (1991)

91 W.J. Yeh, D.R. He   Phy. Rev. Lett. 52 480 (1984)
    and Y. Kao

92 P. Alstrom, M.H.   Phys. Lett. 103A, 171 (1984)
    Jensen and M.T.
    Levinson

93 R.S. Mackay and   Physica 19D, 206 (1986)
    C. Tresser

94 S.E. Brown, G. Mozur- Phy. Rev. Lett.52, 2272 (1984)
    kewich and G.Gruner

95 K. Kaneko   'Collapse of Tori and Genesis
                           of Chaos in Dissipative Systems'
                           (World Scientific, Singapore 1986)

96 R. Delbourgo and   Phy. Rev. 42A, 6230 (1990)
    B.G. Kenny

97 J.A. Glazier and A.   IEEE Trans. Circuits and Systems.
    Libchaher   35, 790 (1988)

98 M.H. Jensen, P.Bak   Phy. Rev. 30A, 1960 (1984)
    and T. Bohr

99 T. Bohr, P. Bak and   Phy. Rev. 30A, 1960 (1984)
    M.H. Jensen

100 P. Bak, T. Bohr,
    M.H. Jensen and   Solid State Comm. 51, 231 (1989)
    Voetmann Christi-
    ansen

101 D.J. Olinger and   Phy. Rev. Lett.60, 797 (1988)
    K.R.Sreenivasan

102 W.J. Tzeng, T.C.Yu,   Phys. Letts. 153A, 117 (1991)
    B. Hu and C.K.Hu

103 B.I. Shraiman   Phy. Rev. 29A, 3464 (1984)

104 B.Hu and J.M. Mao   J.Phys. 20A, 1809 (1987)

105 K.M. Valsamma, G.
    Ambika and K.Babu   Phy. Scr. 42, 19 (1989)
    Joseph

- G 5099 -

106 R.K. Kalia and P. Vashista — 'Melting, localisation and Chaos' (Elsevier, North-Holland 1982)

107 C. Sparrow — 'Lorenz equations, Bifurcations, Chaos and Strange attractors' (Appl. Math. Sci. Springer Verlag 1982)

108 B. Saltzman — J. atmos. Sci. 19, 329 (1962)

109 J.B. Mc Laughlin and P.C. Martin — Phy. Rev. 12A, 186 (1975)

110 G.P. Flessas and PGL Leach — Phys. Lett 154A, 127 (1991)

111 G. Rawlands — J. Phys. 16A, 585 (1983)

112 V. Kirk — Phys. Lett·154A, 243 (1991)

113 O.E. Rössler — Phys. Lett·57A, 397 (1976)

114 R.P. Behringer — Rev. Mod. Phys 57, 657 (1985)

115 D.D. Holm, G.Kovaccic and B. Sundharam — Phys. Lett·154A, 249 (1991)

116 M.Tavis and F. Cummings — Phy. Rev 170, 379 (1968)

117 H. Haken — Phys. Lett 53A, 77 (1975)

118 O.E. Rössler — Z. Naturfersch 31a 259 (1976)

119 D. Ruelle and F. Takens — Comm.Math. Phys·20, 167 (1971)